



UNCLASSIFIED

NACA ACR No. 5A15

NATIONAL ADVISORY COMMITTEE FOR AERONAUTICS

ADVANCE CONFIDENTIAL REPORT

AN EXPERIMENTAL INVESTIGATION OF SEVERAL LOW-DRAG  
WING-NACELLE COMBINATIONS WITH INTERNAL AIR FLOW

By H. Julian Allen, Charles W. Frick,  
and Myles D. Erickson

SUMMARY

The results of an experimental investigation of several low-drag wing-nacelle combinations, incorporating internal air-flow systems, are presented. The external-drag increments due to these nacelles are between one-half and two-thirds of those of conventional nacelle forms. This improvement is accomplished with only minor effects on the lift and moment characteristics of the wing. The procedure employed to determine the external shape of such low-drag nacelles is considered in detail.

The design of an efficient internal-flow system, with or without a blower or throttle, presents no serious problems. The energy losses in the expansion before the engine and the contraction thereafter can be kept small.

It is believed that these nacelles have a wide application in housing engine pusher-propeller units and, with some alteration, jet-propulsion devices. It is probable that the low external drags may not be realized if such nacelles are used with a tractor propeller because of the high level of turbulence in the propeller slipstream.

INTRODUCTION

The results of an experimental investigation of the boundary-layer growth on the surface of a wing-fuselage combination, wherein the nose of the fuselage protrudes forward of the wing, are reported in reference 1. In that investigation it was found that although the transition from laminar

~~CONFIDENTIAL~~  
UNCLASSIFIED

UNCLASSIFIED

to turbulent flow occurred far back along the surface at points distant from the wing-nacelle juncture, in the juncture itself transition moved forward to the wing leading edge.

Some additional drag must inevitably occur with this forward movement of transition in the juncture. This is attributable to (1) the increased surface shear associated with the turbulent boundary layer, and (2) the reduced pressure recovery at the tail which will accompany the thickened boundary layer at the minimum pressure point.

In reference 2 it was contended that premature transition to turbulent flow in such junctures is due to the fact that, on the forward protruding nose of the body, the air close to the surface is first accelerated and then retarded as it approaches the wing. The boundary layer becomes unstable in the region wherein the flow is retarded so that transition to turbulent flow occurs. It was reasoned that by making the nose of the body and the leading edge of the wing coincident, adverse pressure gradients near the leading edge with consequent premature transition could be avoided.

Several wing-nacelle units incorporating this feature were constructed and tested in the Ames 7- by 10-foot wind tunnel (reference 2). The wing and nacelles were so matched that their minimum pressure points were located at the same chordwise station. The experimental results of these tests confirmed the foregoing contention. Over the Reynolds number range of the tests, transition occurred behind the minimum pressure point in the wing-nacelle juncture as well as at all other points on the surface. In consequence, the drag increments for these nacelles were between one-half and two-thirds that for conventional nacelles.

The nacelles of the preliminary investigation (reference 2) were streamline bodies without internal air flow, but it was anticipated that the introduction of internal air flow could be made without destroying the low-drag characteristics. However, it was expected that some difficulties would be encountered in properly shaping nacelles incorporating air-induction systems. In this report, the results of an experimental investigation of several such wing-nacelle combinations with internal flow are presented. A discussion of the proper shaping of such nacelles is included.

~~CONFIDENTIAL~~  
UNCLASSIFIED

~~CONFIDENTIAL~~  
UNCLASSIFIED

## DESCRIPTION OF MODELS

The NACA 35-215 wing of reference 2, the ordinates of which are given in table I, was used again in combination with the nacelles of this report. However, the method of mounting the wing in the tunnel was changed, as is discussed under the section Description of Apparatus.

The nacelle shapes used in this experimental investigation were derived from the NACA 133-30 nacelle shape of reference 2, the ordinates of which are given in table II.

Nacelle nose shapes.— A method was developed in reference 1 for altering the nose of a nacelle to provide a satisfactory nose air inlet. The test results, given in that reference, showed that the pressure gradients over the forward portion of a nacelle so obtained were favorable for all except the lowest inlet-velocity ratios.

The method for altering the nose shape, as outlined in reference 1, is not generally applicable and was accordingly revised to make it suitable for the nacelles of this report. This revised method, which is given in appendix A, was used to develop the shape of the nose  $N_1$  of the first nacelle tested using the nose-shape parameter of reference 1. The subsequent development of noses  $N_2$ ,  $N_3$ ,  $N_4$ , and  $N_5$ , and the reasons for each change are related in the section of this report devoted to a discussion of the results. Figure 1 gives a comparison of these nose shapes. The ordinates are given in table III, and table IV presents the nondimensional nose-shape parameter used in the method of appendix A.

Development of nacelle tail shapes.— Within certain limits, considered in the section Results and Discussion, it is desirable to bring the plane of the pusher propeller as near as possible to the trailing edge of the wing. It is obvious that by so doing, the aerodynamic design of the combination of nacelle and wing becomes more and more critical because of the steep pressure recovery that exists in the juncture of the wing and the nacelle. If this pressure gradient becomes too severe, separation of the flow from the surface will occur with consequent adverse aerodynamic effects. The problem thus confronting the designer is to develop a nacelle fulfilling the design requirements of reference 2 in matching the pressure distribution of wing and nacelle, while at the same time shortening the nacelle without incurring flow separation.

~~CONFIDENTIAL~~

UNCLASSIFIED

UNCLASSIFIED

No rational basis was known for determining to what extent the nacelle tail may be shortened without excessive drag increase. The tail shapes developed herein are the result of judgment and experience gained with the test of each succeeding shape. The first tail  $T_1$  was designed for a propeller position about 15 percent wing chord behind the wing trailing edge. The contour of this tail deviates to a marked degree from the lines of the original NACA 133-30 nacelle, as may be seen in figure 2. Tail  $T_2$  conforms more closely to the original nacelle lines, as may be seen from the same figure, and has a propeller position about 30 percent chord behind the trailing edge. Tail  $T_3$  represents a shape intermediate between the first two contours with a propeller position of about 21 percent wing chord behind the trailing edge. The section of this report devoted to discussion relates the steps involved in this development. Table V gives the ordinates of the various tails.

Outlet and spinner designs.— Since it was desired to test these nacelles throughout a wide range of flow coefficients, it was necessary to provide a variable outlet area. This was accomplished with  $T_1$  and  $T_2$  by using a throttle sliding along the axis of the spinner. This throttle was so designed that the annular duct between the throttle and the inside of the tail cone was of nearly constant area for any given throttle setting to minimize any orifice loss which might occur. Flow coefficients above the maximum value attainable with throttle full open were obtained by using an axial blower in the nose of the model to overcome the internal resistance of the duct.

Spinners of the same shape and length behind the outlet were used with tails  $T_1$  and  $T_2$  with provision for altering the pointed tip to a blunt shape.

The third tail  $T_3$  was tested with a constant outlet area and the variation in flow coefficient obtained by varying the speed of the axial blower. The spinner used with this tail was of approximately the same form as that used with the pusher nacelle of reference 3. Ordinates of all spinners and throttles are given in table VI.

Internal ducts.— It has been shown in reference 4 that the efficient conversion of axial kinetic energy of an air stream that possesses rotational kinetic energy as well, may be made in a diffuser of much shorter length than if the

~~CONFIDENTIAL~~

UNCLASSIFIED

UNCLASSIFIED  
~~CONFIDENTIAL~~

rotational component is not present. Further, the conversion of the rotational kinetic energy itself may be effected by making the diffuser cross section an annulus of increasing area along the axis.

These principles were incorporated in the design of the internal diffuser between the axial blower and the baffle plate simulating the engine. The ordinates of the surfaces are given in table VII. The internal duct between the baffle plate and the outlet did not require refined design except the section along the axis of the throttle, previously mentioned, since the losses suffered in a converging duct are usually small.

The baffle plate simulating the engine was designed to have a conductance  $K$  of 0.25, but most tests were made with a sufficient number of holes plugged to give a value of  $K$  equal to 0.10.

Axial blower.— The axial blower used in these tests consisted of eight blades of Clark Y section so attached to the hub that the blade angle was adjustable. Several blade angles were used in the tests of various nacelles to satisfy the required operating conditions. Part of the tests were made with five Clark Y section countervanes in place. For the purpose of the nacelle-drag tests, the fan is considered of interest only insofar as it was used to vary the flow. A separate report on the fan operation as it affects the internal-flow conditions and as it may be used to improve operating conditions at altitude is proposed.

In discussing the nacelles hereafter, every combination of nose and tail will be noted by grouping the designation of each so that the combination of nose 2 and tail 2, for instance, will be given as  $N_2T_2$ .

A sectional view of  $N_2T_2$  is given in figure 3. Figures 4 to 10 show various views of the nacelles mounted in the tunnel.

#### DESCRIPTION OF APPARATUS

Tests of the various wing-nacelle combinations were made in the Ames 7- by 10-foot wind tunnel. This tunnel is of the closed-throat, rectangular-section, single-return

~~CONFIDENTIAL~~  
UNCLASSIFIED

UNCLASSIFIED

type, capable of airspeeds of 300 miles per hour. The turbulence level of the air stream is such that it was possible to maintain laminar flow over those portions of the wing subject to a favorable pressure gradient up to the maximum attainable test Reynolds number.

Each wing-nacelle combination was mounted as a through model spanning the 7-foot dimension of the test section. End plates flush with the walls of the test section but clearing the walls by a gap of  $3/16$  inch were mounted on the ends of the wing.

The internal drag of all nacelles except nacelle  $N_5T_3$  was obtained prior to the drag tests by measuring the total-head losses and static pressure at the outlet with a rake consisting of 45 total-head and three static tubes. This rake is shown in figure 11. During the force tests of nacelles  $N_5T_3$ ,  $N_5T_4$ , and  $N_5T_5$ , the internal drag was measured with an outlet rake of nine total-head and three static tubes (fig. 8), since all tests were made with the axial blower operating.

The flow quantities measured with the outlet rake were used to calibrate the orifice plate simulating the engine resistance so that the pressure drop across this plate could be used to obtain any desired flow coefficient. This orifice plate of  $1/2$ -inch-thick steel plate was perforated with 90 sharp-edge holes ranging in size from  $25/32$ -inch to  $1/4$ -inch diameter. To adjust the simulated engine conductance to a value of 0.10, a number of the holes were plugged with corks. For tests of other engine conductances, this arrangement of corks was altered to obtain the desired pressure drop.

Wake surveys of the drag were made with a rake of 48 total-head tubes and three static pressure tubes. Section-drag coefficients were computed from these data by an adaptation of the Jones method which considers the effect of fluid compressibility and the temperature rise in the wake.

Boundary-layer profiles were measured with a small surface rake of six total-head tubes and one static tube. Pressures over the nacelle, through the internal duct, and along the wing-nacelle juncture were measured through 0.020-inch-flush orifices.

~~CONFIDENTIAL~~

UNCLASSIFIED

UNCLASSIFIED

TESTS AND TEST METHOD

During all tests, the surfaces of the wing and the nacelles were maintained in an aerodynamically smooth condition. All balance-system measurements were made with the pressure orifices sealed and filled so as to be flush with the model surface.

All data presented, except the pressure-distribution results, have been corrected for tunnel-wall interference. The corrected coefficients (primes indicating test results) are as follows:

$$C_D \quad 0.980 C_D'$$

$$C_L \quad 0.950 C_L'$$

$$C_{m_c/4} \quad 0.980 C_{m_c/4}' + 0.0082 C_L'$$

$$\alpha \quad \alpha' + 0.298 \left[ C_L' + 4 C_{m_c/4}' \right]$$

$$R \quad 1.009 R'$$

$$M \quad 1.009 M'$$

Coefficients for the wing-nacelle combinations are based on a wing chord of 4 feet and a wing area of 28 square feet. Drag coefficients for the nacelles are based on their projected frontal area of 2.58 square feet. The pressure distributions along the wing-nacelle junctures and along the top and bottom meridians of the nacelles are plotted against wing-chord stations so that the data for the various nacelles are comparable.

The drag force due to the internal flow in the duct was determined from measurements of the average total head and static pressure at the outlet, consideration being given to the effects of fluid compressibility. A calibration of the pressure drop across the orifice plate with various internal-flow rates was made to facilitate the determination of the flow coefficient and the internal-drag coefficient when the outlet rake was not installed.

During the course of the tests when the nacelle-drag coefficients obtained from balance measurements were compared

~~CONFIDENTIAL~~

UNCLASSIFIED



UNCLASSIFIED

with nacelle-drag coefficients determined from wake surveys, it was apparent that the presence of the nacelle was influencing the flow at the wing ends to such a degree as to change the tare drag. This was confirmed by a comparison of the drags determined by wake surveys near the ends of the span for the wing and the wing nacelle, the wing nacelle showing a decided increase over that for the wing. The effect was small at low speeds and increased when the speed increased. This discrepancy in tare was discovered during the tests of nacelle  $N_4T_2$ . For this nacelle and for  $N_5T_3$ ,  $N_5T_4$ , and  $N_5T_5$ , tares were determined by making spanwise surveys of the distribution of drag coefficient at a flow coefficient of 0.055, finding the nacelle drag, and computing the tare from the relation of this drag to that determined from the balance force measurements. The tare was then applied to the balance-drag coefficients to obtain the variation of nacelle-drag coefficient with flow coefficient. Two of the surveys from which tares were determined are shown in figures 12 and 13. These exhibit the same type of spanwise distribution of section-drag coefficient as for the nacelles of reference 2. The reasons for the apparently abnormally low section-drag coefficients near the juncture are discussed in that report.

Since nacelle  $N_1T_1$  did not exhibit desirable characteristics, no tare determination was made by the tedious momentum surveys except at the ideal lift  $C_L = 0.213$ . All other data are based on balance measurements only.

It must be noted that the drags determined by wake surveys are low by the amount of the induced drag resulting from the distortion in spanwise lift distribution due to the influence of the nacelle. A theoretical study indicates that the induced-drag coefficient based on projected frontal area of the nacelle is 0.001 at a lift coefficient of 0.23. This induced drag will vary approximately linearly with the lift. Since such an induced drag would vary with propeller thrust for powered nacelles and could be adjusted to practically zero by alteration of the chordwise dimensions of the wing near the nacelle, it is considered that this induced drag is not properly a characteristic of these nacelles. In consequence, no induction correction has been incorporated in any of the test results presented in this report.

~~CONFIDENTIAL~~

UNCLASSIFIED

UNCLASSIFIED

RESULTS AND DISCUSSION

It was found in the tests of the first nacelle  $N_1T_1$  that, as anticipated, laminar flow could be maintained up to the minimum pressure position in the wing-nacelle juncture as well as on the other sections of the wing-nacelle surface. However, a number of undesirable flow characteristics, directly attributable to improper shaping of the nose and the tail of the nacelle, were observed. In the following paragraphs these adverse characteristics are discussed together with the development of satisfactory nose and tail shapes.

Nose development.— The pressure distribution over the exterior and interior surfaces in the vicinity of the nose of a nacelle incorporating an air-induction system is a function of the nose inlet-velocity ratio  $V_1/V_0$ . It is clear that at a sufficiently low inlet-velocity ratio, a low pressure peak, with a consequent local adverse pressure gradient, must occur on the nose exterior. An adverse pressure gradient on the exterior surface will promote premature transition to turbulent flow and so must be avoided if low drag is to be obtained. One criterion, then, in the development of a satisfactory nose shape is that at the lowest inlet-velocity ratio which will occur in high-speed flight at low altitudes, no exterior surface pressure peak is permissible. At a high inlet-velocity ratio, a low pressure peak is too marked, it will lower the critical Mach number of the combination below that dictated by the minimum pressure peak in the wing-nacelle juncture. Another criterion, then, in the development of a satisfactory nose shape is that at the highest inlet-velocity ratios which occur in high-speed flight at high altitudes, the peak pressure on the nose interior must not be as low as the lowest peak pressure on the exterior surface of the wing-nacelle unit.

As a final criterion, in order to insure the attainment of low drag in climb, the range of lift coefficients for low-drag coefficients with moderate to high values of the inlet-velocity ratio should be at least as great as for the wing,

Viewed in the light of these criteria, the nose  $N_1$  was unsatisfactory. As may be seen from the pressure plots of figures 14(a) and 14(b), at the wing ideal lift coefficient (about 0.2), a nose inlet-velocity ratio of over 0.5 was required to prevent the occurrence of an adverse pressure gradient on the nose exterior. Although but one pressure

~~CONFIDENTIAL~~

UNCLASSIFIED

UNCLASSIFIED

orifice was located on the nose interior, the measured pressures at this orifice indicated that an excessively low pressure would occur here at only a moderately high inlet-velocity ratio. Moreover, a pressure survey showed that for moderate to high inlet-velocity ratios, the lift-coefficient range for which no exterior adverse pressure gradients occur was much less than that for the wing.

Two attempts were made to improve the nose shape with noses  $N_2$  and  $N_3$ . The shape  $N_2$  differed from  $N_1$  in having a somewhat larger nose radius as well as some increase of thickness and camber; the shape  $N_3$  incorporated an even larger nose radius as well as some further increase in thickness and camber. These shapes are shown in figure 1. The distribution of pressure over  $N_2$ , shown in figures 15 to 19, indicates a general improvement over nose  $N_1$ . A pressure survey indicated that the nose radius of  $N_3$  was too large, and no further tests using this nose shape were made.

None of these nose shapes permitted a sufficiently wide range of lift coefficients for which no adverse pressure gradients would occur at moderate to high inlet-velocity ratios. An examination of the pressure distributions for the first three nose shapes indicated a means for improving this characteristic. In the case of these noses, at the wing ideal lift coefficient, the upper-lip shape produced an external low pressure peak before the lower lip as the inlet-velocity ratio was reduced. Conversely, as the inlet-velocity ratio was increased, the lower lip produced an internal low pressure peak before the upper lip. If the nacelle axis were curved to the shape of the wing mean-camber line, then, at the ideal lift, the pressure distributions over the nacelle upper and lower nose lip would be similar at any given inlet-velocity ratio. In this case, the lift-coefficient range over which adverse pressure gradients were absent for the wing and the wing-nacelle unit would more closely correspond.

For nose shapes  $N_4$  and  $N_5$ , some nacelle camber was effectively incorporated. The lower lip of  $N_4$  and  $N_5$  was kept the same as for  $N_2$ , since it had been found to be satisfactory. The upper lips of these nose shapes were extended and drooped as shown in figure 1. They differed only in that the leading-edge radius of  $N_4$  was larger than that of  $N_5$ . An examination of the experimental pressure distributions, shown in figures 20 to 29, shows the shape  $N_5$  to

~~CONFIDENTIAL~~

UNCLASSIFIED

UNCLASSIFIED  
~~CONFIDENTIAL~~

be somewhat superior to  $N_4$ , although both are considered satisfactory in light of the three criteria previously discussed.

Tail development.— It has been shown in reference 5 that it is undesirable to place the plane of the propeller closer than 15 percent wing chord behind the trailing edge of the wing in a pusher-propeller wing-nacelle combination because of the adverse effects of the flaps on the propeller characteristics. At the same time, it is desirable to bring the propeller location as near the wing trailing edge as possible because of the saving in weight. Accordingly, the tail shape  $T_1$  was designed to obtain a propeller location 15 percent wing chord behind the wing trailing edge. The tail shape, as noted previously, was obtained by simply contracting the original NACA 133-30 nacelle. This contraction was so severe as to promote flow separation if transition was shifted forward at very low inlet-velocity ratios. This characteristic is exhibited by the data of figure 30 which show the marked hysteresis in the variation of drag coefficient with mass-flow coefficient.

Figure 31 presents the variation of drag coefficient with flow coefficient at the ideal lift, the only lift coefficient for which tare was determined for  $N_1T_1$ . Hysteresis did not occur and it is considered that the flow remained separated at all flow coefficients. In spite of this, the drag of the nacelle is much less than for usual nacelles. This critical characteristic of the flow in the wing-nacelle juncture is further indicated in figure 32 by a reduction in the maximum lift coefficient for this wing-nacelle unit as compared with that for the wing alone or with that for the other wing-nacelle combinations.

In an effort to avoid this undesirable aerodynamic effect in subsequent developments, the ordinates of the tail shapes from the maximum ordinate location to the nacelle station opposite the wing trailing edge were held closely to the ordinates of the NACA 133-30 nacelle, which showed no flow-separation effects. With tail  $T_2$ , for which the propeller location was fixed at 30 percent wing chord behind the wing, the contraction behind the station at the wing trailing edge was slightly more severe than for the original NACA 133-30 nacelle. The test results for the  $N_4T_2$  nacelle, given in figure 33, show that nacelle external-drag increments comparable with those of reference 2 were obtained and

~~CONFIDENTIAL~~  
UNCLASSIFIED

UNCLASSIFIED  
~~CONFIDENTIAL~~

that separation was avoided, as indicated by the absence of hysteresis in the variation of external drag with flow coefficient. Further, the contraction of this tail cone is not so severe as to reduce the maximum lift coefficient appreciably below that for the wing, as is shown by the data of figure 32.

It is considered that while the tail  $T_2$  was satisfactory insofar as aerodynamic characteristics are concerned, the propeller position is too far behind the wing trailing edge for most applications. With  $T_3$  the propeller location was changed to about 21 percent wing chord behind the wing by contracting the tail cone more rapidly behind the wing trailing-edge station than for  $T_2$ . The drag test results for the  $N_5T_3$  nacelle, given in figure 34, show again that low drag was obtained and separation was avoided. In figure 32 the lift curve for the  $N_5T_3$  wing-nacelle unit is shown. It is seen that the lift curve for this wing-nacelle unit is very similar to that for the  $N_2T_2$  unit.

Although  $T_1$  was found to be unsatisfactory, as evidenced by the drag hysteresis with flow coefficient and the reduction of the maximum lift coefficient accompanying the addition of the nacelle to the wing, it is not believed that  $T_3$  necessarily represents the shortest satisfactory nacelle shape with external spinner. Rather, it is considered that  $T_1$  was contracted too rapidly in the region from the maximum diameter to the wing trailing-edge location, which promoted an excessively severe adverse pressure gradient in this region. Using the tail contracted at a rate midway between that for  $T_1$  and  $T_3$ , with a spinner similar to that for  $T_3$ , would allow a propeller location about 15 percent wing chord behind the wing. Such a nacelle would probably have satisfactory aerodynamic characteristics.

In the investigation of reference 1, several nacelles were tested from which air was exhausted through a circular opening at the end of the nacelle. Such nacelles might be considered to be representative of a jet-propulsion unit or a propeller-propulsion unit with a submerged propeller hub. For comparison with these nacelles, the tails  $T_4$  and  $T_5$  were constructed. Both were formed from tail  $T_3$  by removing the spinner and extending the skirt so as to reduce the diameter of the exhaust opening. However, with  $T_4$  the trailing edge was sharp but not cusped as with  $T_5$ .

CONFIDENTIAL

UNCLASSIFIED

UNCLASSIFIED  
~~CONFIDENTIAL~~

The results of the tests of these tail shapes are shown in figures 35(a) and 35(b). No indication of hysteresis of the drag coefficient with flow coefficient was found. It is noteworthy that the external drag of the cusped  $T_5$  tail is less than that for the  $T_4$  tail. This characteristic of cusped tail nacelles was predicted in reference 1 and later realized in the tests of reference 6. It is considered that the cusp-type skirt trailing edge would be similarly beneficial for nacelles with annular exhaust openings, as for tails  $T_1$ ,  $T_2$ , and  $T_3$ .

Tabulated below are the external-drag coefficients for the nacelles  $N_1T_1$ ,  $N_4T_2$ ,  $N_5T_3$ , and  $N_5T_4$  obtained at the wing ideal lift coefficient (0.213) and at the design flow coefficient (0.044):

Nacelle $N_1T_1$	$C_D = 0.0325$
Nacelle $N_4T_2$	$C_D = 0.0258$
Nacelle $N_5T_3$	$C_D = 0.0240$
Nacelle $N_5T_4$	$C_D = 0.0257$

It is seen that with the exception of  $N_1T_1$ , these drag coefficients are very nearly the same and are approximately equal to those for the nacelles of reference 2. While the  $N_1T_1$  nacelle is inferior to the others, it still represents a considerable improvement over nacelles of the usual form. The drag coefficient for nacelle  $N_5T_5$  is not included in this table since the minimum flow coefficient obtainable was greater than the design value even though the outlet area was the same as for  $T_4$ . This effective increase in the outlet area is due to the cusped tail cone and was noted also in the tests of reference 6.

The drag coefficients of the nacelles were investigated at low lift coefficients throughout the Reynolds number range, but only minor variations were found. At  $C_L = 0.325$  the drag coefficient decreased slightly, while at  $C_L = 0.525$  the drag coefficient showed a slight increase with Reynolds number. These data are not presented since they show only these small changes.

Tests of the nacelle  $N_4T_2$  through the Reynolds number range were made at low lift coefficient with blunt spinner.

~~CONFIDENTIAL~~

UNCLASSIFIED

An increase in the nacelle drag coefficient of about 0.001 over that for the pointed spinner was found.

The variation of drag coefficient with lift coefficient for the  $N_4T_2$  combinations at a Reynolds number of 3,700,000 is shown in figure 36. This variation was typical of all the nacelles excepting  $N_1T_1$ . The peculiar variation of nacelle drag coefficients as exhibited by these data, insofar as the drag coefficients at  $C_L = 0$  and  $C_L = 0.525$  are concerned, is understandable if a study of the effect of the nacelle on the pressure distribution over the portion of the wing outboard of the nacelle is made. The presence of the nacelle so distorts the flow pattern in this region that a sharp pressure peak usually appearing on the nose of the wing at these lift coefficients does not occur so that the transition point does not move forward. Consequently, these portions of the wing experience lower drag coefficients than are usually obtained at these lift coefficients, so that the total increment in drag due to the nacelle is less than for the other angles of attack. This phenomenon occurred with all the nacelles tested.

An investigation of the variation of external-drag coefficient with internal-flow coefficient for nacelle  $N_4T_2$  (fig. 33) reveals that as the flow coefficient is increased from zero, a marked reduction in drag is obtained. This is attributed to the reduction in mean velocity over the exterior of the nacelle and to the favorable effect of increasing flow coefficient on the location of transition on the nacelle which is brought about by the reduction and eventual elimination of the pressure peak on the nose exterior. As the flow coefficient is further increased, the drag is reduced but at a lesser rate and is a minimum for the minimum flow coefficient with wide-open throttle; that is, when the ratio of the velocity of discharge to the velocity on the nacelle at the outlet is a minimum. When this flow coefficient is exceeded, the drag coefficient at first remains sensibly constant then rises at an increasing rate.

It will be noted on figure 37 that for all the nacelles except  $N_5T_5$  this characteristic increase in drag coefficient, which accompanies an increase in the ratio of the velocity of discharge to the velocity over the nacelle at the outlet, is present.

UNCLASSIFIED

These results were obtained with varying flow coefficient. In order to eliminate the effect of flow coefficient, the drag characteristics of nacelle  $N_1T_1$  were measured at a constant-flow coefficient over a wide range of outlet velocities by suitably varying the blower speed and throttle opening. The results shown in figure 38, when compared with the previously mentioned data, indicate that these data are little affected by changing the flow coefficient. While the characteristic increase of drag coefficient with velocity of discharge is not well understood, consideration should be given to this effect in the choice of the outlet area in any nacelle design. Cusping the tail outlet, as for  $N_5T_5$ , is seen to minimize this effect for the test range of flow coefficients.

Internal drag due to air induction.— The results of these tests indicate that the internal-flow systems of the nacelles were satisfactory in that the losses associated with the initial expansions up to the baffle plate (simulating the engine) and the contractions thereafter were small. This is evident from figure 39, where it is shown that the total internal-drag coefficient is only moderately greater than the drag due to the baffle plate. There is no reason to believe that the introduction of the blower had a detrimental effect on the efficiency of expansion and contraction. As seen in this figure, a windmilling fan does not add appreciably to the internal losses.

Boundary layer.— The laminar boundary layer in the wing-nacelle juncture was found to be uniquely stable, as was also observed in the tests of reference 2. The formation of a pressure peak on the exterior surface of the nacelle nose, sufficient to move transition very far forward on the nacelle at points removed from the juncture, produced no change on the laminar boundary layer at the minimum pressure point in the juncture. This effect is not understood.

Boundary-layer tests at the pressure minimum over the span of the model showed that the flow remained laminar on the upper surface of the model at lift coefficients up to about 0.4 to the highest Reynolds number tested, about 10,000,000, for a flow coefficient of 0.055. Those results agree well with those of the extensive transition-location surveys presented in reference 2.

~~CONFIDENTIAL~~

UNCLASSIFIED



UNCLASSIFIED  
~~CONFIDENTIAL~~

Pressure distribution,— In reference 2, it was shown that the velocity distribution in the wing-nacelle juncture could be calculated with reasonable accuracy by the superposition method of reference 7. When the nacelle is altered to provide air induction at the nose, however, an accurate calculation of the velocity distribution is practically an impossibility. The velocity distribution may be approximated, though, by the method of appendix B, which considers what changes to the effective body dimensions result from so altering the nacelle.

This velocity distribution calculated by the method of appendix B may be combined with that for the wing by the superposition method of reference 7 to obtain the velocity distribution in the wing-nacelle juncture shown in figure 40.

The experimental velocity distributions in the juncture corrected to zero Mach number, using Von Karman's relation of reference 8, are shown in figure 41 along with the calculated distribution.

Some variation of the velocity distribution with Reynolds number is shown. This is attributed to boundary-layer cross flow, a phenomenon which was observed during the tests of reference 2 and is discussed therein. The calculated curve of velocity distribution lies somewhat above even the experimental values for the highest test Reynolds number. The agreement, though, is reasonably good.

Figure 42 shows a comparison of the juncture velocity distributions for nacelles  $N_1T_1$ ,  $N_4T_2$ , and  $N_5T_3$ . These are seen to be very nearly the same. Examination of figure 43 showing the velocity distributions over the top and bottom meridians of the same nacelles shows, as previously mentioned, that nacelle  $N_1T_1$  has its minimum pressure at 60 percent wing chord. Nacelles  $N_4T_2$  and  $N_5T_3$  are very similar to the NACA 133-30 nacelle of reference 2.

The pressure distributions at a flow coefficient of 0.055 throughout the angle-of-attack range are given for nacelle  $N_2T_2$  juncture and top and bottom meridians in tables VIII and IX and for nacelle  $N_5T_3$  in tables X and XI.

Critical speed,— The variation of critical Mach number as predicted from subcritical pressure measurements is shown

~~CONFIDENTIAL~~

UNCLASSIFIED

UNCLASSIFIED

in figures 44, 45, and 46 for nacelles  $N_2T_2$ ,  $N_4T_2$ , and  $N_5T_3$ , respectively. Through the middle range, as expected from the considerations of the foregoing section,  $M_{cr}$  increases slowly with flow coefficient. The marked decrease in the critical speed at very high and very low flow coefficients results from the formation of a sharp pressure peak on the interior or on the exterior of the nose for these conditions. This effect is more properly associated with the inlet-velocity ratio which, for these tests, bears a direct relationship with the flow coefficient as indicated on the figures. As previously explained, very high inlet-velocity ratios cause the formation of a sharp pressure peak on the interior surface of the nose which determines the critical Mach number. The formation of a local shock in the internal duct with a consequent loss of total head of great magnitude may be especially serious because of its effect on the flow of cooling air to the engine. The design of the nose inlet should be such as to avoid this critical condition. The formation of an external pressure peak at low inlet-velocity ratios is not so serious, though it may be influential in limiting the diving speed. However, for some of the noses ( $N_5$ , for instance) the exterior pressure peak did not appear at certain low angles of attack or, if present, was not of sufficient magnitude to fix the critical Mach number.

At a moderate flow coefficient of 0.055, the critical Mach number for nacelle  $N_5T_3$  is 0.61. This represents an appreciable increase over the value of 0.57 found for the nacelles of reference 2. This increase in critical Mach number, of course, results from the fact that when air flow is permitted through the nacelle, the flow behaves as though the fineness ratio of the nacelle were effectively increased so that the external velocities are decreased.

While a critical Mach number of 0.61 is satisfactory for most airplanes employing propeller propulsion, it cannot be considered allowable in the usual case for those employing jet propulsion. For the latter cases some alteration of these nacelles is necessary to improve the critical speed. In the initial investigation of the wing-nacelle combinations of reference 2, it was found that the velocity gradients over the nacelle top meridians were so favorable that the transition points were located behind the corresponding points on the wing. Moreover, the laminar-boundary layer at the wing-nacelle juncture exhibited uniquely stable characteristics

~~CONFIDENTIAL~~

UNCLASSIFIED

UNCLASSIFIED

in that it was difficult to promote transition to turbulent flow ahead of the minimum pressure location. An experimental investigation of the position of the transition line on the wing-nacelle combination employing the  $N_1T_1$  nacelle was made, and it was found that the velocity gradient over the nacelle was again more favorable than necessary. Consequently, a less favorable velocity gradient for the nacelle would still allow low drags to be maintained and, at the same time, permit a considerable increase in the critical Mach number to be effected. For example, using a body of revolution with the same fineness ratio but with a slightly blunter nose shape than for an ellipse, while still providing what is considered to be a satisfactory favorable gradient, would allow a critical Mach number of about 0.64 for a wing-nacelle combination incorporating the NACA 35-215 wing section. This critical Mach number is nearly as high as that for the wing alone ( $M_{cr} = 0.67$  for the wing), so that any further improvement in critical speed could most profitably be made by reducing the wing thickness. As a further point, the nacelles of this report would permit the installation of large diameter jet units. Using smaller diameter jet units would permit the nacelle thickness ratio to be materially reduced so that further increases in critical Mach number would automatically be effected. Finally, it was found in the tests of reference 3 that, by lowering the nacelle with respect to the wing, a marked increase in critical speed could be obtained. It is considered that a similar alteration for the wing-nacelle combinations of this report would likewise be beneficial.

#### CONCLUSIONS

The results of tests of the wing-nacelle combinations of this report demonstrate that, by following the design principles of reference 2, premature transition to turbulent flow in the wing-nacelle juncture can be avoided for a nacelle with air induction at the nose as well as for a streamline body without internal-air flow. The nacelle-drag coefficient, based on the projected frontal area, for a combination incorporating these principles is reduced to one-half to two-thirds that for the usual nacelle not incorporating these principles.

It is considered that these low-drag coefficients may be realized only with jet-propulsion units and pusher-propeller installations. The use of a tractor propeller would probably preclude the attainment of low drag since the turbulence level

~~CONFIDENTIAL~~

UNCLASSIFIED

UNCLASSIFIED

NACA ACR No. 5A15

~~CONFIDENTIAL~~

19

in a propeller slipstream is high, so that in the propeller wake transition would probably move forward of the location of minimum pressure.

The addition of the nacelle to the wing resulted in only minor effects on the lift and moment characteristics of the wing. The rate of variation of the quarter-chord-moment coefficient with lift coefficient was increased and the maximum lift was slightly decreased.

The critical Mach number, as determined from subcritical pressure measurements in the juncture, was increased over that for the low-drag wing-nacelle combinations of reference 2. The effect of air induction was found to have some influence on the velocity distribution over the nacelle, increasing the critical speed with increasing flow coefficient, until, when the flow coefficient was excessive, the critical speed was determined by the low pressure occasioned at the inner lip of the duct opening.

The use of superposition in predicting the velocity distribution in the wing-nacelle juncture was found to give too high velocities. This is believed due to the difficulty in accounting for the effect of air induction on the velocities over the nacelle, as well as to the effective thinning of the wing profile at the juncture due to boundary-layer cross flow.

Ames Aeronautical Laboratory,  
National Advisory Committee for Aeronautics,  
Moffett Field, Calif.

~~CONFIDENTIAL~~

UNCLASSIFIED

UNCLASSIFIED

APPENDIX A

METHOD FOR DERIVING NACELLE NOSE SHAPES

The following more general method for deriving nose shapes for nacelles is based on the more restricted method evolved in reference 2. The procedure is as follows: Using the known quantity of air required for cooling, the mass flow coefficient is calculated. This coefficient is given by

$$\frac{\rho Q}{\rho_0 F V_0} \cdot$$

where

$\rho Q$  mass flow rate

$\rho_0$  air mass density in the free stream

$F$  maximum cross-sectional area of the nacelle

$V_0$  free-stream velocity

The ratio of the nose air-inlet diameter to the maximum diameter of the nacelle is then found from

$$\frac{d}{D_{\max}} = \sqrt{\frac{\frac{\rho Q}{\rho_0 F V_0}}{\frac{V_i \rho_i}{V_0 \rho_0}}}$$

where  $V_i/V_0$  is the ratio of the nose air-inlet velocity to the free-stream velocity, and  $\rho_i/\rho_0$  is the ratio of the density of the air at the nose air inlet to that of the free stream.

The value of  $\frac{V_i}{V_0} \frac{\rho_i}{\rho_0}$  will depend on the range of altitudes and speeds to be encountered in flight. When the wing operates at its ideal lift coefficient, the desired value of  $\frac{V_i}{V_0} \frac{\rho_i}{\rho_0}$  will usually lie between 0.4 and 0.6. In the design

~~CONFIDENTIAL~~

UNCLASSIFIED

UNCLASSIFIED

of the nacelles of this report, a value of 0.5 was chosen.

Using the method of reference 1 for reshaping the nacelle nose, the nacelle is shortened by an amount  $l$  as shown in figure 47. In order to retain the same nose location relative to the station corresponding to the minimum pressure position (which is very nearly coincident with that corresponding to the maximum diameter station), it is necessary therefore to lengthen the basic nacelle shape by the amount  $l$  before the method is applied.

To this end, from the basic nacelle shape (fig. 2) the value of  $x_0 = x_0'$  corresponding to  $y_0 = y_0' = 1.34 r$  is found, where  $x_0$  and  $y_0$  are the axial and radial coordinates of the basic nacelle and  $r$  is the radius of the nose opening (i.e.,  $d/2$ ).

The length  $l$  is then given by

$$l = \left( \frac{x_0'}{m_0 L_0 - x_0'} \right) m_0 L_0$$

where  $m_0 L_0$  is the axial distance from the nose to the station at the maximum diameter for the basic nacelle as shown in figure 48.

The ordinates for the extended nacelle forward of the maximum diameter station are calculated using the relations

$$y_e = y_0$$
$$x_e = \left( 1 + \frac{l}{m_0 L_0} \right) x_0 - l$$

The distance along the axis of the ducted body from the nose opening to the point where the nose ordinates fair into ordinates of the extended nacelle, shown in figure 47, is designated  $X$  and is given by

$$X = 1.172 \left( \frac{d}{D_{\max}} \right) m_0 L_0$$

The ordinates of the nacelle between  $x = 0$  and  $x = X$  are

~~CONFIDENTIAL~~

UNCLASSIFIED

UNCLASSIFIED

~~CONFIDENTIAL~~

$$y = y_e - Y (y_e - r)$$

where  $Y$  is the nose-shape parameter which is a function of  $x/X$ .

The nose-shape parameter  $Y$  for the nacelle  $N_1$  was obtained from the corresponding values given in reference 1. The nose-shape parameters for all the nose shapes discussed in this report are given in table IV. It should be noted that all the noses were developed for the same value of  $X$  and from the same extended version of the NACA 133-30 nacelle.

## APPENDIX B

The velocity distribution over a nacelle, designed to incorporate internal air flow by the method of appendix A, may be calculated as indicated in the following (all symbols are defined in appendix A):

The basic nacelle of length  $L_0$  is increased to

$$L_e = L_0 + l$$

where  $l$  is the nose extension determined by the method of appendix A.

Moreover, the internal air flow effectively reduces the cross-sectional area of the nacelle to

$$F_e = F - \rho Q / \rho_0 V$$

so that the effective diameter becomes

$$D_e = D_0 \sqrt{1 - \rho Q / \rho_0 F V_0}$$

The effective diameter-length ratio is then

$$\frac{D_e}{L_e} = \frac{D_0}{L_0} \left[ \frac{\sqrt{1 - \rho Q / \rho_0 F V_0}}{1 + \frac{l}{L_0}} \right]$$

The increment by which the velocity at any point on a streamline body exceeds that of the free stream is roughly

~~CONFIDENTIAL~~

UNCLASSIFIED

proportional to the diameter-length ratio of the body. Hence, for the nacelle incorporating the nose air inlet, the velocity at any point behind the maximum ordinate station

$$\frac{U}{V_0} = 1 + \left[ \left( \frac{U}{V_0} \right)_0 - 1 \right] \frac{\sqrt{1 - \rho Q / \rho_0 V_0}}{1 + \frac{l}{L_0}}$$

where

$\frac{U}{V_0}$  velocity at  $x_e = x_0$  on the nacelle with the nose air inlet

$\left( \frac{U}{V_0} \right)_0$  velocity at  $x_0$  on the basic nacelle

At stations forward of the maximum ordinate station the velocity given by the same equation applies at a point

$$x_e = \left( 1 + \frac{l}{m_0 L_0} \right) x_0 - l$$

rather than  $x_e = x_0$ .

These calculated values will apply except at stations close to the nose opening where the velocity curve must be faired to  $U/V_0 = 0$  at the nose opening.

#### REFERENCES

1. Becker, John V.: Wind-Tunnel Tests of Air Inlet and Outlet Openings on a Streamline Body. NACA ACR, Nov. 1940.
2. Allen, H. Julian, and Frick, Charles W., Jr.: Experimental Investigation of a New Type of Low-Drag Wing-Nacelle Combination. NACA ACR, July 1942.
3. Becker, John V.: High-Speed Tests of Radial-Engine Nacelles on a Thick Low-Drag Wing. NACA ACR, May 1942.



UNCLASSIFIED

NACA ACR No. 5A15

~~CONFIDENTIAL~~

24

4. Paterson, G. N.: Modern Diffuser Design. Aircraft Engineering, vol. 10, no. 115, Sept. 1938, pp. 267-273.
5. Thompson, J. S., Smelt, R., Davison, B., and Smith, F.: Comparison of Pusher and Tractor Airscrews Mounted on a Wing. British R.A.E. Rep. No. B.A. 1614, June 1940.
6. Becker, John V., and Baals, Donald D.: Wind-Tunnel Tests of a Submerged-Engine Fuselage Design. NACA ACR, Oct. 1940.
7. Robinson, Russell G., and Wright, Ray H.: Estimation of Critical Speeds of Airfoils and Streamline Bodies. NACA ACR, March 1940.
8. von Kármán, Th.: Compressibility Effects in Aerodynamics. Jour. Aero. Sci., vol. 8, no. 9, July 1941, pp. 337-356.

~~CONFIDENTIAL~~

UNCLASSIFIED

UNCLASSIFIED  
~~CONFIDENTIAL~~

TABLE I.- ORDINATES OF NACA 35-215 WING  $a = 0.50$ 

Upper surface				Lower surface			
x Distance along chord		y Ordinate		x Distance along chord		y Ordinate	
Percent chord	Inches	Percent chord	Inches	Percent chord	Inches	Percent chord	Inches
0	0	0	0	0	0	0	0
.376	.18	1.137	.55	.624	.30	-.999	-.48
.609	.29	1.403	.67	.891	.43	-1.209	-.58
1.087	.52	1.828	.88	1.413	.68	-1.534	-.74
2.308	1.11	2.544	1.26	2.693	1.29	-2.026	-1.01
4.784	2.30	3.711	1.78	5.214	2.50	-2.829	-1.36
7.276	3.49	4.534	2.18	7.722	3.71	-3.346	-1.61
9.777	4.69	5.215	2.50	10.223	4.91	-3.763	-1.81
14.788	7.10	6.328	3.04	15.212	7.30	-4.432	-2.13
19.809	9.51	7.200	3.46	20.191	9.69	-4.952	-2.38
24.838	11.92	7.889	3.79	25.162	12.08	-5.361	-2.57
29.873	14.34	8.408	4.04	30.127	14.46	-5.672	-2.72
34.913	16.76	8.770	4.21	35.087	16.84	-5.884	-2.82
39.958	19.18	8.967	4.30	40.042	19.22	-5.995	-2.88
45.009	21.60	8.977	4.31	44.991	21.60	-5.981	-2.87
50.077	24.04	8.732	4.19	49.923	23.96	-5.792	-2.78
55.130	26.46	8.109	3.89	54.869	26.34	-5.323	-2.56
60.150	28.87	7.262	3.49	59.850	28.73	-4.700	-2.26
65.150	31.27	6.283	3.02	64.850	31.13	-3.993	-1.92
70.137	33.67	5.228	2.51	69.863	33.54	-3.246	-1.56
75.113	36.05	4.140	1.99	74.888	35.95	-2.488	-1.19
80.086	38.44	3.062	1.47	79.914	38.36	-1.756	-.84
85.056	40.83	2.042	.98	84.944	40.77	-1.084	-.52
90.029	43.21	1.134	.54	89.971	43.19	-.520	-.25
95.009	45.60	.424	.20	94.991	45.60	-.136	-.07
100.00	48.00	0	0	100.00	48.00	0	0

~~CONFIDENTIAL~~  
UNCLASSIFIED

UNCLASSIFIED  
CONFIDENTIAL

TABLE II.- ORDINATES OF NACA 133-30 NACELLE

x Distance along center line		r Radius	
Percent length	Inches	Percent length	Inches
0	0	0	0
1.250	.90	3.318	2.39
2.500	1.80	4.680	3.37
5.000	3.60	6.598	4.75
7.500	5.40	8.043	5.79
10.000	7.20	9.238	6.65
15.000	10.80	11.164	8.04
20.00	14.40	12.656	9.11
25.00	18.00	13.789	9.93
30.00	21.60	14.573	10.49
35.00	25.20	15.002	10.80
40.00	28.80	15.098	10.87
45.00	32.40	14.919	10.74
50.00	36.00	14.532	10.46
55.00	39.60	13.991	10.07
60.00	43.20	13.329	9.60
65.00	46.80	12.563	9.05
70.00	50.40	11.697	8.42
75.00	54.00	10.725	7.72
80.00	57.60	9.626	6.93
85.00	61.20	8.360	6.02
90.00	64.80	6.841	4.93
95.00	68.40	4.846	3.49
100.00	72.00	0	0

CONFIDENTIAL

UNCLASSIFIED

TABLE III.- NOSE COORDINATES, IN INCHES TO  $D_{max}$

N <sub>1</sub>			N <sub>2</sub>			N <sub>3</sub>			N <sub>4</sub>			N <sub>5</sub>		
Station	Ordinates		Station	Ordinates		Station	Ordinates		Station	Ordinates		Station	Ordinates	
	Outside	Inside		Outside	Inside		Outside	Inside		Outside	Inside		Outside	Inside
0	4.12	4.12	0	4.24	4.24	0	4.30	4.30	-0.285	3.90	3.90	-0.275	3.85	3.85
.08	4.48	4.01	.03	4.38	4.12	.03	4.46	4.17	-.25	4.08	4.08	-.25	4.04	4.04
.16	4.63	4.001	.06	4.45	4.07	.06	4.53	4.12	-.20	4.19	4.19	-.20	4.12	4.12
.25	4.75	4.00	.12	4.56	4.03	.12	4.64	4.07	-.15	4.27	4.27	-.15	4.31	4.31
.33	4.84	4.00	.18	4.65	4.01	.18	4.75	4.04	-.10	4.35	4.35	-.10	4.45	4.45
.50	5.01	4.00	.24	4.73	4.00	.24	4.83	4.02	-.05	4.43	4.43	.10	4.57	4.57
.66	5.15	4.00	.31	4.81	4.00	.31	4.90	4.01	0	4.49	4.49	.20	4.68	4.68
.83	5.28	4.00	.37	4.88	4.00	.37	4.97	4.00	.05	4.55	4.55	.30	4.78	4.78
1.00	5.39	4.00	.43	4.94	4.00	.43	5.07	4.00	.10	4.62	4.62	.40	4.88	4.88
1.33	5.69	4.00	.44	5.00	---	.44	5.19	4.00	.15	4.68	4.68	.50	4.98	4.98
1.66	5.79	4.00	.49	---	---	.62	5.29	4.00	.20	4.73	4.73	.75	5.20	5.20
2.49	6.22	4.00	.62	---	---	.74	5.46	4.00	.30	4.83	4.83	1.00	5.37	5.37
3.32	6.59	---	.74	---	---	.99	5.62	4.00	.40	4.92	4.92	1.25	5.55	5.55
4.00	6.87	---	.99	---	---	1.24	5.95	4.00	.50	5.01	5.01	1.50	5.70	5.70
4.15	6.92	---	1.24	---	---	1.86	6.24	4.00	.60	5.12	5.12	1.75	5.84	5.84
4.98	7.23	---	1.86	---	---	2.48	6.51	4.00	.74	5.24	5.24	2.00	5.98	5.98
6.64	7.77	---	2.48	---	---	3.11	6.76	---	.80	5.41	5.41	2.50	6.23	6.23
8.31	8.25	---	3.11	---	---	3.72	6.87	---	.99	5.59	5.59	3.00	6.46	6.46
9.97	8.69	---	3.72	---	---	4.00	---	---	1.00	5.87	5.87	3.50	6.67	6.67
11.63	9.09	---	4.00	---	---	---	---	---	1.24	6.87	6.87	4.00	6.87	6.87
13.29	9.46	---	---	---	---	---	---	---	1.40	---	---	---	---	---
14.95	9.76	---	---	---	---	---	---	---	1.86	---	---	---	---	---
16.62	10.01	---	---	---	---	---	---	---	2.48	---	---	---	---	---
17.20	10.11	---	---	---	---	---	---	---	3.11	---	---	---	---	---
20.30	10.49	---	---	---	---	---	---	---	3.72	---	---	---	---	---
24.60	10.80	---	---	---	---	---	---	---	4.00	---	---	---	---	---
28.23	10.87	---	---	---	---	---	---	---	---	---	---	---	---	---

Note: Ordinates for stations 4.000 to 28.23 of Noses N<sub>2</sub>, N<sub>3</sub>, N<sub>4</sub>, and N<sub>5</sub> are the same as those of N<sub>1</sub>.

CONFIDENTIAL

TABLE IV.- NOSE-SHAPE PARAMETER, Y

x X	Outside					Inside				
	N <sub>1</sub>	N <sub>2</sub>	N <sub>3</sub>	N <sub>4</sub>	N <sub>5</sub>	N <sub>1</sub>	N <sub>2</sub>	N <sub>3</sub>	N <sub>4</sub>	N <sub>5</sub>
-0.0228	----	----	----	1.083	----	----	----	----	1.083	----
-.022	----	----	----	.980	1.125	----	----	----	1.154	1.125
-.020	----	----	----	.934	.967	----	----	----	1.204	1.205
-.015	----	----	----	.835	.864	----	----	----	1.259	1.260
-.010	----	----	----	.758	.782	----	----	----	1.274	1.271
-.005	----	----	----	.692	.726	----	----	----	1.281	1.272
0	0.860	0.820	0.780	.637	.670	0.860	0.820	0.780	1.282	1.267
.005	.730	.670	.608	.585	.600	.995	.950	.910	1.275	1.254
.010	.614	.600	.526	.538	.576	.997	.980	.950	1.263	1.240
.015	.540	.540	.474	.500	.538	.998	.990	.970	1.250	1.225
.020	.490	.490	.434	.466	.502	1.000	.997	.984	1.238	1.209
.025	.447	.447	.399	.434	.468	----	1.000	.994	1.224	1.194
.030	.411	.411	.364	.406	.438	----	----	1.000	1.210	1.178
.035	.381	.381	.340	.380	.407	----	----	----	1.195	1.162
.040	.355	.355	.316	.355	.378	----	----	----	1.180	1.146
.045	.331	.331	.293	.329	.352	----	----	----	1.167	1.133
.050	.310	.310	.272	.307	.329	----	----	----	1.150	1.120
.055	.294	.294	.254	.284	.308	----	----	----	1.135	1.107
.060	.274	.274	.239	.262	.288	----	----	----	1.121	1.095
.065	.259	.259	.224	.246	.272	----	----	----	1.109	1.085
.070	.244	.244	.210	.230	.258	----	----	----	1.097	1.075
.075	.230	.230	.197	.216	.244	----	----	----	1.084	1.066
.080	.217	.217	.184	.204	.230	----	----	----	1.072	1.056
.085	.206	.206	.174	.192	.218	----	----	----	1.061	1.049
.090	.195	.195	.165	.182	.207	----	----	----	1.050	1.041
.100	.174	.174	.149	.163	.186	----	----	----	1.031	1.027
.110	.156	.156	.136	.147	.168	----	----	----	1.017	1.017
.120	.140	.140	.124	.134	.153	----	----	----	1.006	1.009
.130	.127	.127	.114	.122	.139	----	----	----	1.000	1.005
.140	.115	.115	.104	.111	.126	----	----	----	----	1.002
.150	.104	.104	.096	.101	.115	----	----	----	----	1.001
.160	.095	.095	.089	.094	.105	----	----	----	----	1.000
.170	.087	.087	.083	.087	.096	----	----	----	----	----
.180	.080	.080	.077	.080	.089	----	----	----	----	----
.190	.074	.074	.071	.075	.082	----	----	----	----	----
.200	.067	.067	.066	.070	.077	----	----	----	----	----
.210	.062	.062	.062	.064	.071	----	----	----	----	----
.220	.058	.058	.058	.061	.067	----	----	----	----	----
.230	.054	.054	.054	.057	.063	----	----	----	----	----
.240	.050	.050	.050	.054	.059	----	----	----	----	----
.250	.047	.047	.047	.050	.055	----	----	----	----	----
.275	.041	.041	.041	.044	.045	----	----	----	----	----
.300	.037	.037	.037	.038	.039	----	----	----	----	----
.350	.032	.032	.032	.032	.032	----	----	----	----	----
.400	.027	.027	.027	.027	.027	----	----	----	----	----
.450	.024	.024	.024	.024	.024	----	----	----	----	----
.500	.021	.021	.021	.021	.021	----	----	----	----	----
.550	.018	.018	.018	.018	.018	----	----	----	----	----
.600	.015	.015	.015	.015	.015	----	----	----	----	----
.650	.013	.013	.013	.013	.013	----	----	----	----	----
.700	.012	.012	.012	.012	.012	----	----	----	----	----
.750	.010	.010	.010	.010	.010	----	----	----	----	----
.800	.008	.008	.008	.008	.008	----	----	----	----	----
.850	.006	.006	.006	.006	.006	----	----	----	----	----
.900	.004	.004	.004	.004	.004	----	----	----	----	----
1.000	0	0	0	0	0	----	----	----	----	----

CONFIDENTIAL

UNCLASSIFIED





UNCLASSIFIED

~~CONFIDENTIAL~~

TABLE VII.- ORDINATES OF INTERNAL DIFFUSER INCLUDING FAN SPINNER

Inner shell				Inner Cowl			
Station (in.)	Ordinate (in.)	Station (in.)	Ordinate (in.)	Station (in.)	Ordinate (in.)	Station (in.)	Ordinate (in.)
2.00	4.00	24.50	7.01	-1.25	0	19.50	4.42
2.50	4.00	25.50	7.19	-1.11	.71	20.50	4.59
5.00	4.00	26.50	7.46	-.86	1.16	21.50	4.77
5.50	4.00	27.50	7.82	-.61	1.67	22.50	4.95
6.50	4.09	28.50	8.32	0	1.91	23.50	5.12
7.50	4.19	29.50	8.98	.14	1.97	24.50	5.29
8.50	4.30	29.63	9.09	.64	2.17	25.50	5.47
9.50	4.44	30.00	9.12	1.64	2.31	26.50	5.52
10.50	4.58	31.00	9.12	2.00	2.31	27.50	5.34
11.50	4.74	32.00	9.12	3.00	2.31	28.50	5.03
12.50	4.91	32.50	9.12	4.00	2.31	29.50	4.72
13.50	5.07	-----	-----	5.00	2.31	30.50	4.52
14.50	5.24	-----	-----	5.50	2.31	31.50	4.37
15.50	5.42	-----	-----	6.50	2.37	32.50	4.27
16.50	5.59	-----	-----	7.50	2.45	(Baffle Plate)	
17.50	5.77	-----	-----	8.50	2.54	-----	-----
18.50	5.94	-----	-----	9.50	2.67	-----	-----
19.50	6.12	-----	-----	10.50	2.81	-----	-----
20.50	6.30	-----	-----	11.50	2.98	-----	-----
21.50	6.48	-----	-----	12.50	3.16	-----	-----
22.50	6.66	-----	-----	13.50	3.34	-----	-----
23.50	6.83	-----	-----	14.50	3.52	-----	-----
-----	-----	-----	-----	15.50	3.69	-----	-----
-----	-----	-----	-----	16.50	3.87	-----	-----
-----	-----	-----	-----	17.50	4.05	-----	-----
-----	-----	-----	-----	18.50	4.23	-----	-----

~~CONFIDENTIAL~~

UNCLASSIFIED



UNCLASSIFIED

CONFIDENTIAL

TABLE VIII.- EXPERIMENTAL VALUES OF  $(U/V)^2$  FOR  $N_2T_2$  WING-NACELLE JUNCTURE<sup>1</sup>  
 REYNOLDS NUMBER =  $3.59 \times 10^6$  MACH NUMBER = 0.13

CL	-0.252	-0.012	0.107	0.224	0.343	0.686	1.120	1.370	1.415
% Chord	-3	-1	0	1	2	5	9	13	15
Upper surface									
0	0.273	0.024	0.016	0	0.048	0.618	2.152	4.018	4.747
.50	.016	.186	.353	.538	.755	1.695	3.451	5.307	5.967
1.00	.129	.364	.554	.755	.964	1.847	3.469	4.825	5.173
1.50	.233	.502	.691	.884	1.093	1.927	3.310	4.589	4.995
2.50	.402	.704	.900	1.092	1.301	2.088	3.301	4.474	4.810
5.00	.691	.980	1.157	1.333	1.510	2.160	3.079	3.919	4.128
10.00	.940	1.166	1.317	1.446	1.566	2.016	2.687	3.241	3.283
15.00	1.093	1.288	1.414	1.518	1.615	1.984	2.505	2.891	2.868
20.00	1.206	1.385	1.478	1.575	1.663	1.967	2.400	2.670	2.587
25.00	1.318	1.466	1.575	1.647	1.711	1.984	2.360	2.482	2.369
30.00	1.431	1.563	1.671	1.735	1.791	2.048	2.352	2.368	2.160
35.00	1.495	1.611	1.719	1.767	1.815	2.048	2.304	2.163	1.975
40.00	1.575	1.684	1.784	1.831	1.880	2.080	2.280	1.960	1.823
45.00	1.640	1.749	1.831	1.880	1.912	2.089	2.233	1.805	1.727
50.00	1.704	1.790	1.872	1.912	1.936	2.071	2.121	1.699	1.655
55.00	1.624	1.700	1.767	1.800	1.815	1.910	1.842	1.633	1.630
60.00	1.543	1.603	1.655	1.679	1.695	1.743	1.723	1.625	1.639
65.00	1.455	1.498	1.542	1.558	1.566	1.558	1.675	1.633	1.663
70.00	1.350	1.393	1.414	1.430	1.438	1.494	1.635	1.649	1.622
80.00	1.165	1.182	1.205	1.205	1.229	1.341	1.316	1.535	1.575
Lower surface									
0.50	1.125	0.599	0.386	0.225	0.088	0.016	0.491	1.127	1.462
1.00	1.431	.882	.634	.450	.265	.008	.080	.490	.683
1.50	1.559	1.037	.803	.594	.402	.056	.016	.220	.353
2.50	1.712	1.231	.996	.803	.602	.201	.032	.160	.056
5.00	1.744	1.368	1.173	1.004	.836	.412	.112	.008	.016
10.00	1.672	1.393	1.261	1.125	.988	.683	.335	.171	.145
15.00	1.648	1.425	1.317	1.205	1.093	.819	.502	.335	.305
20.00	1.672	1.482	1.382	1.285	1.180	.932	.630	.474	.442
25.00	1.672	1.506	1.446	1.333	1.273	1.020	.750	.572	.570
30.00	1.672	1.530	1.478	1.382	1.294	1.076	.837	.662	.675
35.00	1.720	1.579	1.526	1.446	1.350	1.165	.925	.768	.779
40.00	1.720	1.587	1.558	1.478	1.398	1.229	1.005	.849	.876
45.00	1.752	1.652	1.607	1.527	1.462	1.301	1.092	.947	.972
50.00	1.752	1.660	1.623	1.558	1.486	1.341	1.148	1.028	1.068
55.00	---	---	---	---	---	---	---	---	---
60.00	1.543	1.490	1.478	1.414	1.365	1.260	1.116	1.028	1.092
65.00	1.463	1.401	1.398	1.333	1.310	1.221	1.084	1.037	1.052
70.00	1.350	1.304	1.285	1.245	1.221	1.149	1.037	1.012	1.036
80.00	1.190	1.142	1.125	1.092	1.085	1.036	.957	.972	.996

<sup>1</sup> These data are uncorrected for tunnel-wall effect.

CONFIDENTIAL

UNCLASSIFIED

~~CONFIDENTIAL~~

TABLE IX.- EXPERIMENTAL VALUES OF  $(U/V)^2$  FOR NACA NACAELLE TOP AND BOTTOM MERIDIAN<sup>1</sup>  
 REYNOLDS NUMBER =  $3.59 \times 10^6$  MACH NUMBER = 0.13

$\frac{C_L}{\alpha}$	-0.252		-0.012		+0.107		0.224		0.343		0.686		1.120		1.370		1.415	
	-3		-1		0		1		2		5		9		13		15	
Upper Surface																		
0	0.056	0.032	0.209	0.405	0.779	2.129	3.771	5.486	5.894									
.50	.281	.591	.771	1.020	1.255	2.209	3.492	4.417	4.673									
1.00	.426	.713	.916	1.108	1.340	2.138	3.220	4.015	4.257									
2.50	.691	.956	1.117	1.269	1.462	2.071	2.885	3.494	3.679									
5.00	.812	1.053	1.148	1.285	1.446	1.871	2.471	3.003	3.115									
10.00	.932	1.109	1.213	1.309	1.414	1.742	2.216	2.565	2.601									
20.00	1.101	1.247	1.435	1.414	1.486	1.750	2.064	2.270	2.249									
30.00	1.230	1.360	1.430	1.510	1.566	1.767	2.018	2.131	2.080									
40.00	1.310	1.425	1.486	1.542	1.599	1.775	1.970	2.000	1.911									
50.00	1.358	1.458	1.502	1.550	1.599	1.719	1.866	1.861	1.750									
60.00	1.358	1.433	1.470	1.518	1.550	1.639	1.730	1.706	1.605									
70.00	1.294	1.344	1.374	1.382	1.406	1.502	1.563	1.543	1.558									
90.00	1.197	1.215	1.229	1.245	1.253	1.285	1.284	1.380	1.519									
110.00	---	---	---	---	---	---	---	---	---									
Lower Surface																		
0.00	1.246	0.518	0.225	0.056	0.048	0.072	0.423	0.824	1.004									
.50	1.584	1.068	.819	.618	.434	.064	.064	.016	.032									
1.00	1.600	1.166	.924	.755	.586	.201	.024	.057	.048									
2.50	1.648	1.295	1.117	.948	.804	.442	.136	.016	.024									
5.00	1.559	1.303	1.148	1.020	.900	.594	.287	.131	.080									
10.00	1.519	1.312	1.197	1.092	1.012	.755	.471	.294	.249									
20.00	1.519	1.360	1.277	1.205	1.125	.916	.670	.505	.458									
30.00	1.568	1.433	1.358	1.302	1.229	1.052	.821	.686	.642									
40.00	1.568	1.449	1.398	1.333	1.285	1.132	.925	.808	.771									
50.00	1.600	1.441	1.398	1.350	1.301	1.173	.996	.898	.884									
60.00	1.479	1.409	1.374	1.333	1.294	1.197	1.044	.972	.964									
70.00	1.350	1.295	1.277	1.269	1.229	1.157	1.028	.988	.996									
90.00	1.140	1.072	---	---	---	---	1.023	1.028	1.046									
110.00	1.021	1.028	1.036	1.044	1.028	1.036	1.021	1.110	1.180									

<sup>1</sup>These data are uncorrected for tunnel-wall effect.

~~CONFIDENTIAL~~

UNCLASSIFIED  
~~CONFIDENTIAL~~

TABLE X.- EXPERIMENTAL VALUES OF  $(U/V)^2$  FOR  $N_5T_3$  WING-NACELLE JUNCTURE <sup>1</sup>  
REYNOLDS NUMBER =  $3.59 \times 10^6$  MACH NUMBER = 0.13

$C_L$	-0.231	-0.007	0.110	0.228	0.347	0.685	1.101	1.350	1.417
$\alpha$	-3	-1	0	1	2	5	9	13	15
Upper surface									
0	0.263	0.040	0.024	0.048	0.120	0.675	2.222	3.951	4.560
.50	.056	.215	.377	.562	.781	1.664	3.309	4.900	5.329
1.00	.159	.399	.578	.779	1.004	1.821	3.340	4.473	4.763
1.50	.255	.518	.699	.892	1.108	1.884	3.140	4.224	4.467
2.50	.422	.710	.900	1.100	1.299	2.025	3.130	4.104	4.293
5.00	.661	.941	1.060	1.229	1.387	-----	-----	-----	-----
10.00	.924	1.156	1.293	1.430	1.538	1.978	2.608	3.029	2.990
15.00	1.060	1.260	1.382	1.495	1.578	1.907	2.415	2.682	2.559
20.00	1.179	1.348	1.462	1.550	1.625	1.899	2.319	2.490	2.243
25.00	1.267	1.427	1.526	1.615	1.674	1.915	2.280	2.312	1.985
30.00	1.379	1.539	1.615	1.695	1.754	1.962	2.280	2.138	1.836
35.00	1.435	1.570	1.646	1.720	1.770	1.962	2.222	1.911	1.680
40.00	1.498	1.635	1.703	1.767	1.809	1.970	2.191	1.766	1.593
45.00	1.578	1.699	1.760	1.824	1.856	1.993	2.151	1.639	1.539
50.00	1.641	1.746	1.808	1.855	1.889	1.986	2.058	1.550	1.515
55.00	1.578	1.666	1.720	1.760	1.785	1.844	1.801	1.519	1.515
60.00	1.506	1.586	1.623	1.663	1.674	1.687	1.681	1.535	1.530
65.00	1.426	1.475	1.519	1.543	1.554	1.523	1.619	1.559	1.555
70.00	1.339	1.388	1.414	1.430	1.442	1.460	1.554	1.575	1.570
80.00	1.171	1.204	1.221	1.237	1.243	1.311	1.363	1.519	1.555
84.00	1.115	1.148	1.165	1.180	1.180	1.240	1.283	1.486	1.539
Lower surface									
0.50	1.115	0.590	0.410	0.249	0.120	0.031	0.422	1.109	1.358
1.00	1.379	.845	.634	.458	.287	.047	.120	.506	.636
1.50	1.490	.981	.771	.586	.406	.094	.032	.257	.322
2.50	-----	-----	-----	-----	-----	-----	-----	-----	-----
5.00	-----	1.322	1.142	.980	.974	.455	.136	.048	0
10.00	1.616	1.340	1.221	1.117	.988	.675	.359	.225	.134
15.00	1.601	1.380	1.293	1.197	1.091	.816	.518	.386	.290
20.00	1.601	1.435	1.350	1.277	1.171	.926	.646	.514	.416
25.00	1.609	1.460	1.398	1.325	1.227	1.004	.757	.602	.542
30.00	1.616	1.484	1.422	1.358	1.267	1.060	.844	.699	.644
35.00	1.641	1.530	1.479	1.422	1.330	1.146	.982	.804	.746
40.00	1.665	1.579	1.526	1.462	1.386	1.217	1.012	.892	.840
45.00	1.690	1.604	1.559	1.510	1.442	1.272	1.091	.988	.942
50.00	1.681	1.620	1.575	1.535	1.466	1.311	1.155	1.060	1.028
55.00	-----	-----	-----	-----	-----	-----	-----	-----	-----
60.00	1.514	1.451	1.430	1.398	1.347	1.240	1.124	1.076	1.060
65.00	1.426	1.395	1.365	1.334	1.291	1.193	1.100	1.085	1.083
70.00	1.339	1.300	1.285	1.261	1.227	1.146	1.060	1.069	1.067
80.00	1.187	1.164	1.149	1.133	1.108	1.052	1.004	1.052	1.067
84.00	1.131	1.100	1.085	1.068	1.052	1.004	.964	1.020	1.044

<sup>1</sup> These data are uncorrected for tunnel-wall effect.

~~CONFIDENTIAL~~  
UNCLASSIFIED

UNCLASSIFIED

~~CONFIDENTIAL~~

TABLE XI.- EXPERIMENTAL VALUES OF  $(U/V)^2$  FOR  $N_{S,T_3}$  NACELLE TOP AND BOTTOM MERIDIAN<sup>1</sup>  
 REYNOLDS NUMBER =  $3.59 \times 10^6$  MACH NUMBER = 0.13

CL % Chord	$\alpha$	-0.231	-0.007	0.110	0.228	0.347	0.685	1.101	1.350	1.417
		-3	-1	0	1	2	5	9	13	15
Upper surface										
-0.60		0.048	0.048	0.040	0.040	0.088	1.146	3.038	4.780	5.353
0		.279	.534	.691	.884	1.075	1.789	2.790	3.799	4.043
1.00		.510	.782	.932	1.108	1.275	1.868	2.665	3.470	3.689
5.00		.828	1.036	1.156	1.285	1.403	1.805	2.354	2.780	2.872
10.00		.924	1.124	1.213	1.310	1.395	1.727	2.120	2.432	2.472
20.00		1.091	1.244	1.325	1.398	1.474	1.695	2.009	2.169	2.251
30.00		1.219	1.348	1.422	1.478	1.546	1.727	1.975	2.056	2.096
40.00		1.290	1.404	1.460	1.519	1.562	1.711	1.905	1.920	1.930
50.00		1.339	1.435	1.486	1.526	1.570	1.680	1.816	1.783	1.765
60.00		1.339	1.427	1.470	1.495	1.530	1.601	1.714	1.646	1.664
70.00		1.235	1.275	1.293	1.301	1.307	1.303	1.291	1.397	1.585
90.00		.964	.957	.964	.964	.956	.926	.964	1.205	1.366
110.00										
Lower surface										
0		1.084	0.495	0.281	0.121	0.016	0.047	0.590	1.446	1.790
.50		1.498	1.037	.852	.651	.478	.157	0	.080	.157
1.00		1.498	1.085	.916	.739	.574	.251	.016	.008	.031
2.50		1.609	1.275	1.133	.972	.821	.487	.175	.048	.024
5.00		1.530	1.285	1.165	1.036	.908	.628	.327	.177	.126
10.00		1.450	1.276	1.173	1.076	1.004	.754	.502	.321	.361
20.00		1.474	1.331	1.261	1.189	1.123	.918	.685	.530	.573
30.00		1.514	1.404	1.350	1.285	1.227	.936	.844	.699	.738
40.00		1.514	1.419	1.381	1.325	1.275	1.114	.940	.820	.872
50.00		1.482	1.427	1.382	1.341	1.299	1.162	1.020	.924	.981
60.00		1.435	1.398	1.365	1.325	1.291	1.178	1.060	.996	1.060
70.00		1.323	1.275	1.269	1.261	1.227	1.146	1.060	1.012	1.083
90.00		1.203	1.196	1.189	1.173	1.155	1.114	1.100	1.116	1.225
110.00		.876	.893	.900	.900	.900	.910	.924	1.028	1.162

<sup>1</sup> These data are uncorrected for tunnel-wall effect.

UNCLASSIFIED



Figure 1.- Comparison of nose shapes.

NATIONAL ADVISORY COMMITTEE  
FOR AERONAUTICS

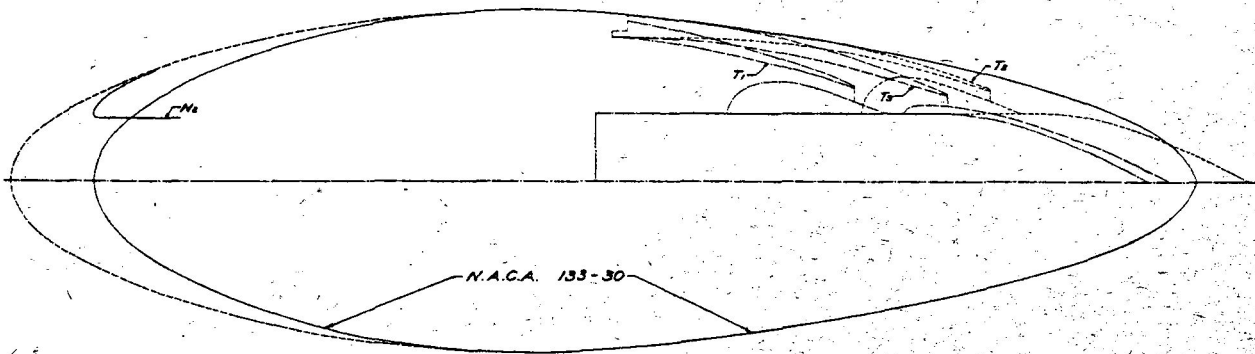
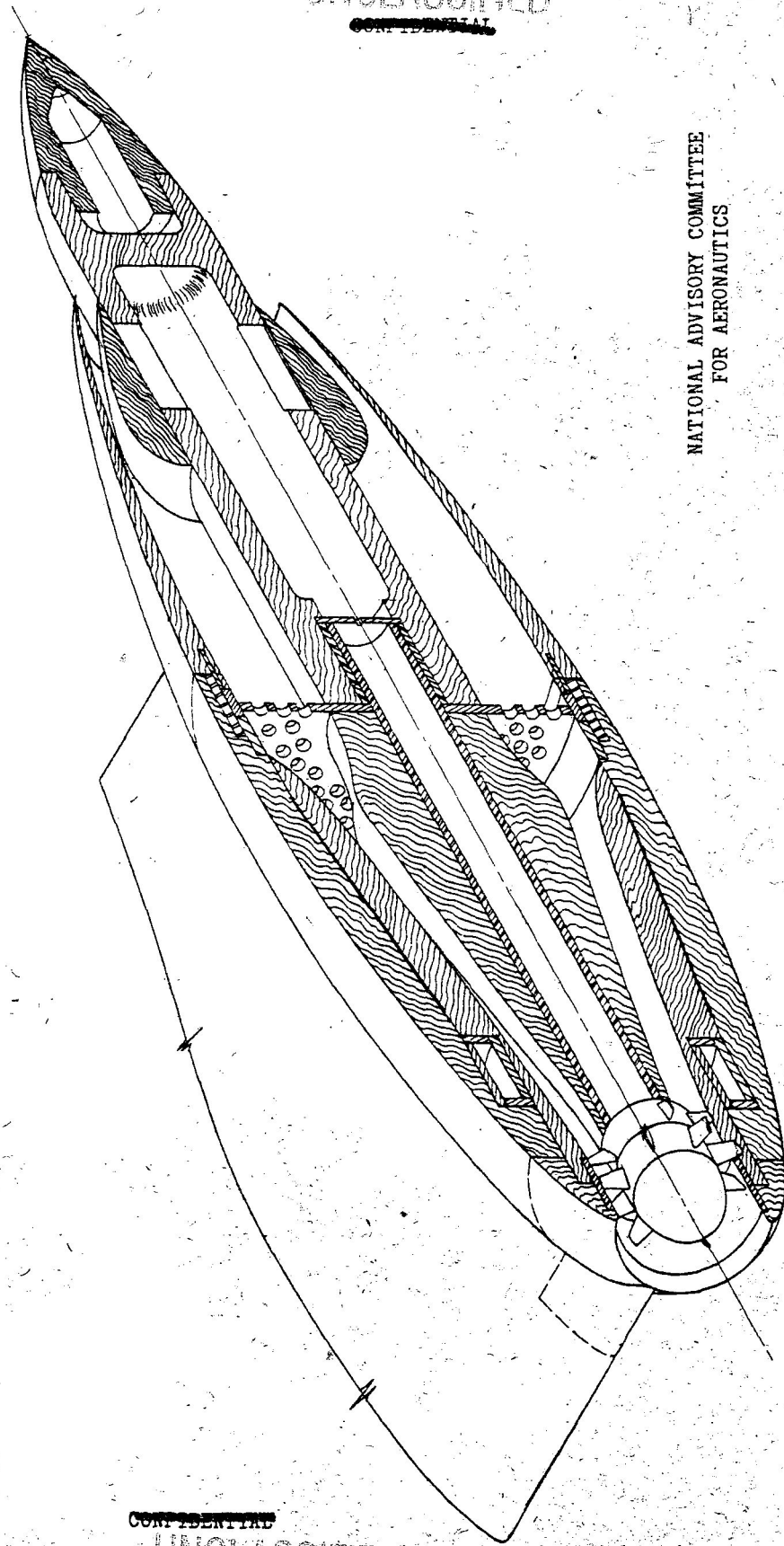


Figure 2.- Comparison of nacelle lines with NACA 133-30 nacelle.

UNCLASSIFIED



NATIONAL ADVISORY COMMITTEE  
FOR AERONAUTICS

Figure 3.- Sectional view of test model N<sub>2</sub>T<sub>2</sub>.

~~CONFIDENTIAL~~

UNCLASSIFIED

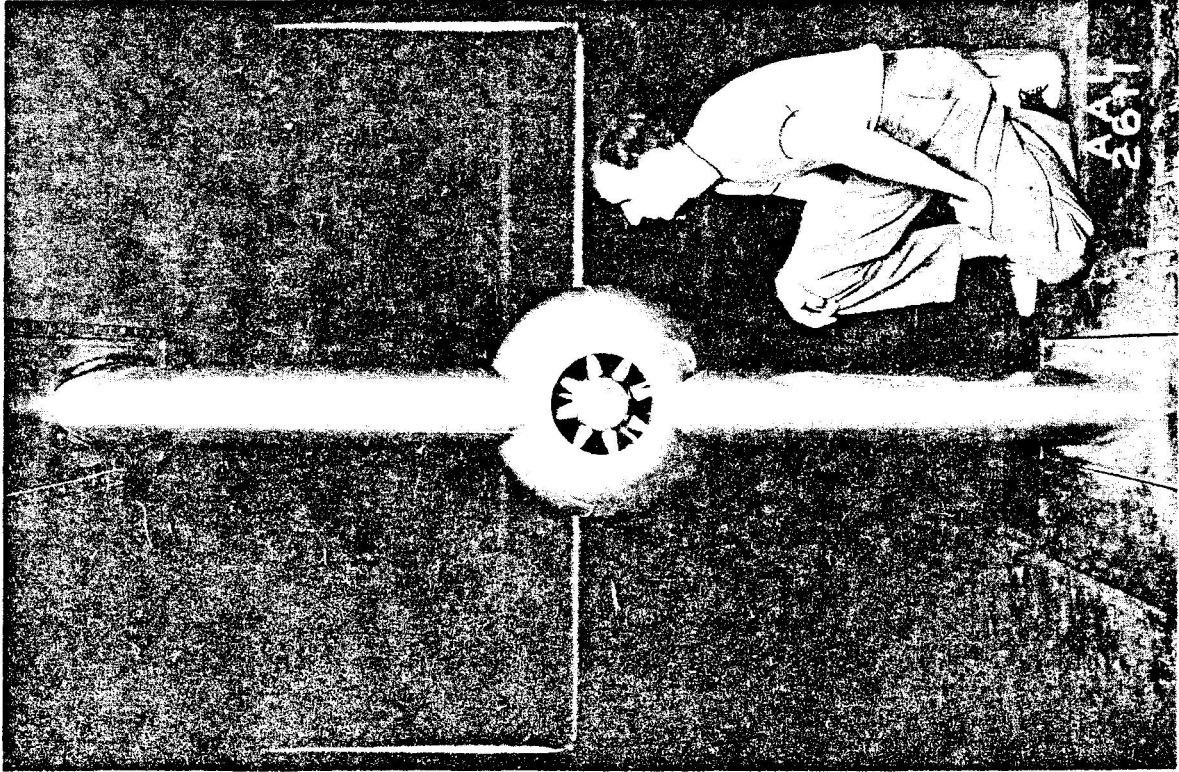


Figure 5. - Front view of nacelle N1T1.

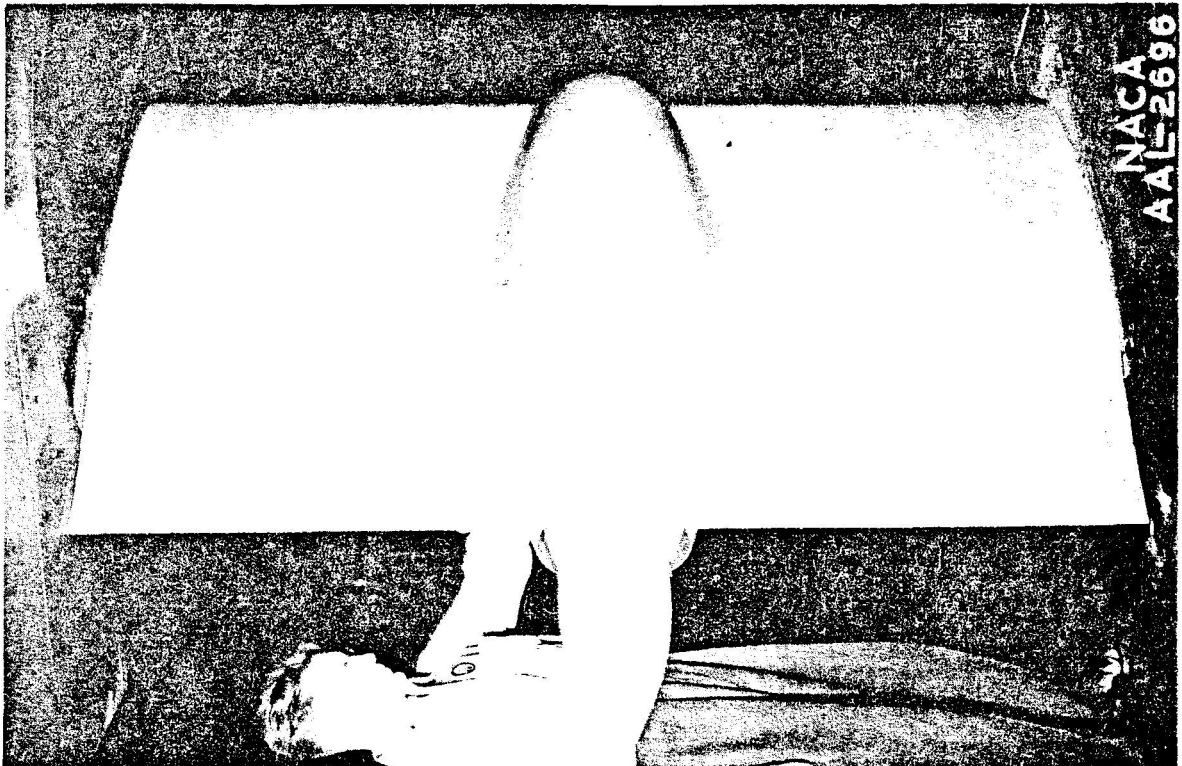


Figure 4. - Rear view of nacelle N1T1.

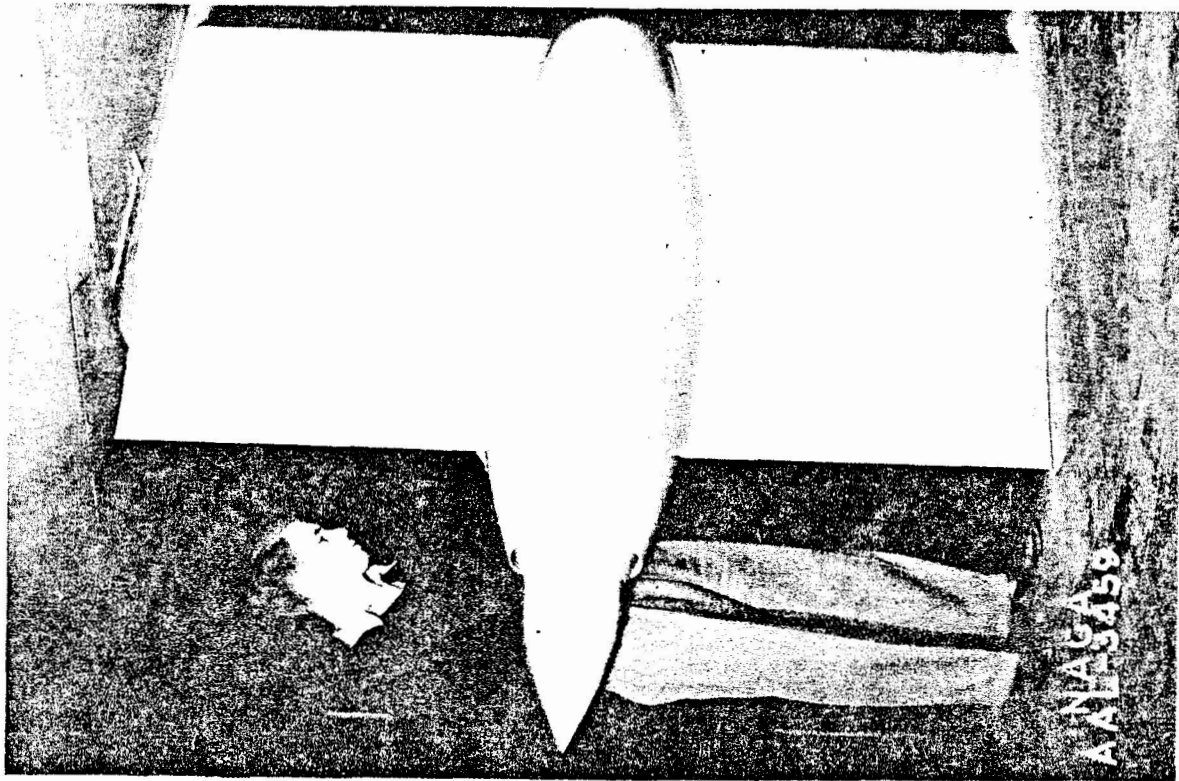


Figure 7.- View of lower surface of nacelle  
N4T2.

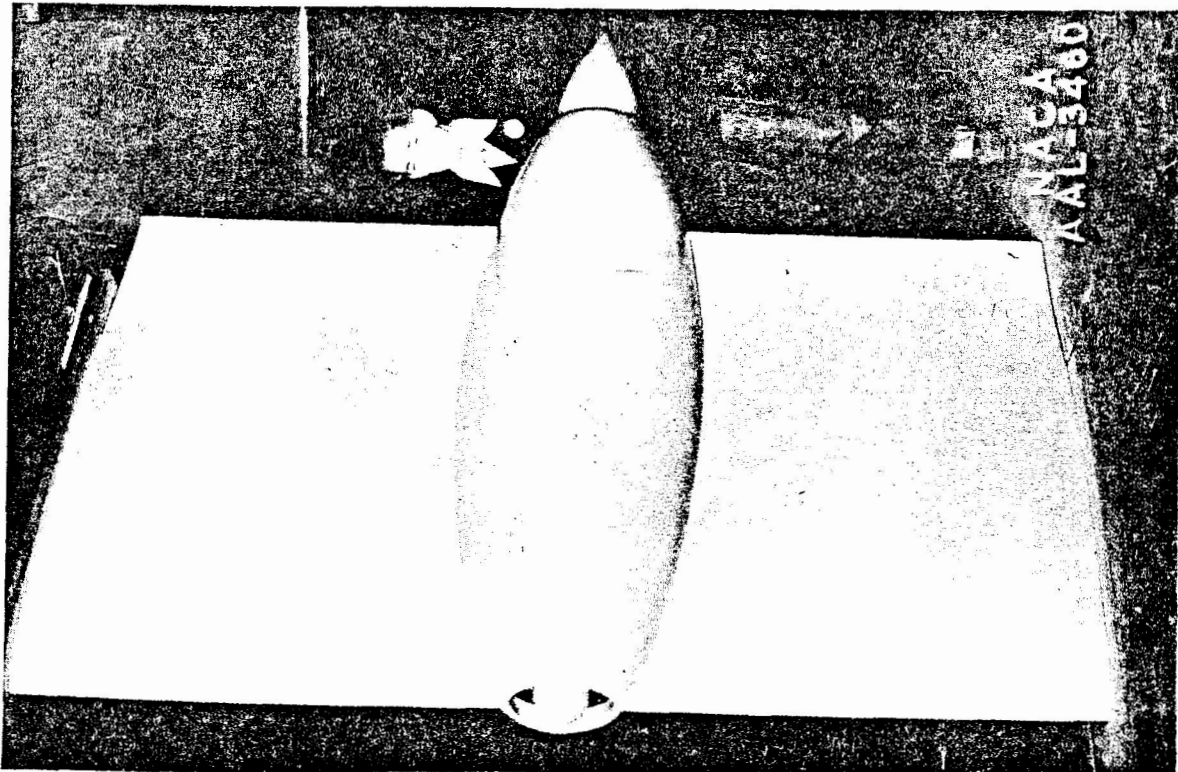


Figure 6.- View of upper surface of nacelle  
N4T2.



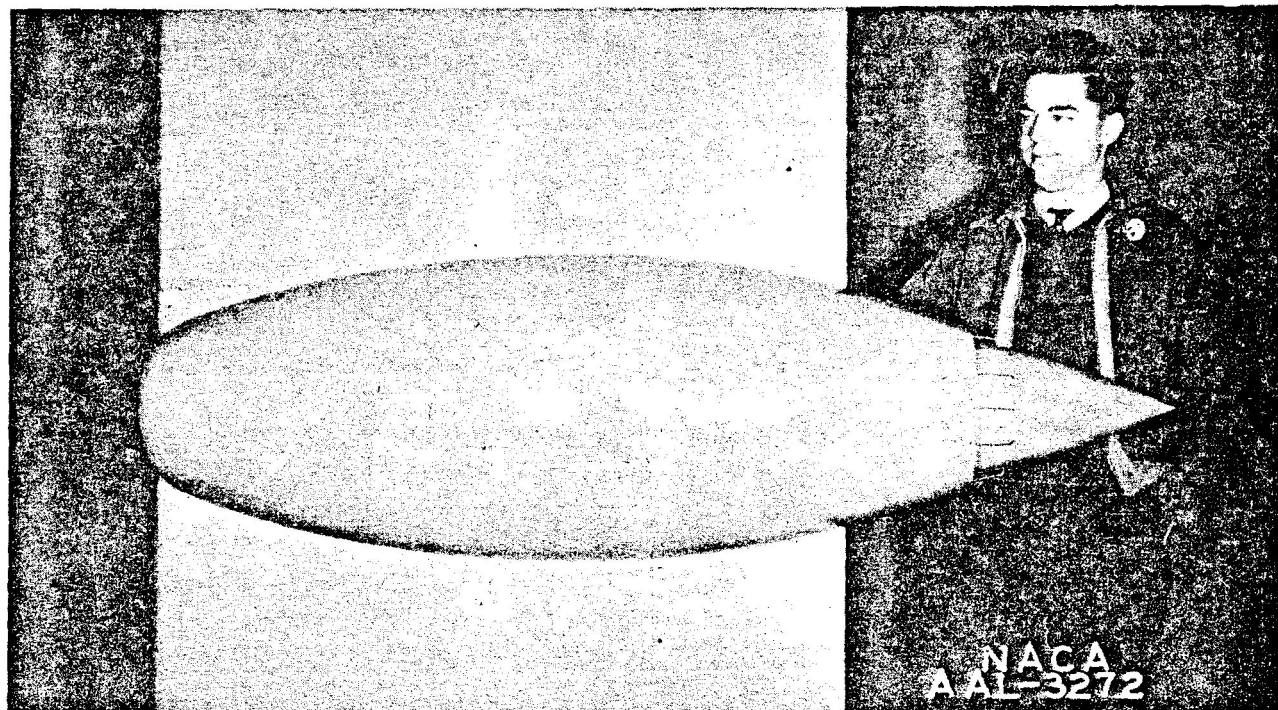


Figure 8.- View of upper surface of nacelle N<sub>5</sub>T<sub>3</sub>.

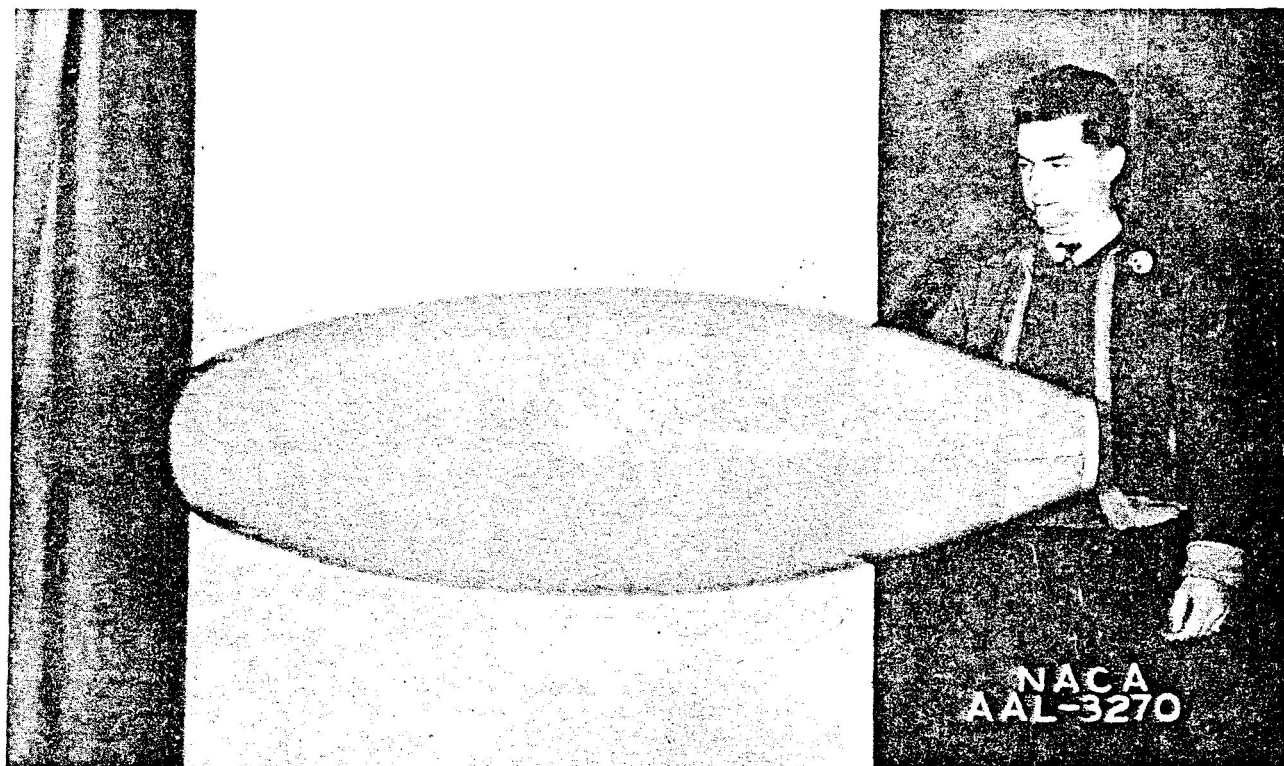


Figure 9.- View of upper surface of nacelle N<sub>5</sub>T<sub>4</sub>.

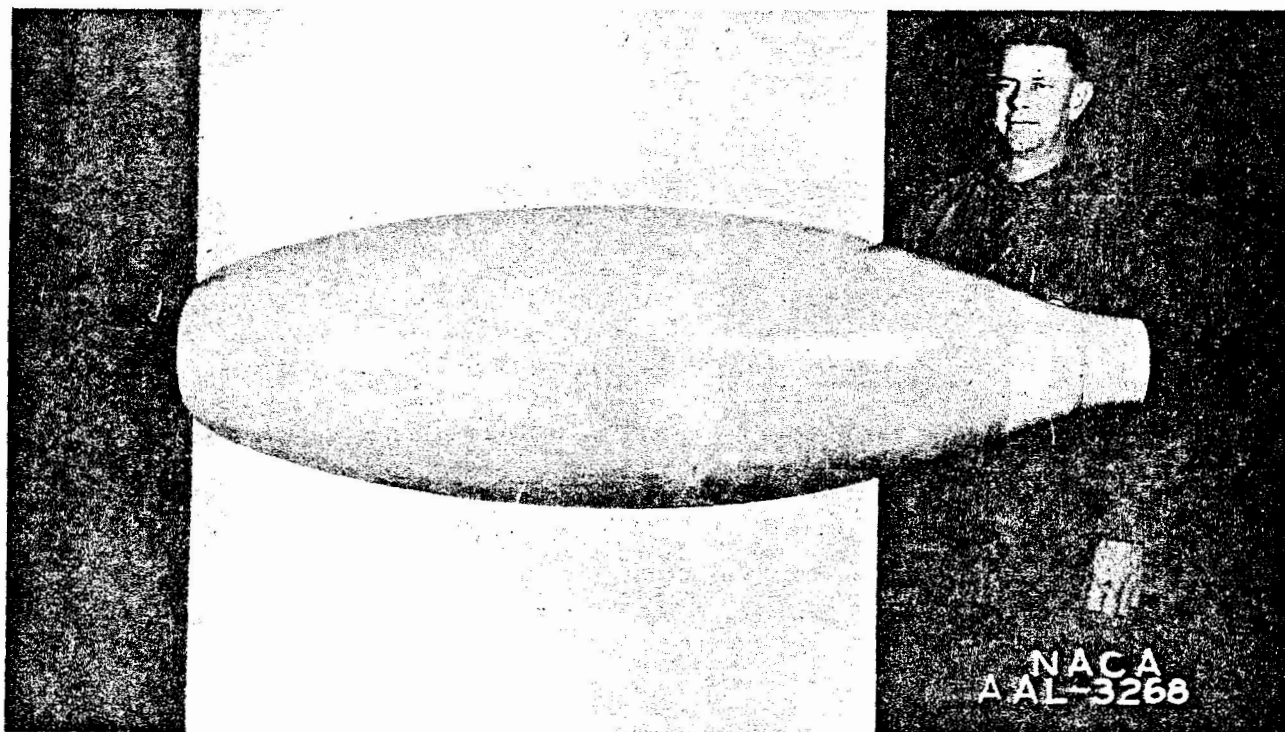


Figure 10.- View of upper surface of nacelle N<sub>5</sub>T<sub>5</sub>.

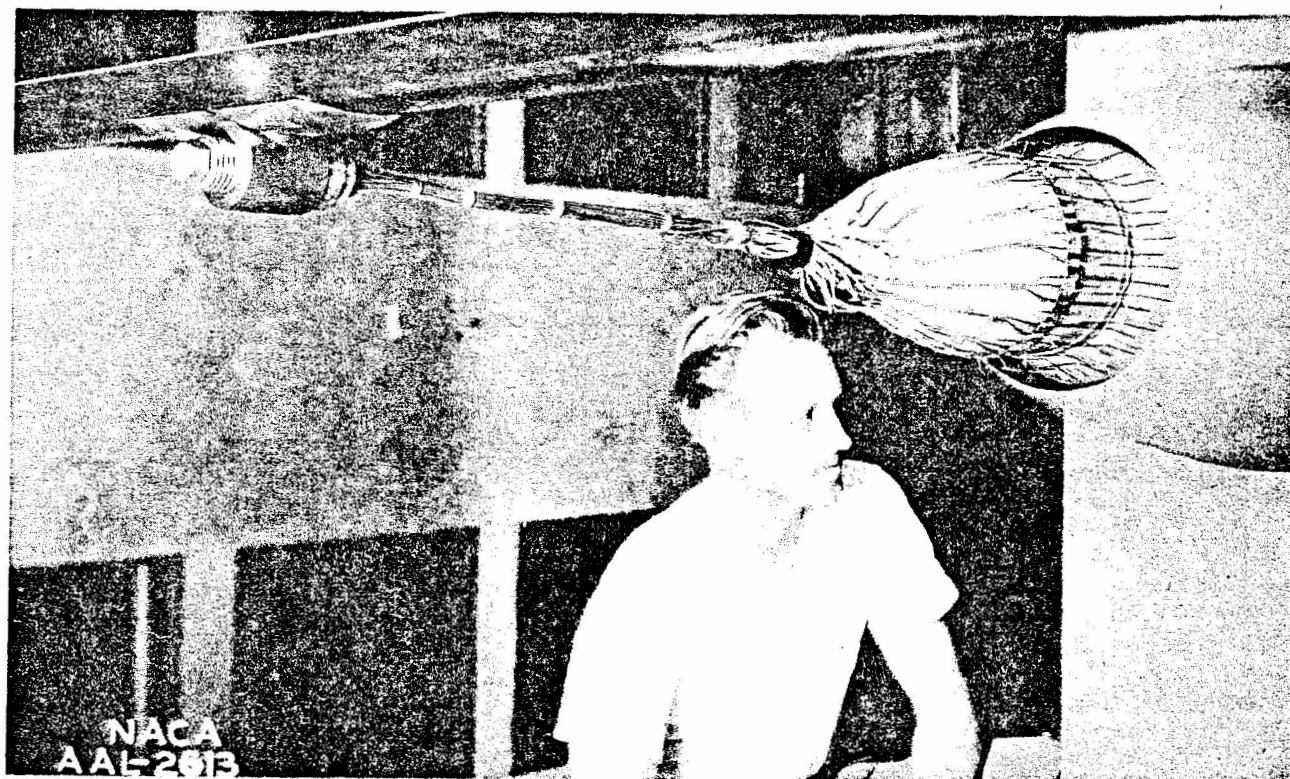


Figure 11.- View of outlet rake on nacelle N<sub>1</sub>T<sub>1</sub>.

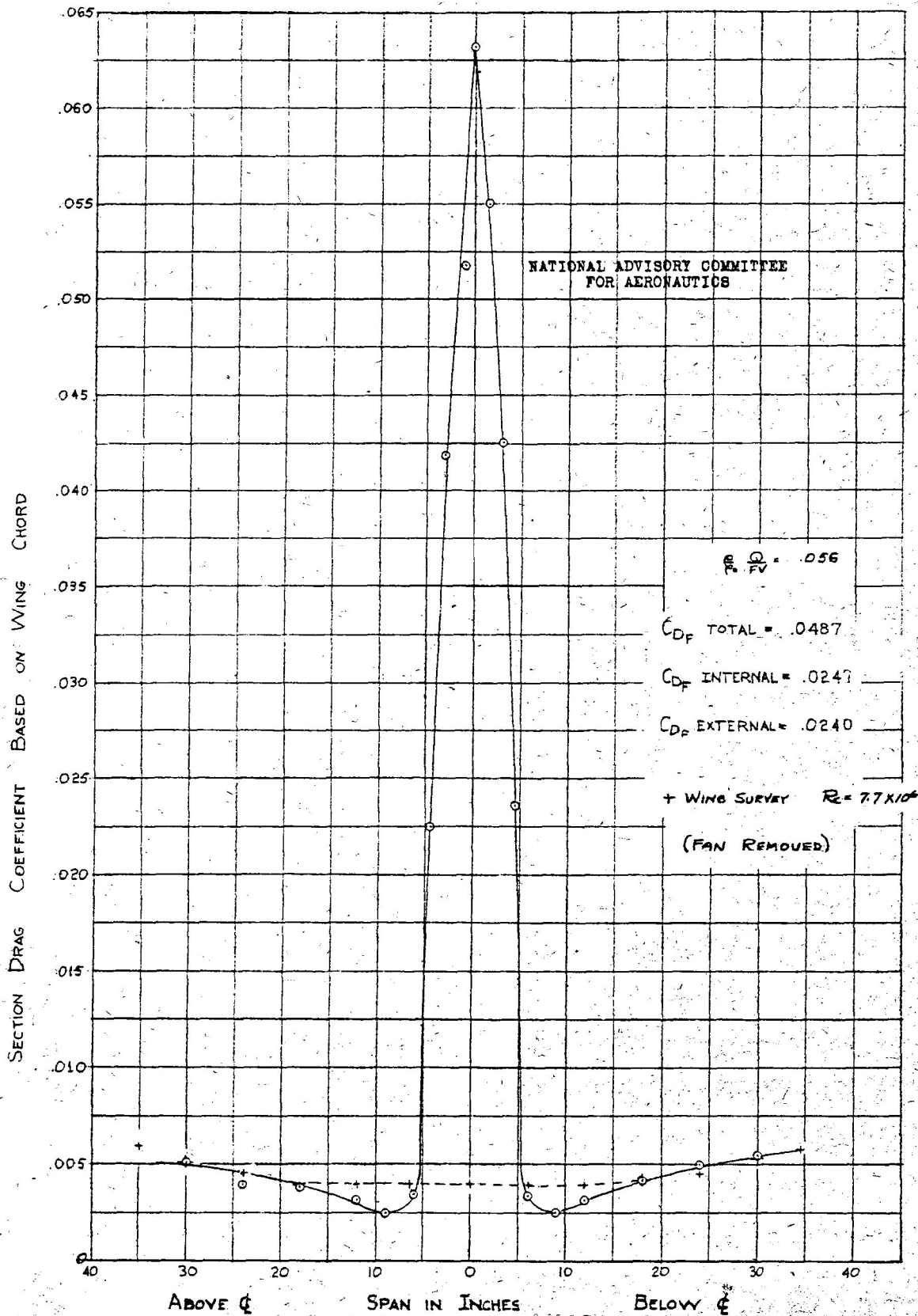
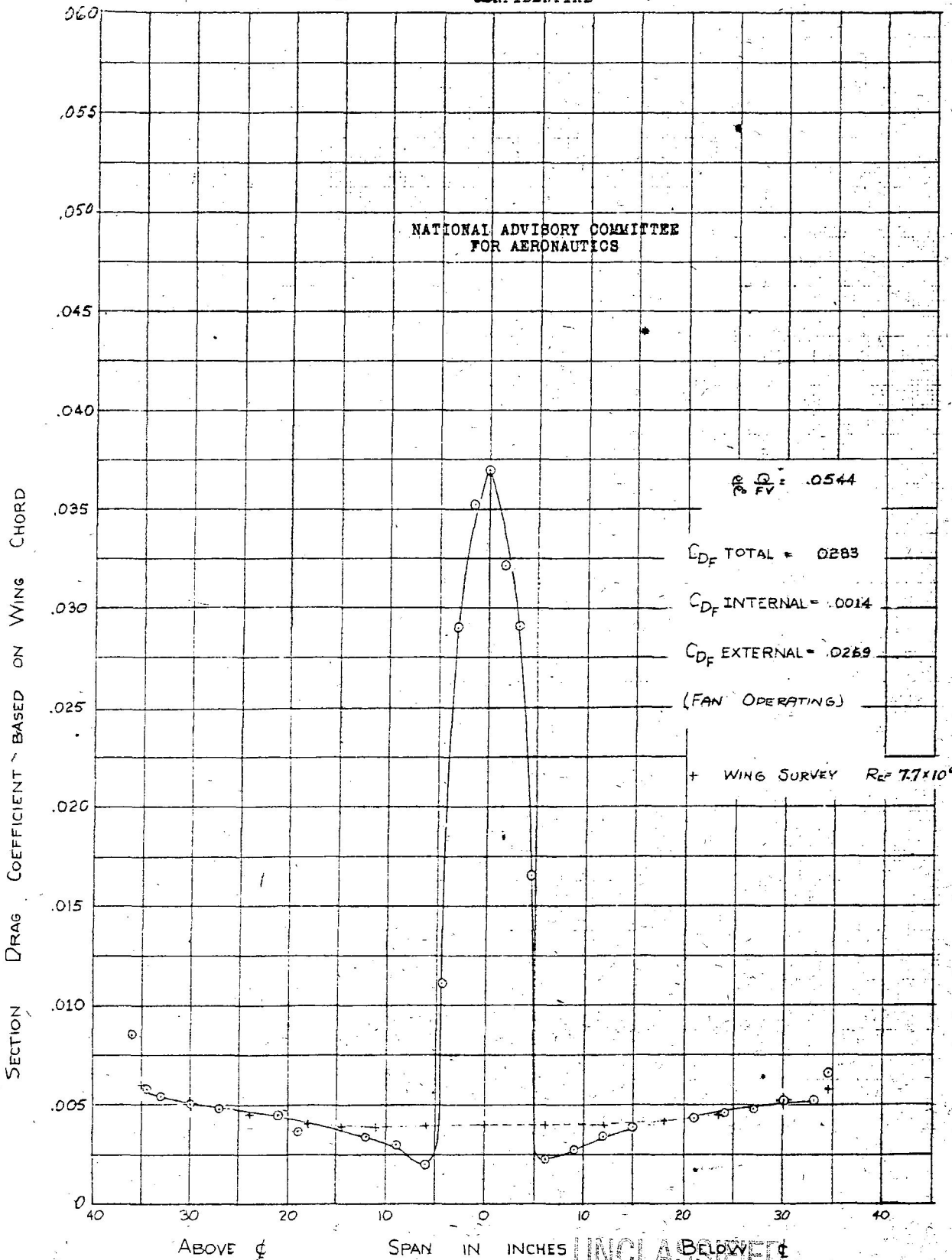


FIGURE 12.-SPANWISE VARIATION OF SECTION DRAG COEFFICIENT OBTAINED FROM WAKE SURVEY  $N_4 T_2$   $\alpha = 1.03^\circ$   $C_L = .213$  REYNOLDS NUMBER =  $7.5 \times 10^6$  MACH NUMBER = .27

~~CONFIDENTIAL~~



UNCLASSIFIED

FIGURE 13.- SPANWISE VARIATION OF SECTION DRAG COEFFICIENT OBTAINED FROM WAKE SURVEY.  $N_5 T_3$   $\alpha = 1.03^\circ$   $C_L = .213$  REYNOLDS NUMBER  $7.5 \times 10^6$  MACH NUMBER .27

~~CONFIDENTIAL~~

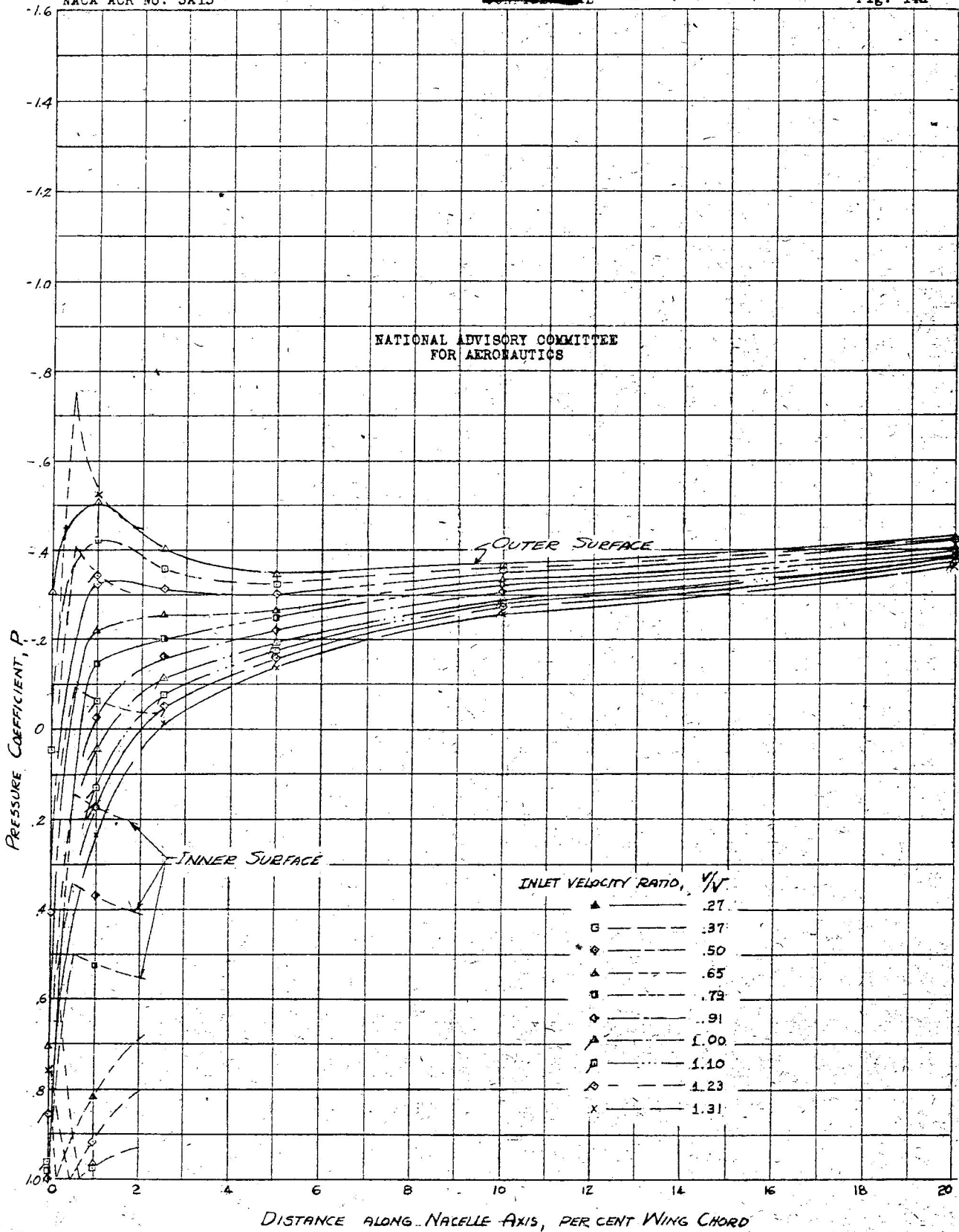


FIGURE 14a: PRESSURE DISTRIBUTION OVER THE UPPER LIP OF NOSE  $N_1$ ,  $\alpha = 1.05^\circ$ ,  $C_L = .215$

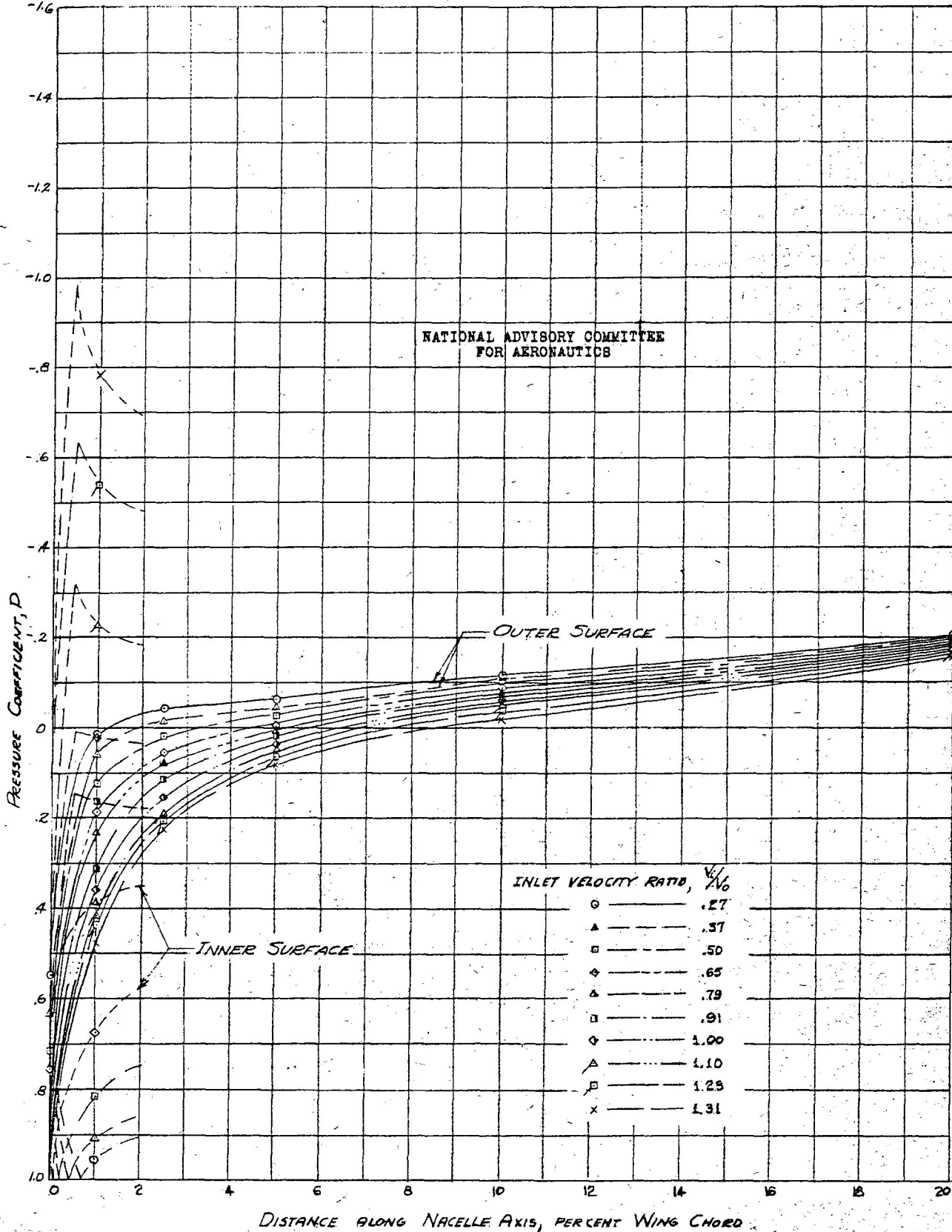


FIGURE 14b: PRESSURE DISTRIBUTION OVER THE LOWER LIP OF NOSE  $N_1$ ,  $\alpha = 1.05^\circ$ ,  $C_L = .215$

UNCLASSIFIED

NACA ACR No. 5A15

CONFIDENTIAL

Fig. 15a

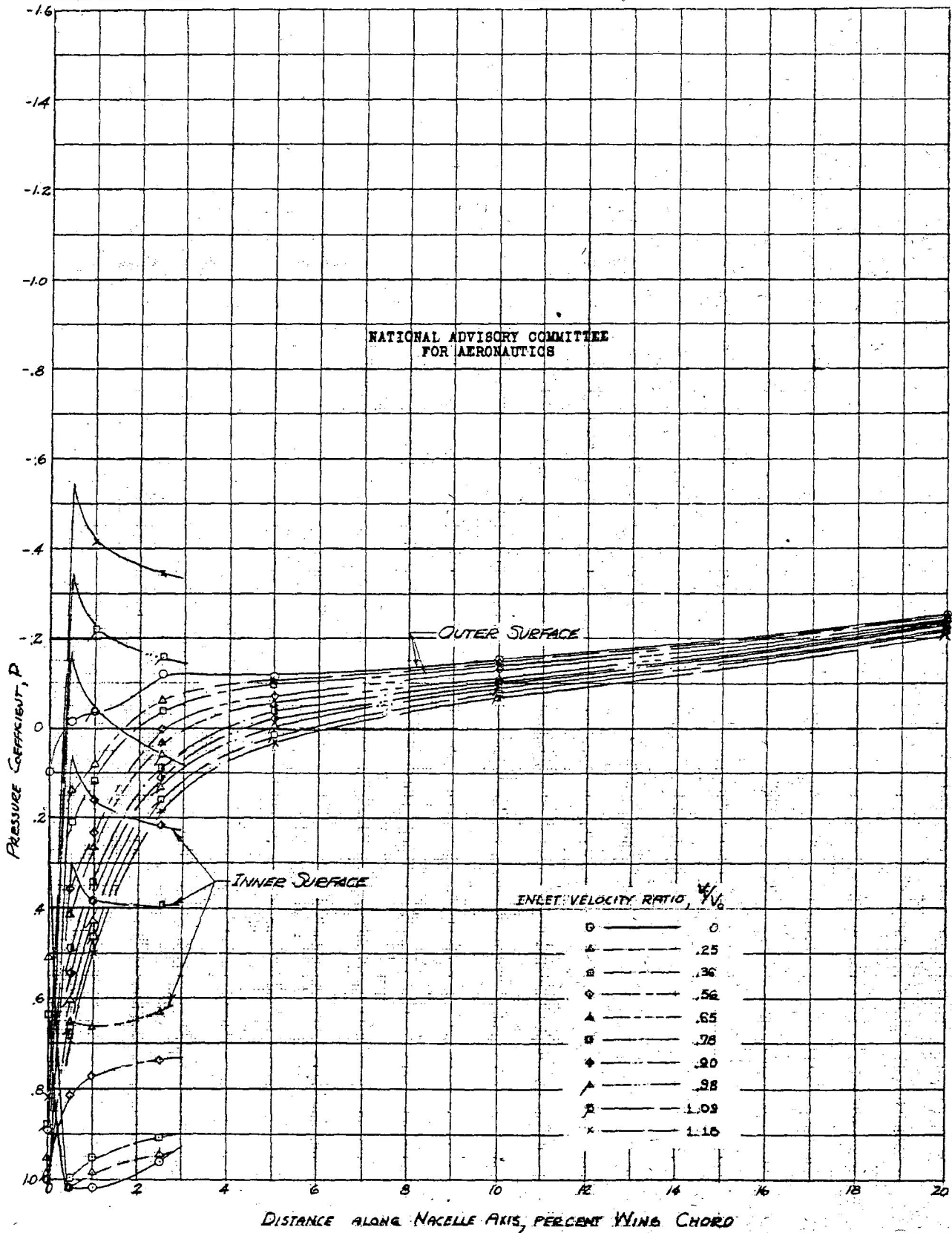


FIGURE 15. Pressure Distribution over the Upper Lip of Nose  $N_2$   $\alpha=1.00^\circ$   $C_L=0.12$

UNCLASSIFIED

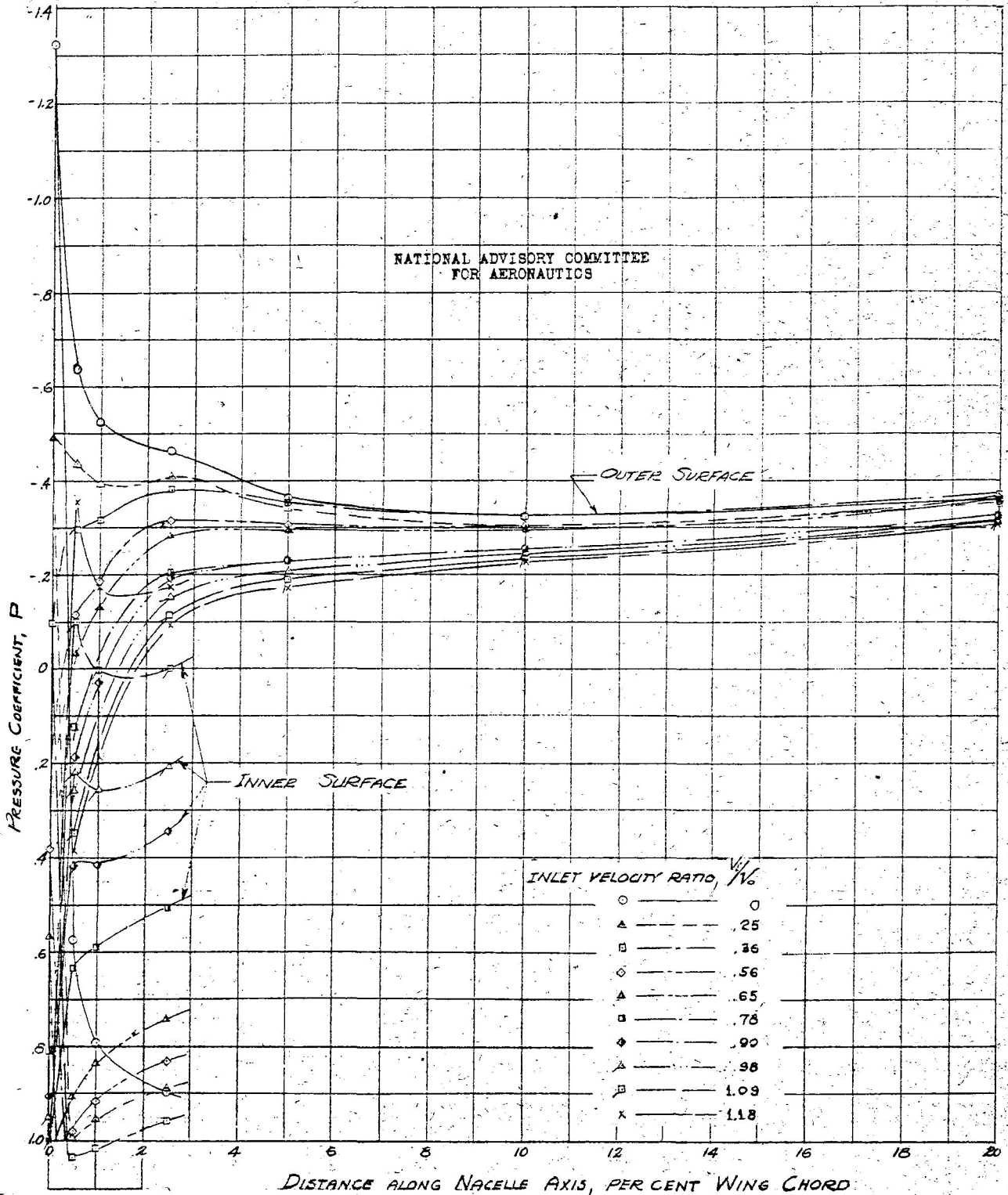


FIGURE 15b—PRESSURE DISTRIBUTION OVER THE LOWER LIP OF NOSE  $N_2$ .  $\alpha = -1.00^\circ$   $C_L = 0.12$



UNCLASSIFIED

NACA ACR No. 5A15

~~CONFIDENTIAL~~

Fig. 16a

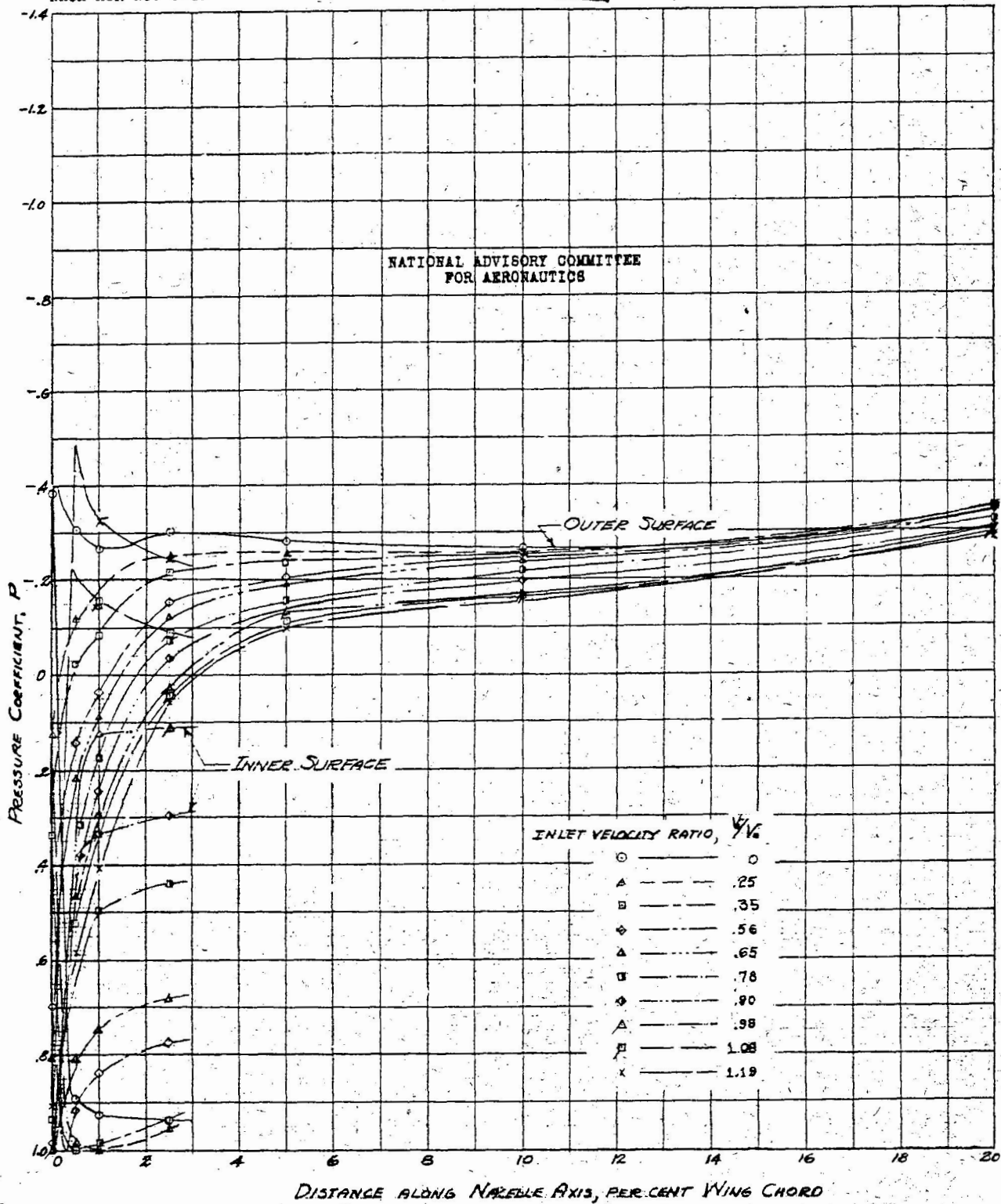


FIGURE 16a.- PRESSURE DISTRIBUTION OVER THE UPPER LIP OF NOSE  $N_2$ ,  $\alpha=0^\circ$ ,  $C_L=.105$

~~CONFIDENTIAL~~  
UNCLASSIFIED

UNCLASSIFIED

CONFIDENTIAL

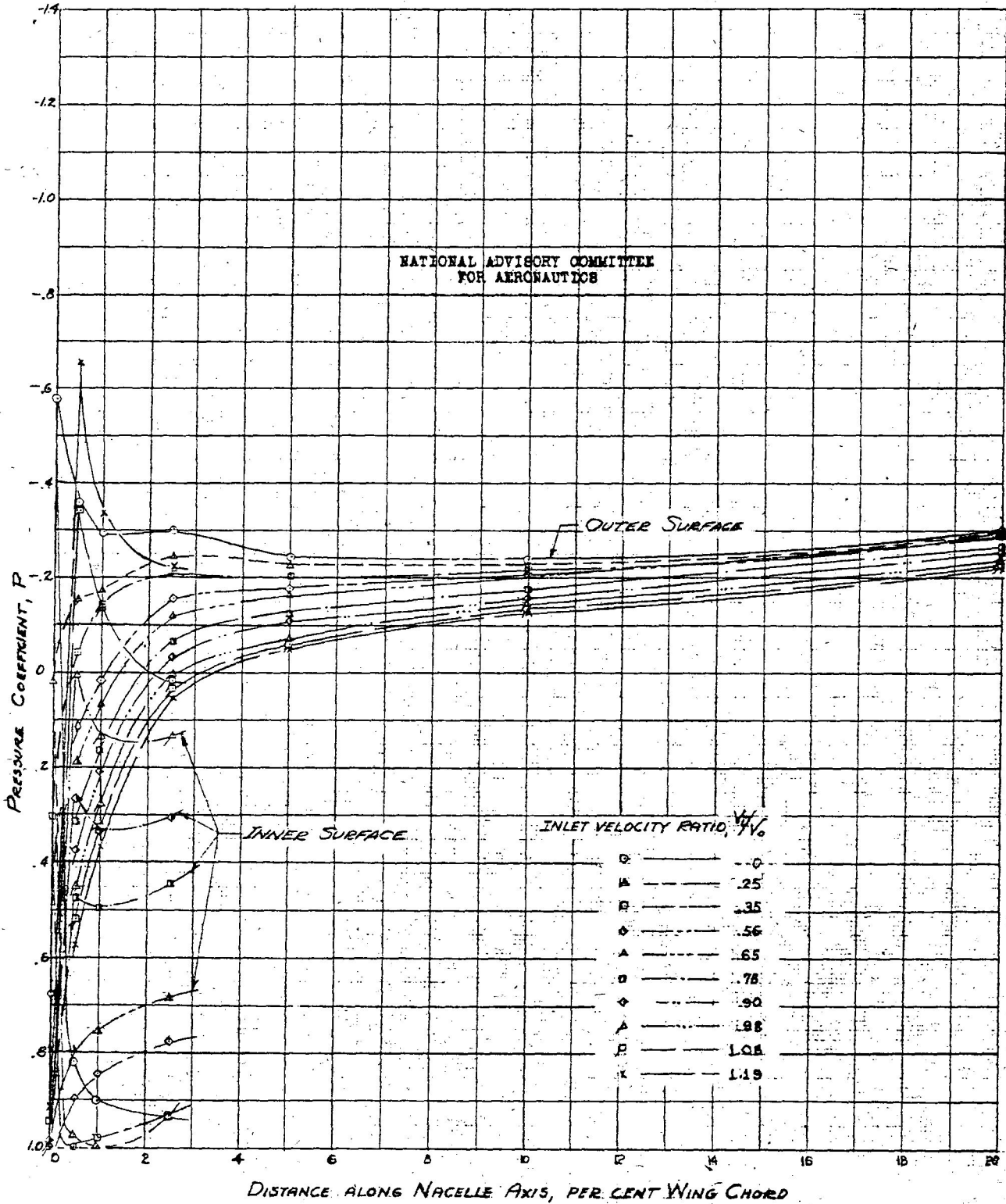


FIGURE 16b.-PRESSURE DISTRIBUTION OVER THE LOWER LIP OF NOSE  $N_2$ ,  $\alpha = 2^\circ$ ,  $C_{L_2} = .105$

UNCLASSIFIED

UNCLASSIFIED

~~CONFIDENTIAL~~

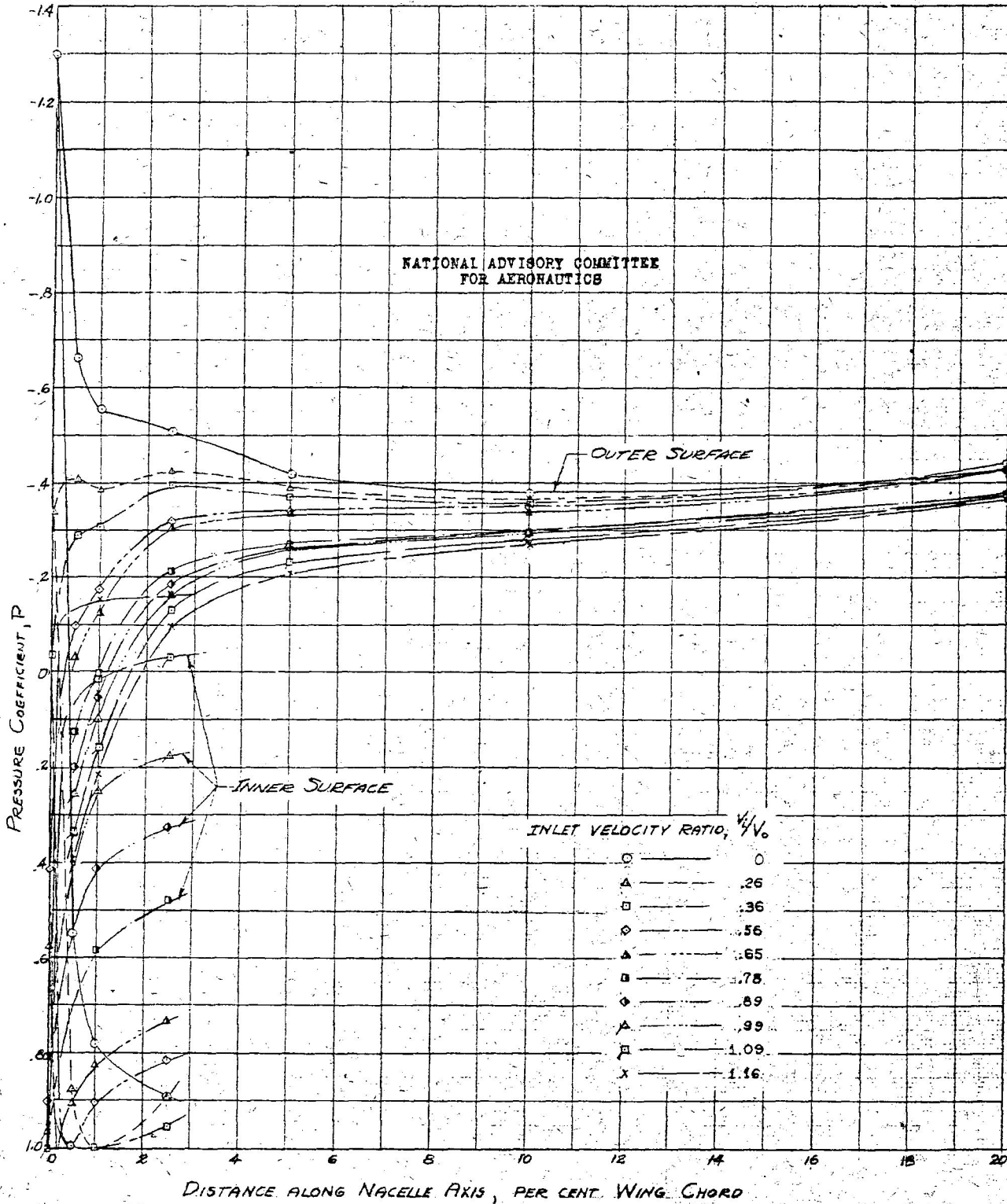
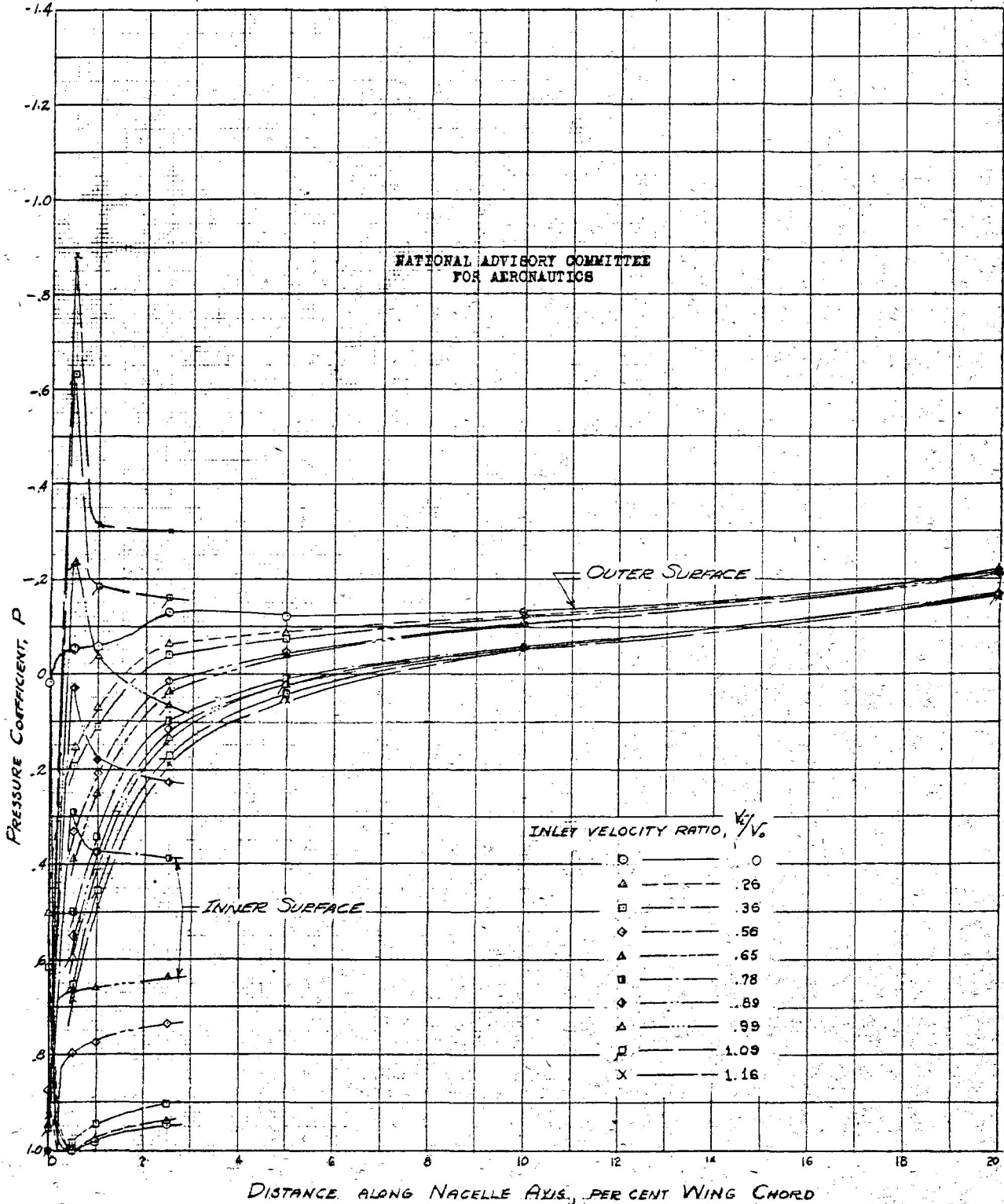


FIGURE 17a: PRESSURE DISTRIBUTION OVER THE UPPER LIP OF NOSE  $N_2$ ,  $\alpha = 1.05^\circ$   $C_L = .215$

~~CONFIDENTIAL~~

UNCLASSIFIED

UNCLASSIFIED



CONFIDENTIAL

FIGURE 17b: PRESSURE DISTRIBUTION OVER THE LOWER LIP OF NOSE  $N_2$ ,  $\alpha = 1.05^\circ$ ,  $C_L = 0.215$

UNCLASSIFIED

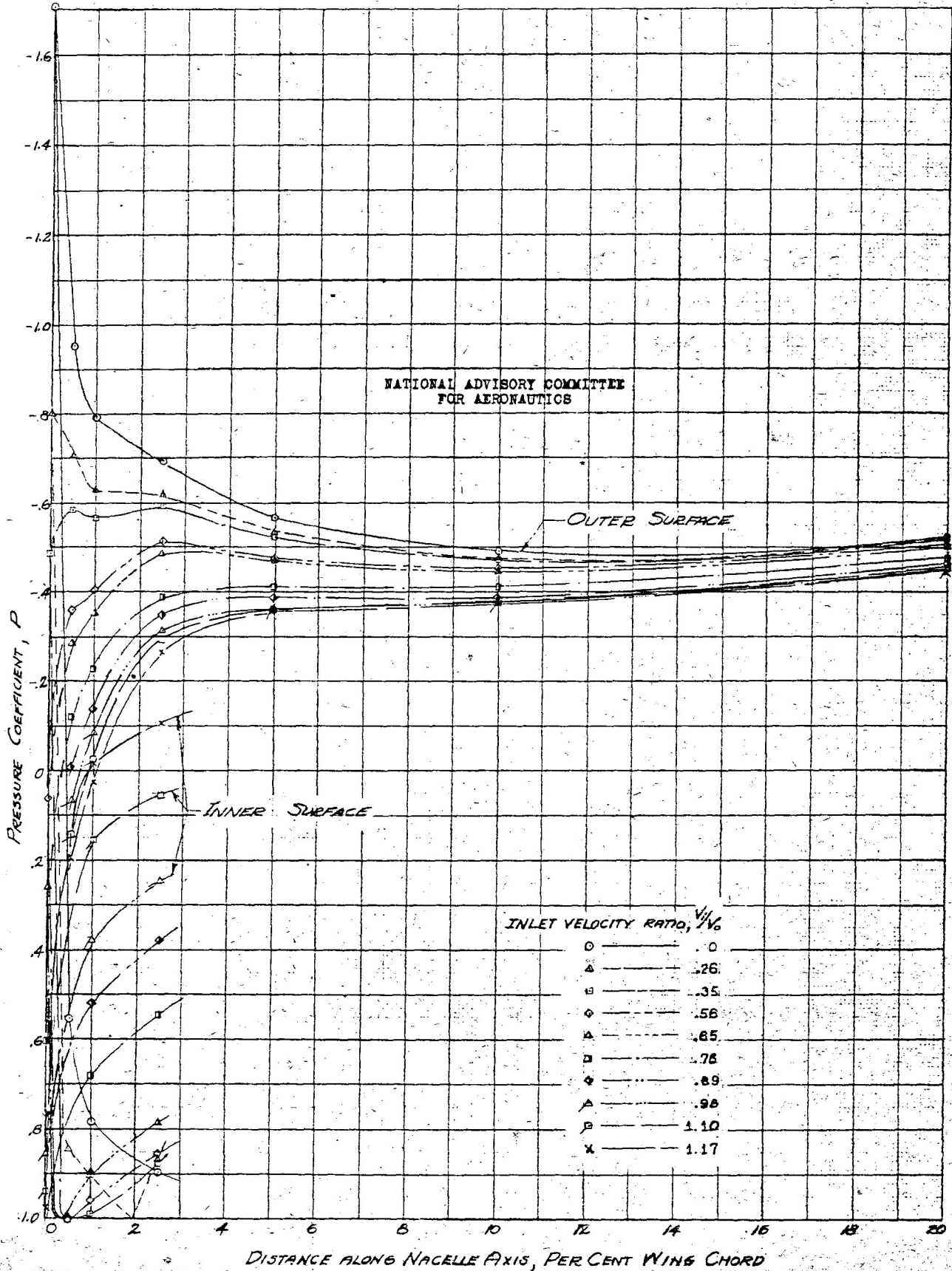


FIGURE 18a.-PRESSURE DISTRIBUTION OVER UPPER LIP OF NOSE  $N_2$   $\alpha = 2.11^\circ$   $C_L = .325$

UNCLASSIFIED

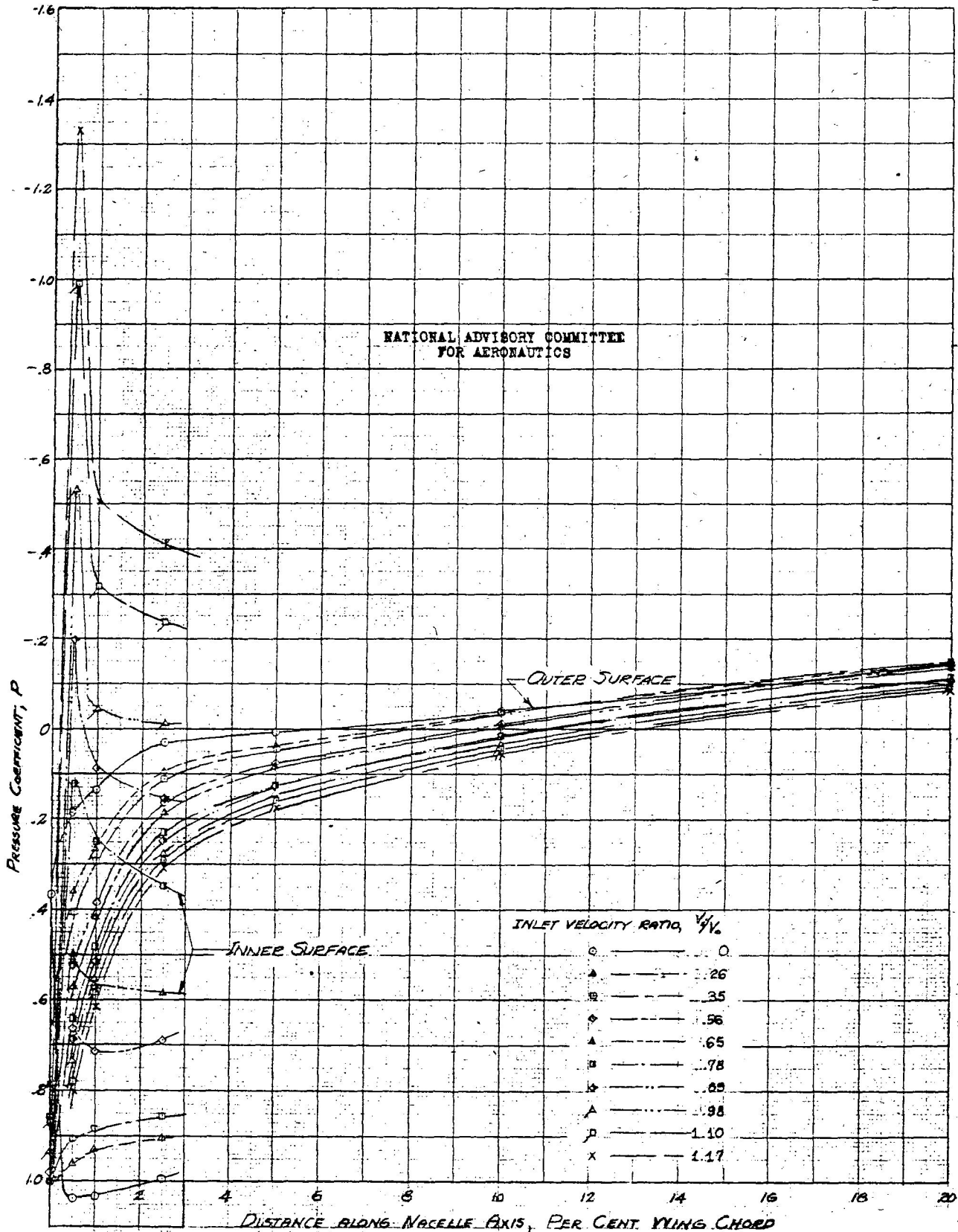


FIGURE 18b. PRESSURE DISTRIBUTION OVER LOWER LIP OF NOSE  $N_2$ ,  $\alpha = 2.11^\circ$   $C_L = 3.25$

UNCLASSIFIED

UNCLASSIFIED

NACA ACR No. 5A15

CONFIDENTIAL

Fig. 19a

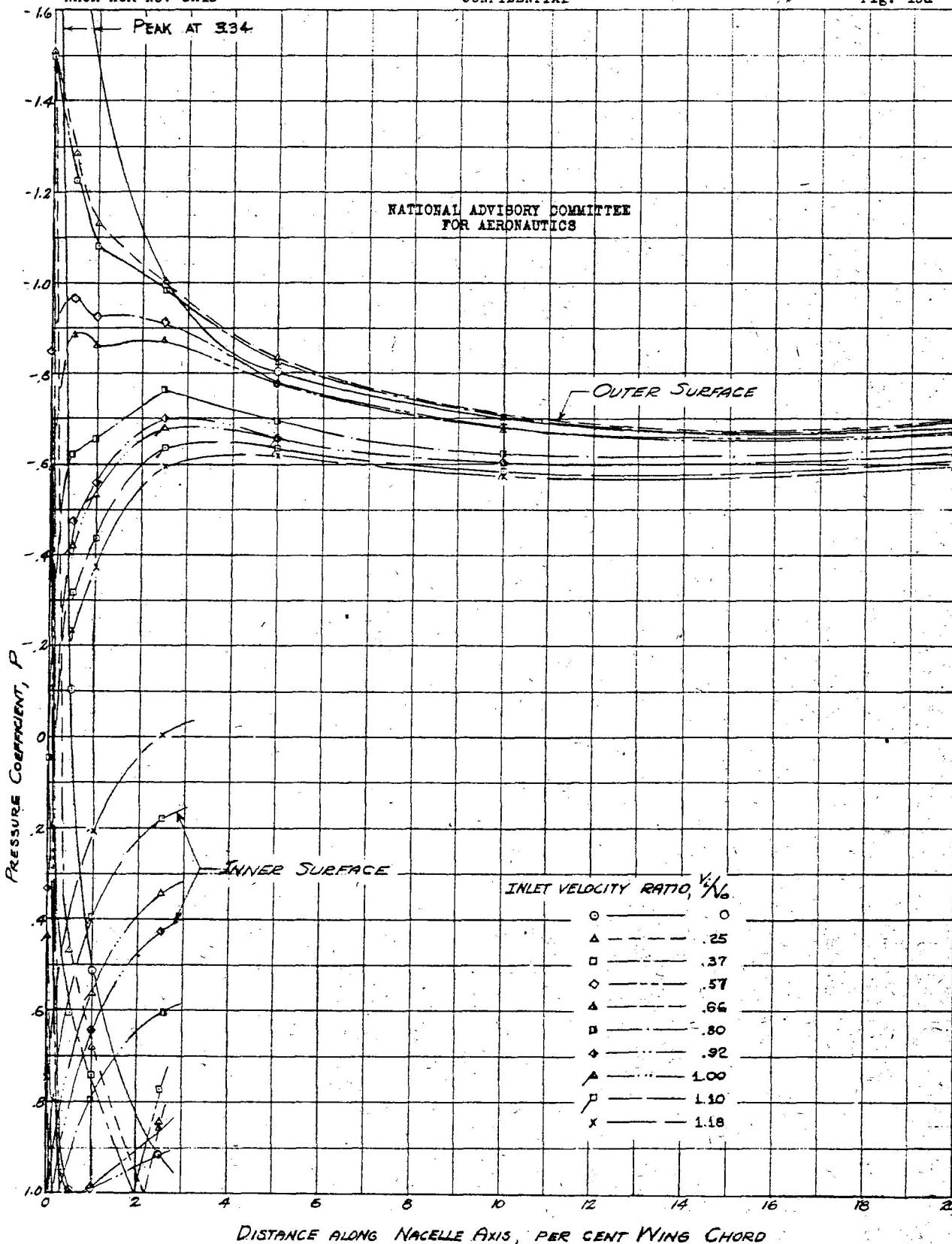


FIGURE 19a: PRESSURE DISTRIBUTION OVER UPPER LIP OF NOSE  $N_2$ ,  $\alpha = 4.25^\circ$ ,  $C_L = .565$

UNCLASSIFIED

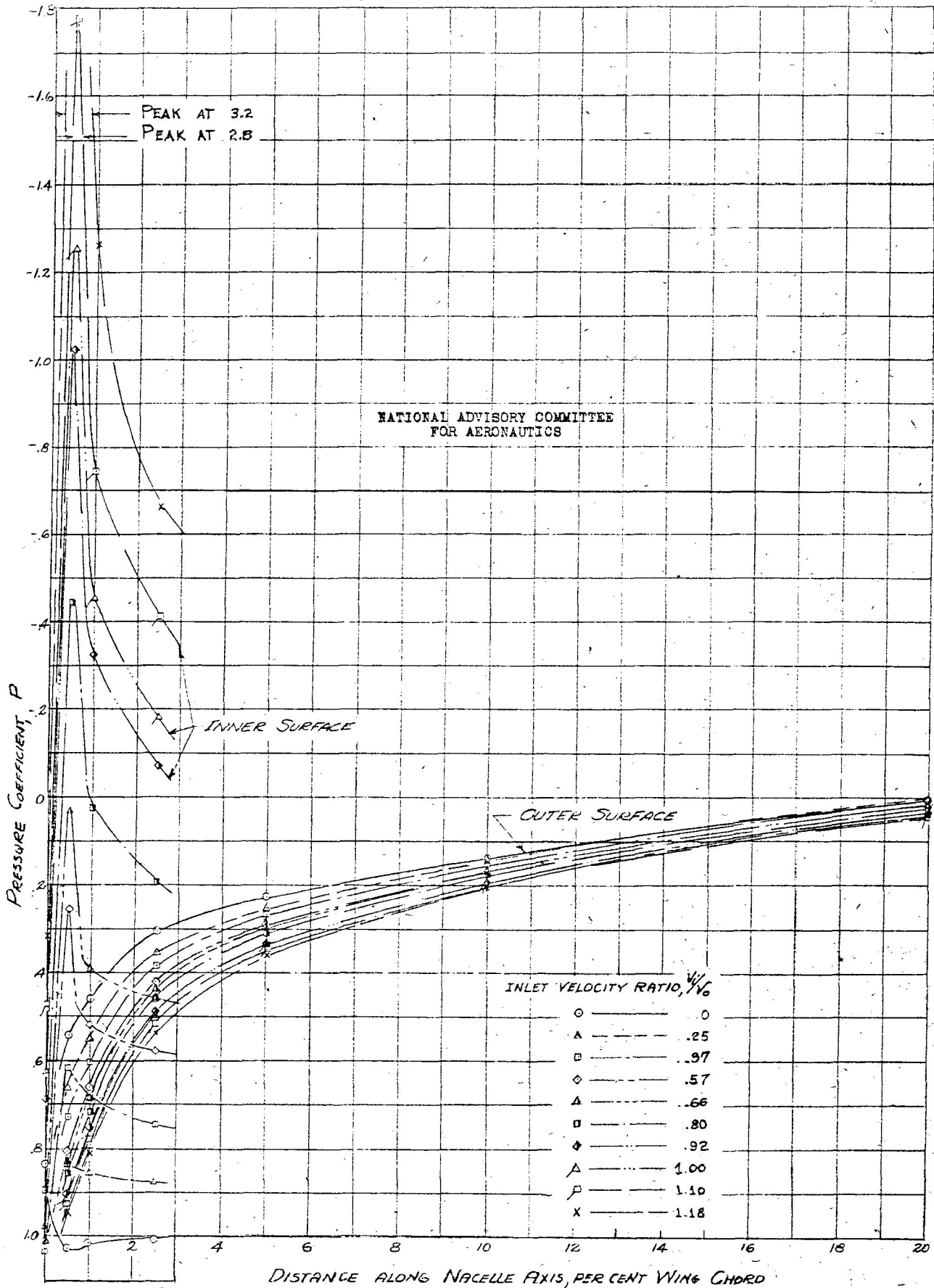


FIGURE 19b—PRESSURE DISTRIBUTION OVER THE LOWER LIP OF NOSE  $N_2$ ,  $\alpha = 4.25^\circ$   $C_L = .565$



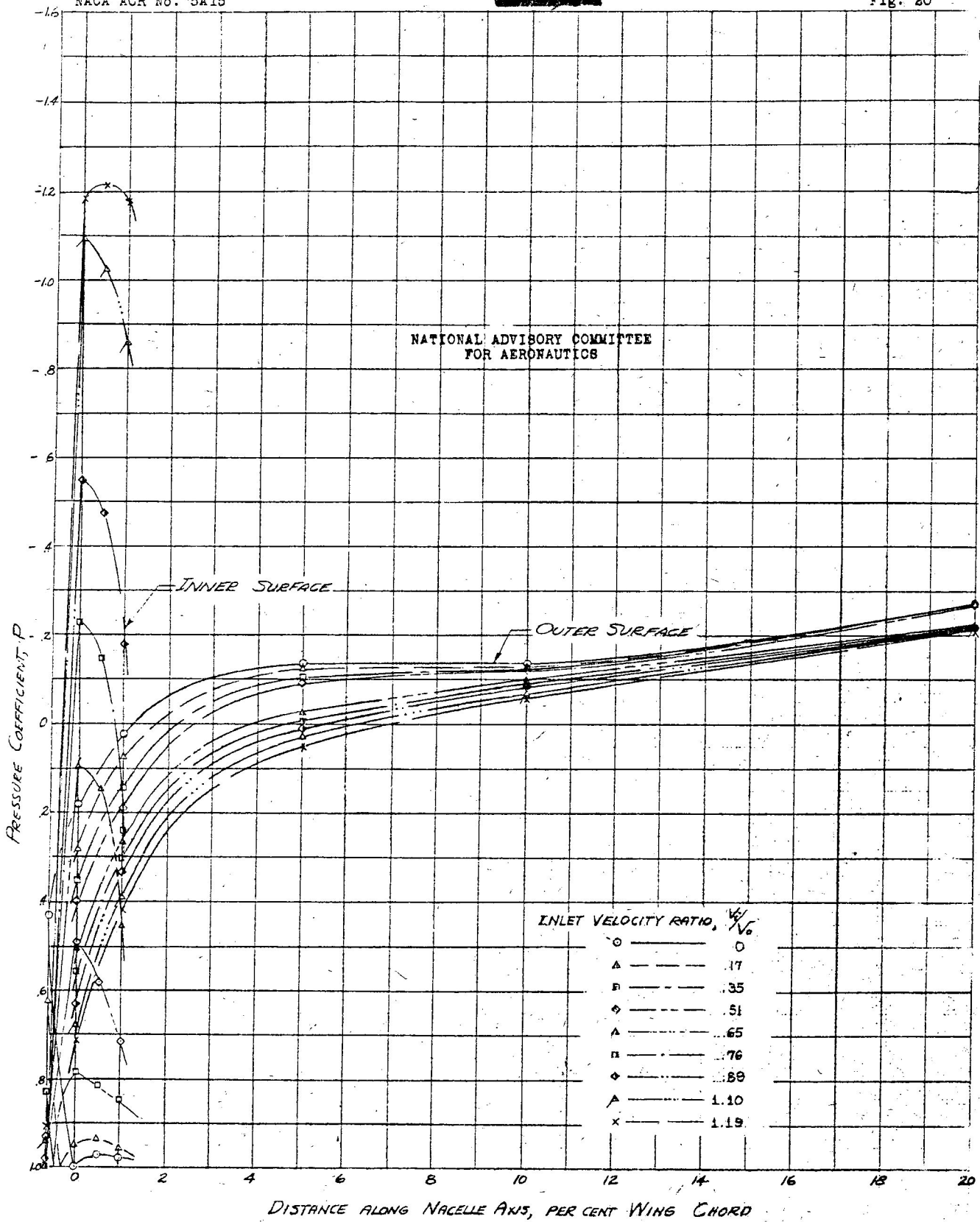
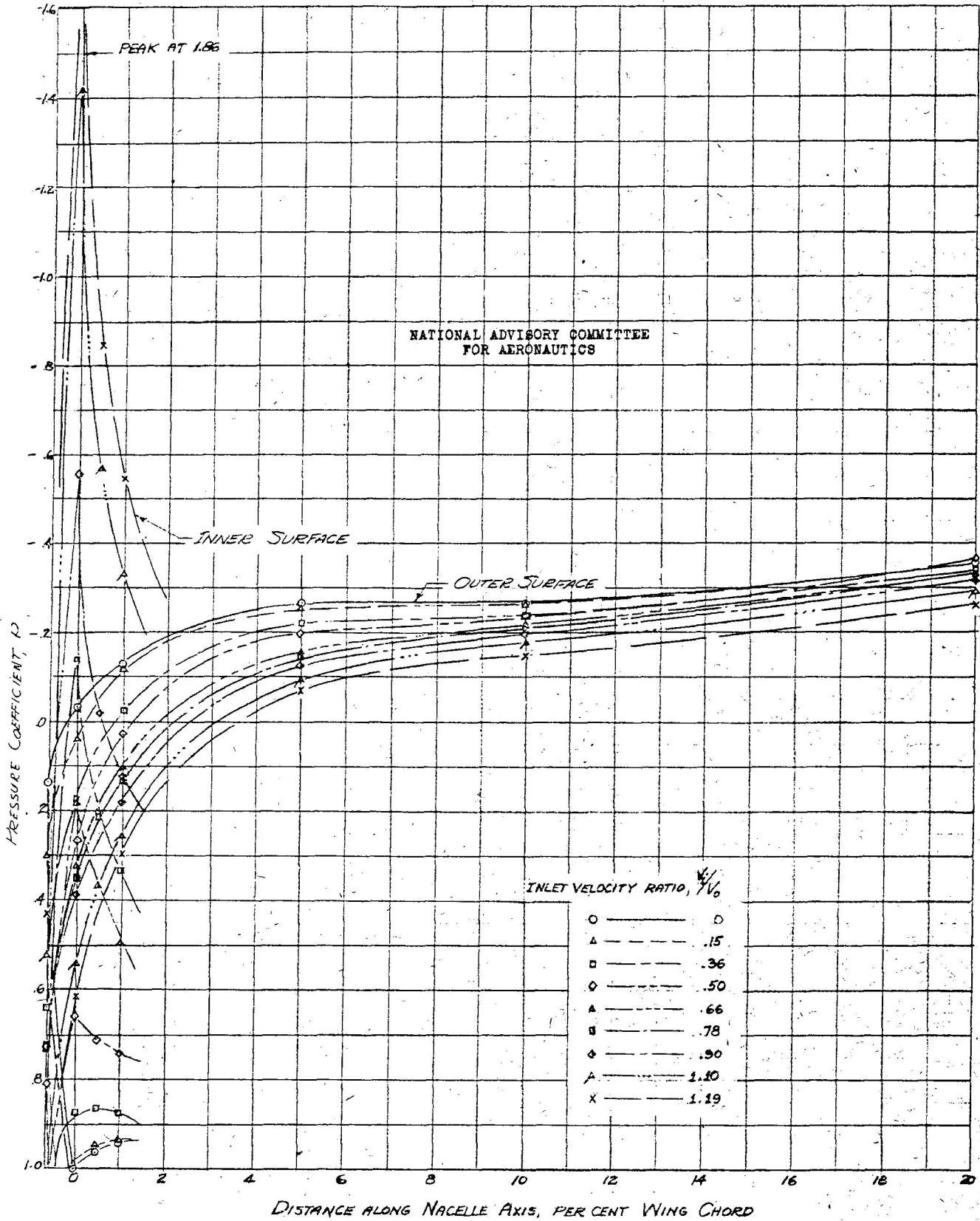


FIGURE 20.-PRESSURE DISTRIBUTION OVER THE UPPER LIP OF NOSE  $N_4$ .  $\alpha = -1.00$   $C_L = .012$



CONFIDENTIAL  
FIGURE 21.—PRESSURE DISTRIBUTION OVER THE UPPER LIP OF NOSE  $N_4$ .  $\alpha = 0^\circ$   $C_L = .105$

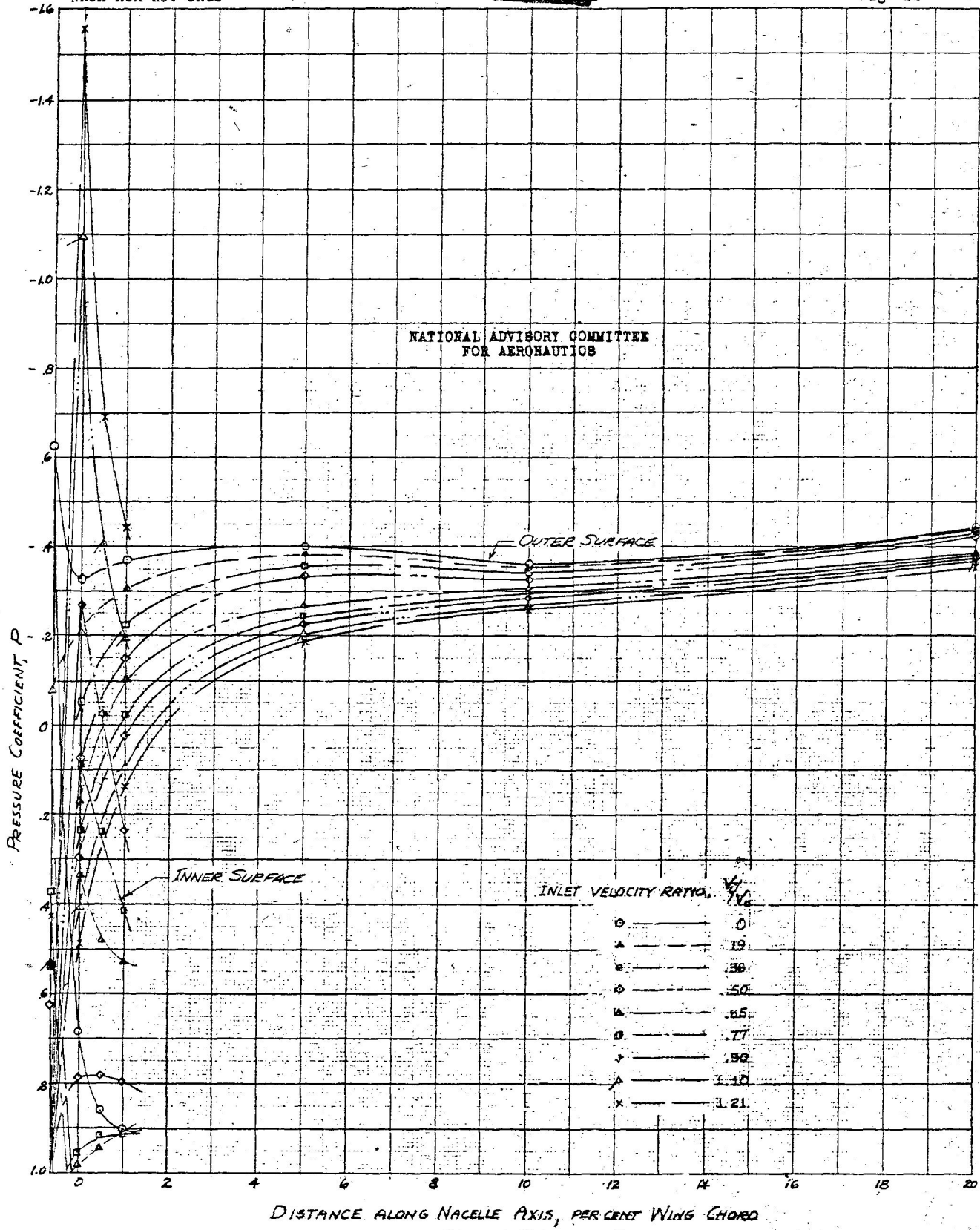


FIGURE 22.—PRESSURE DISTRIBUTION OVER THE UPPER LIP OF NOSE  $N_4$ ,  $\alpha = 1.05^\circ$ ,  $C_L = .215$

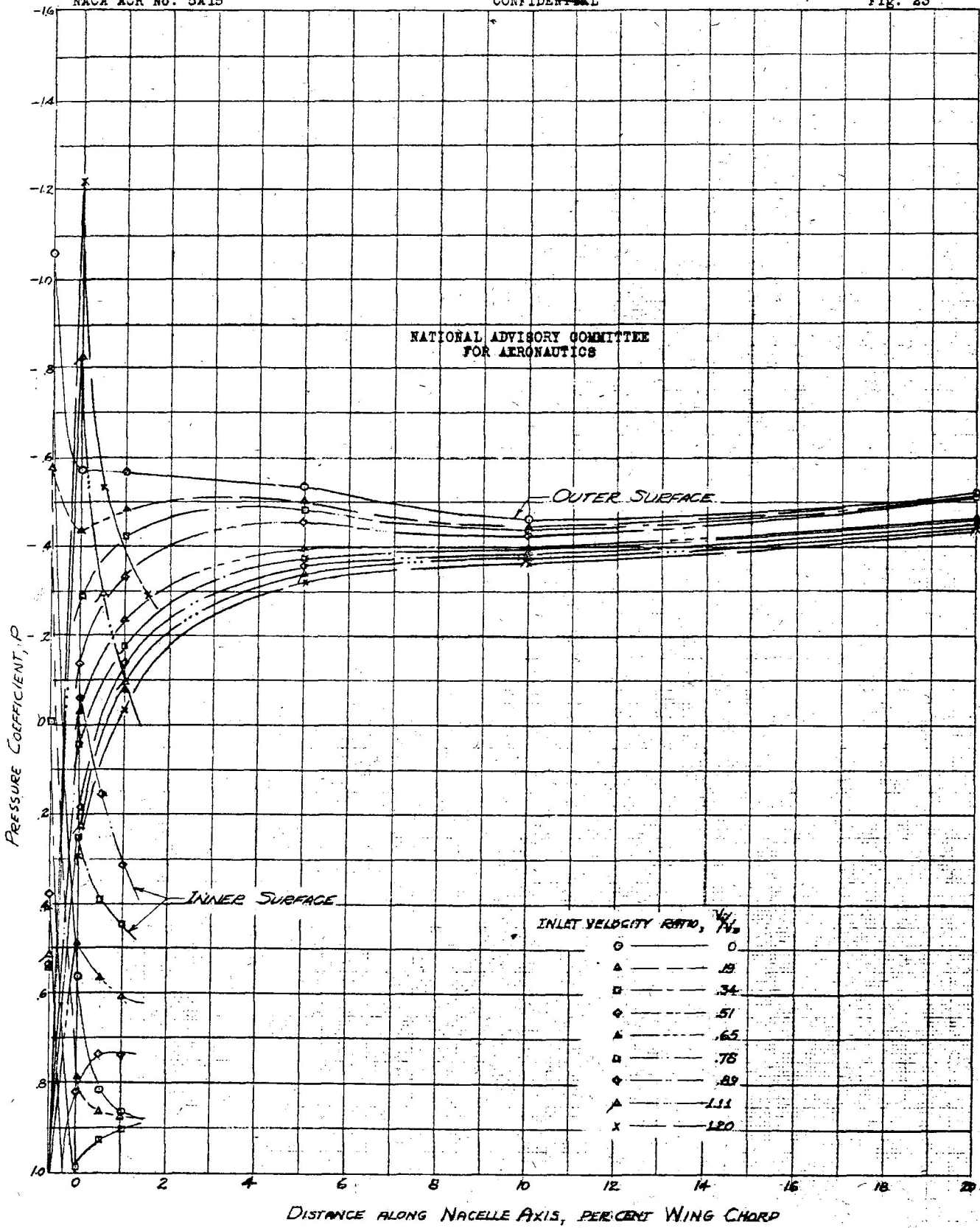


FIGURE 23.-PRESSURE DISTRIBUTION OVER THE UPPER LIP OF NOSE N<sub>2</sub> QCR11  $C_p = .325$

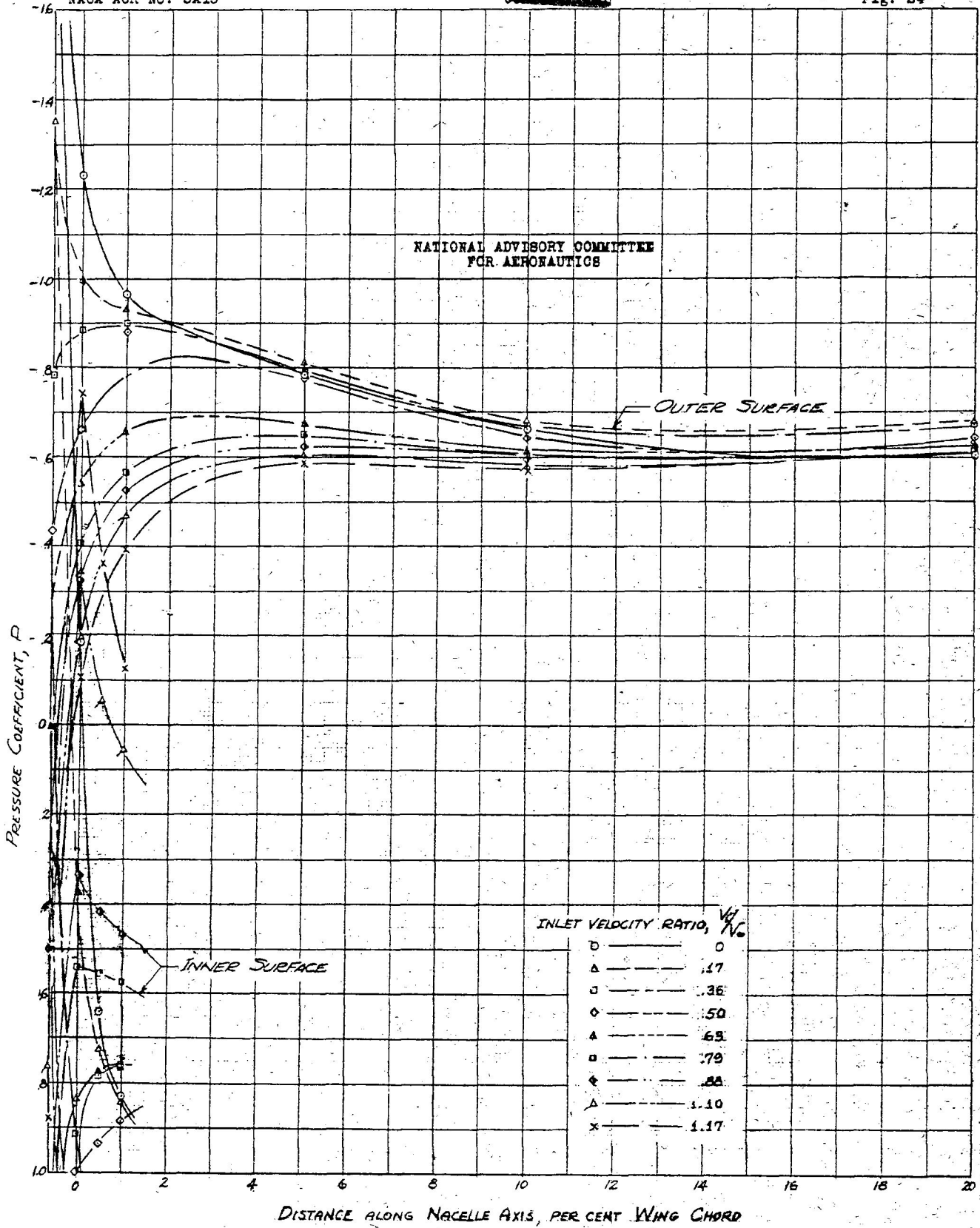


FIGURE 24.-PRESSURE DISTRIBUTION OVER THE UPPER LIP OF NOSE  $N_4$   $\alpha=4.25^\circ$   $C_L=.565$

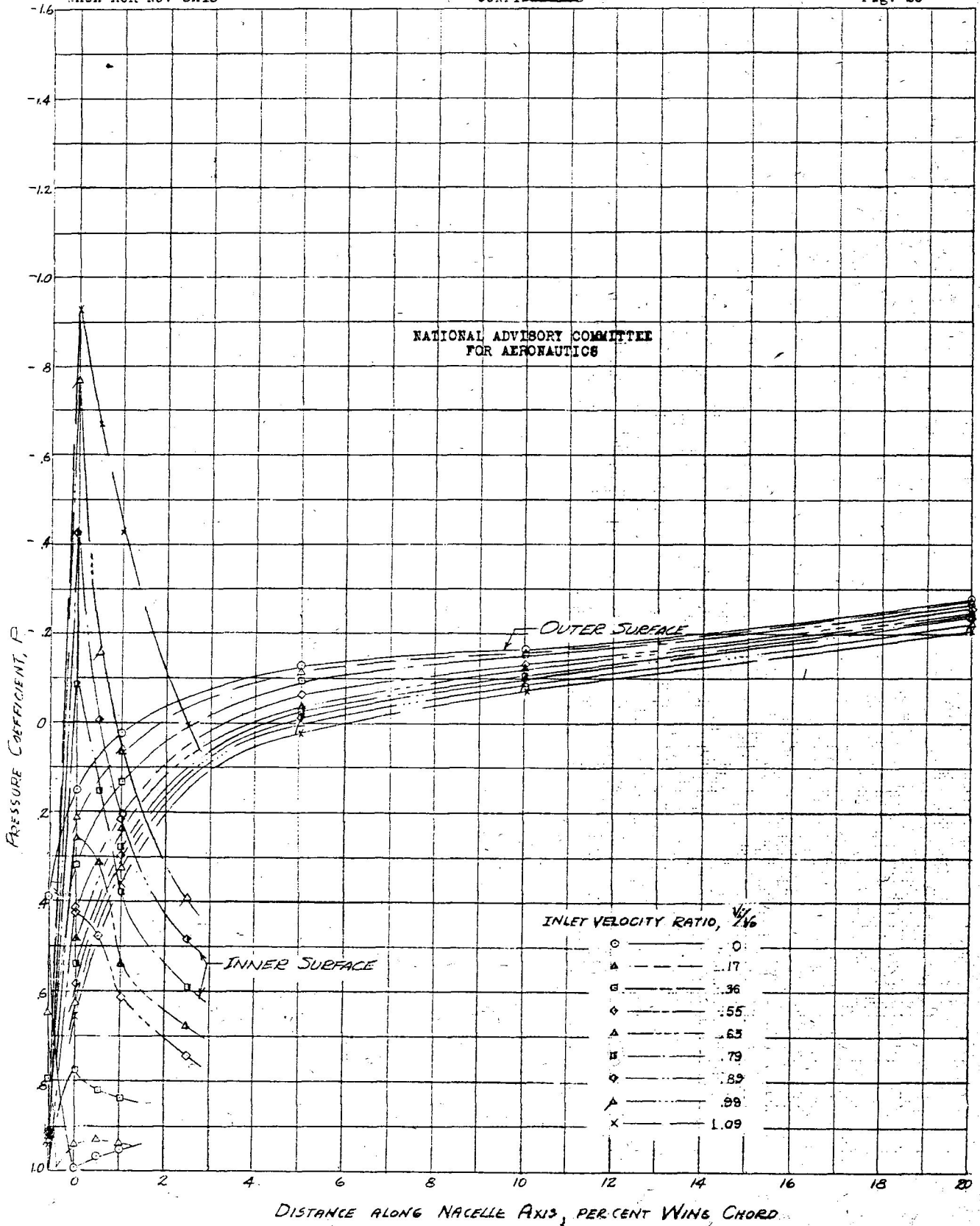


FIGURE 25.- PRESSURE DISTRIBUTION OVER THE UPPER LIP OF NOSE  $N_5$ .  $\alpha = -1.00^\circ$   $C_L = .012$

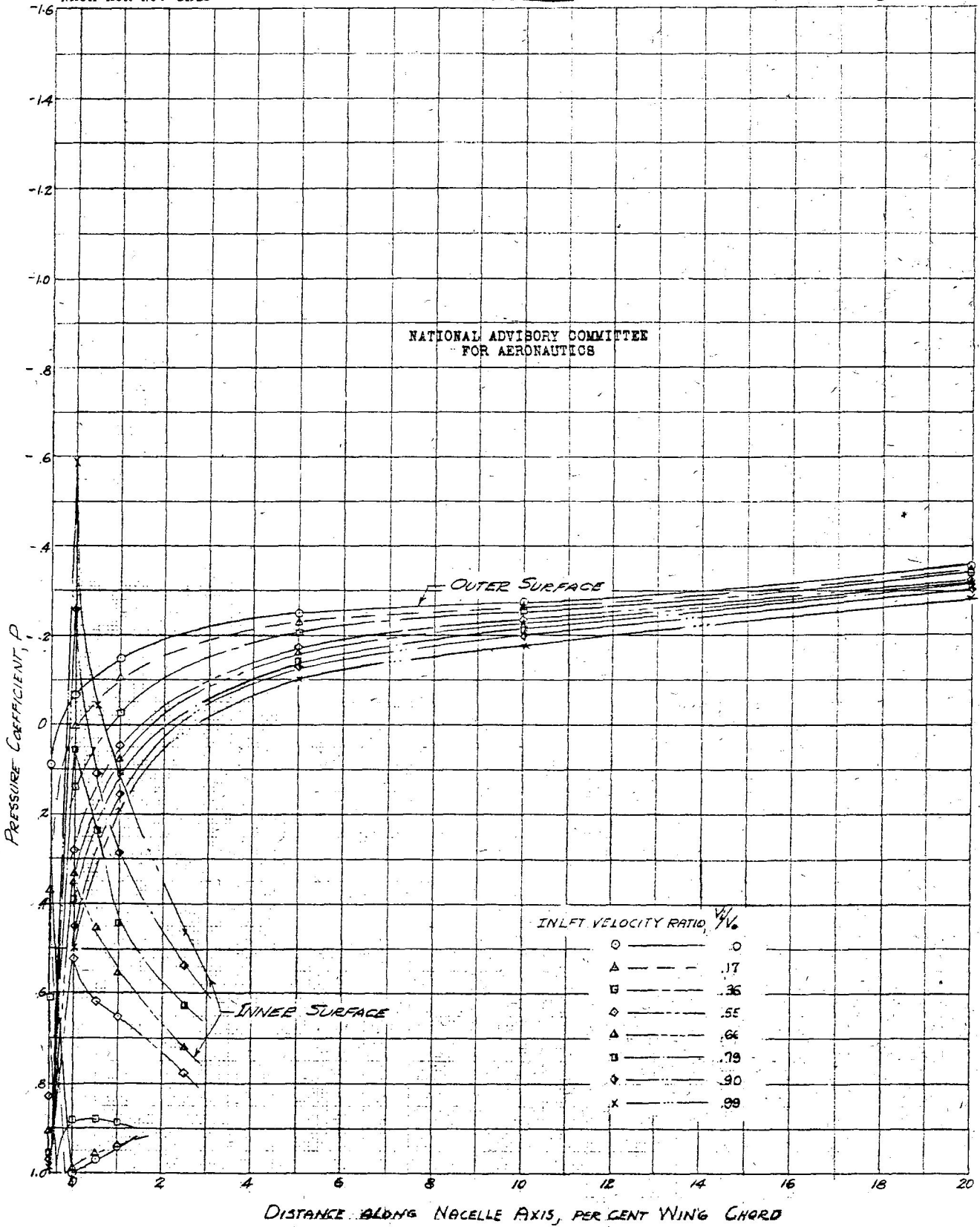


FIGURE 26—PRESSURE DISTRIBUTION OVER THE UPPER LIP OF NOSE  $N_5$ .  $\alpha = 0^\circ$ .  $C_L = .105$ .

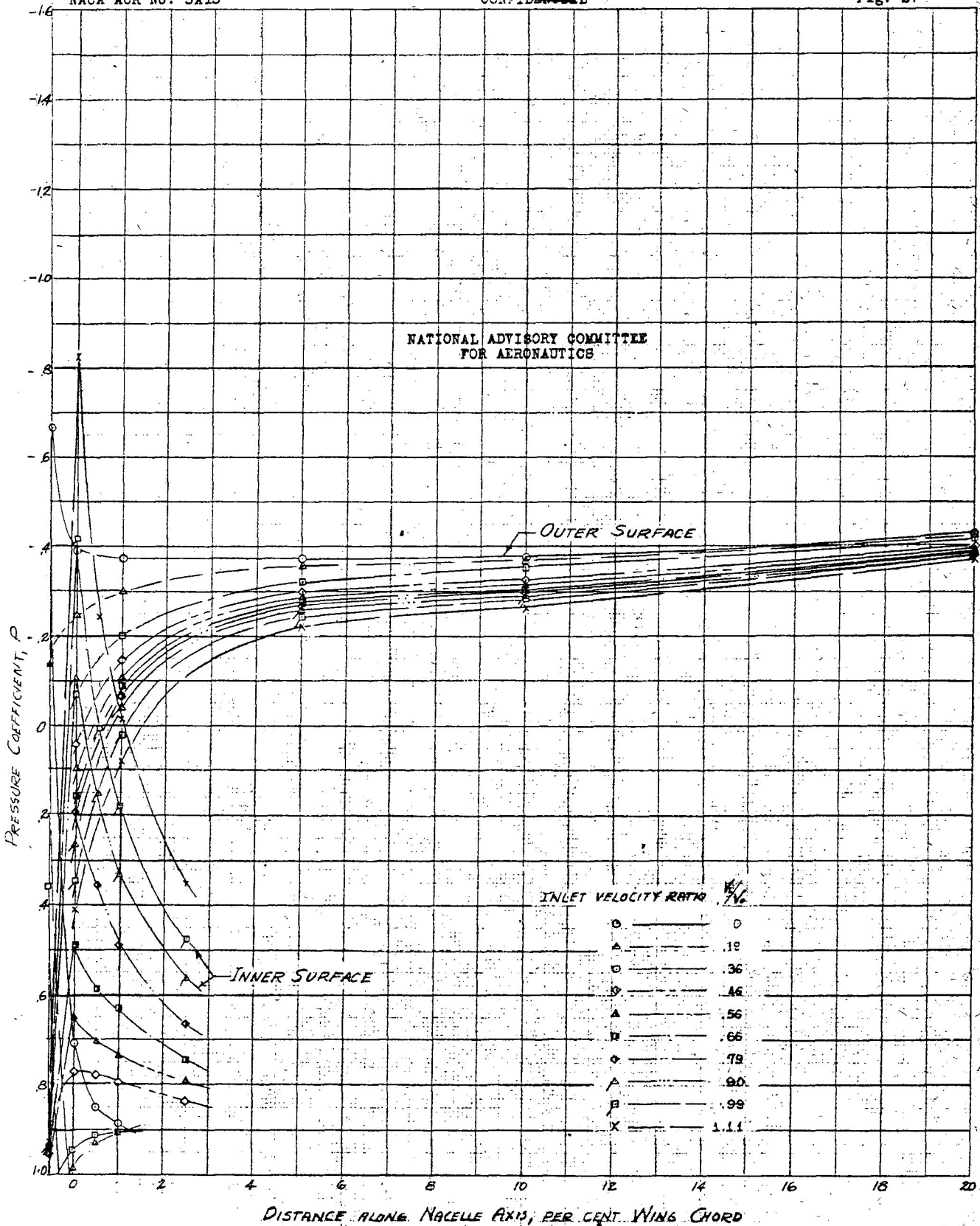


FIGURE 27.- PRESSURE DISTRIBUTION OVER THE UPPER LIP OF NOSE  $N_5$   $\alpha = 1.05^\circ$   $C_L = .215$



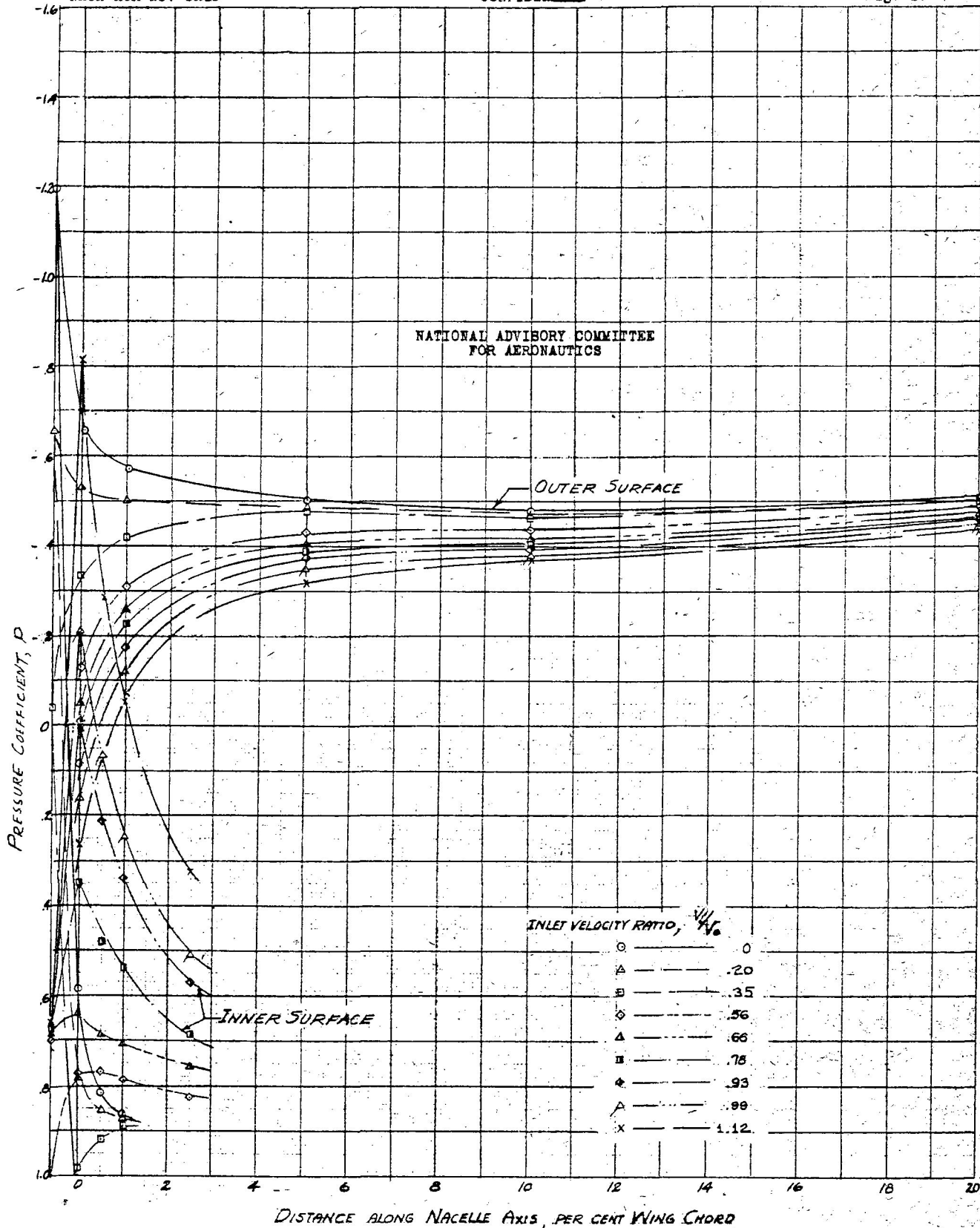


FIGURE 28.-PRESSURE DISTRIBUTION OVER THE UPPER LIP OF NOSE  $N_5$ .  $\alpha = 2.11^\circ$   $C_L = .525$

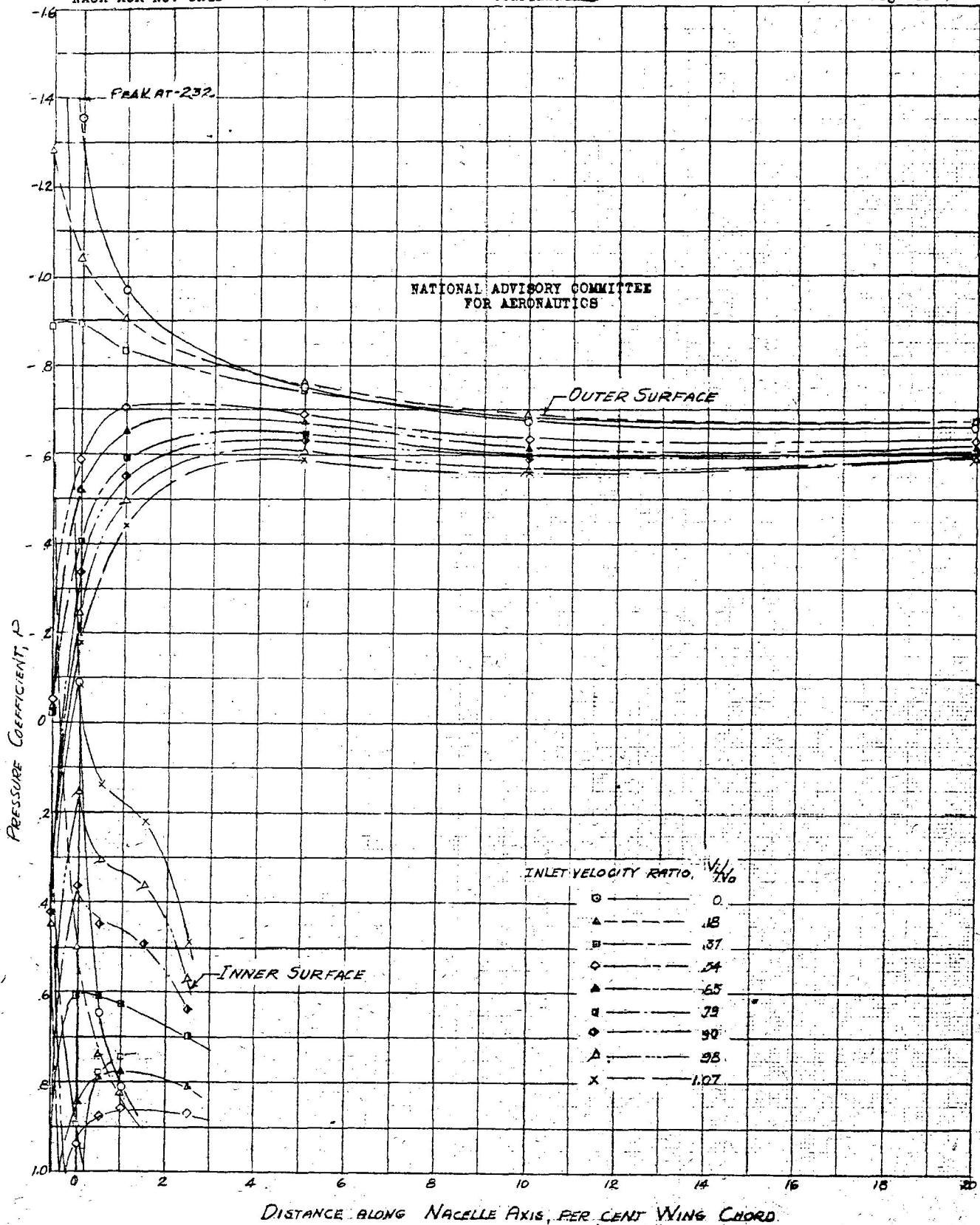


FIGURE 29—PRESSURE DISTRIBUTION OVER THE UPPER LIP OF NOSE  $N_5$   $\alpha = 4.25^\circ$   $C_L = 5.65$

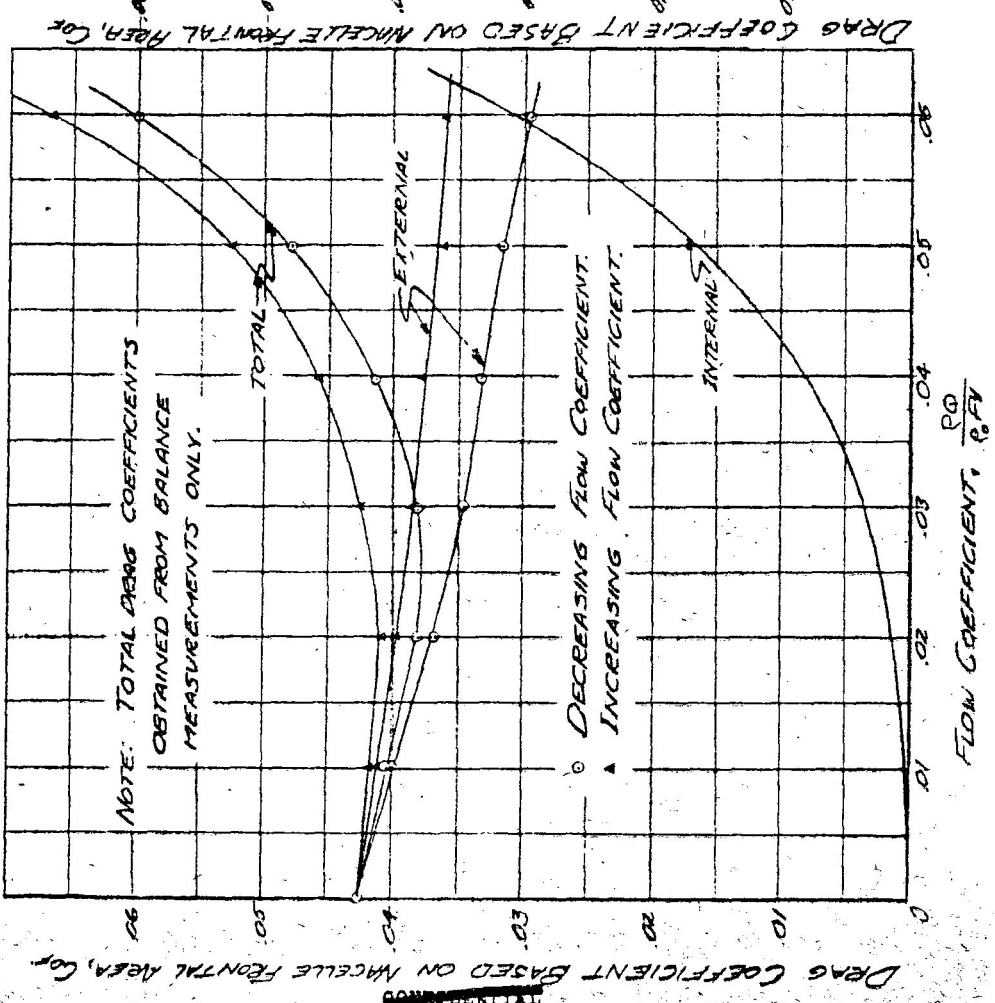
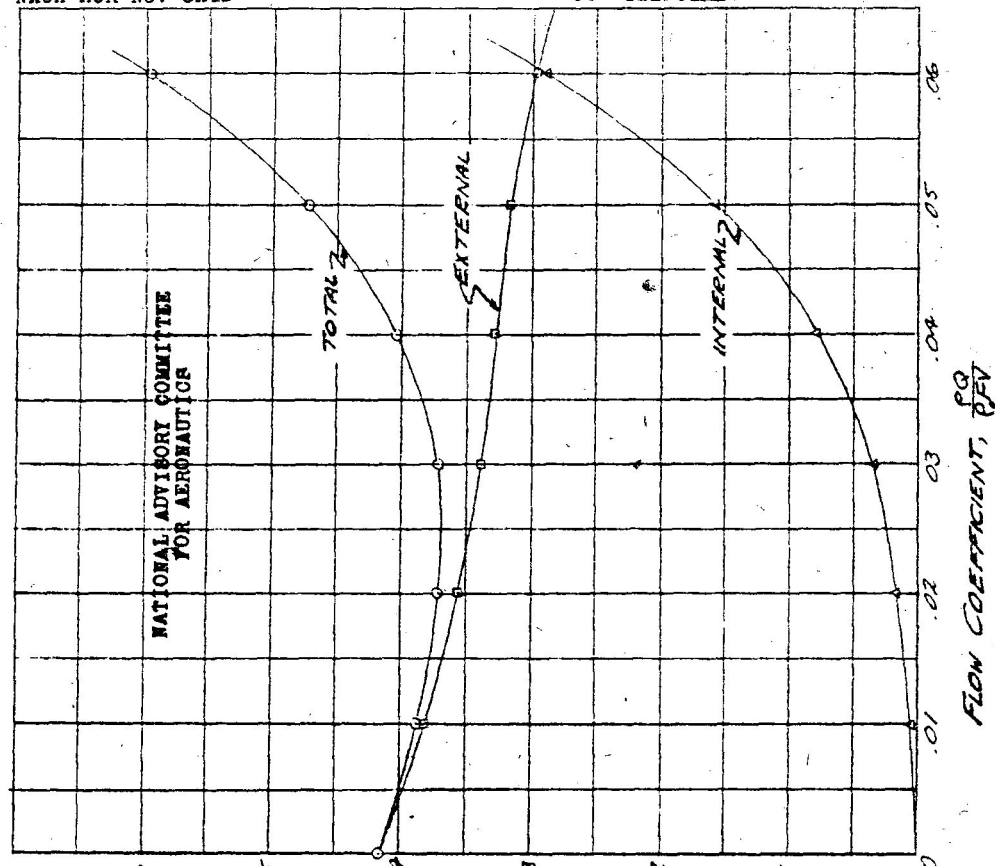


FIGURE 30.- VARIATION OF NACELLE  $N/T$ , DRAG COEFFICIENT WITH MASS FLOW COEFFICIENT.  $\alpha = 0^\circ$ ,  $C_L = .105$ . REYNOLDS NUMBER =  $7.6 \times 10^6$ . MACH NUMBER = .27

FIGURE 31.- VARIATION OF NACELLE  $N/T$ , DRAG COEFFICIENT WITH MASS FLOW COEFFICIENT.  $\alpha = 1.03^\circ$ ,  $C_L = .213$ . REYNOLDS NUMBER =  $7.6 \times 10^6$ . MACH NUMBER = .27

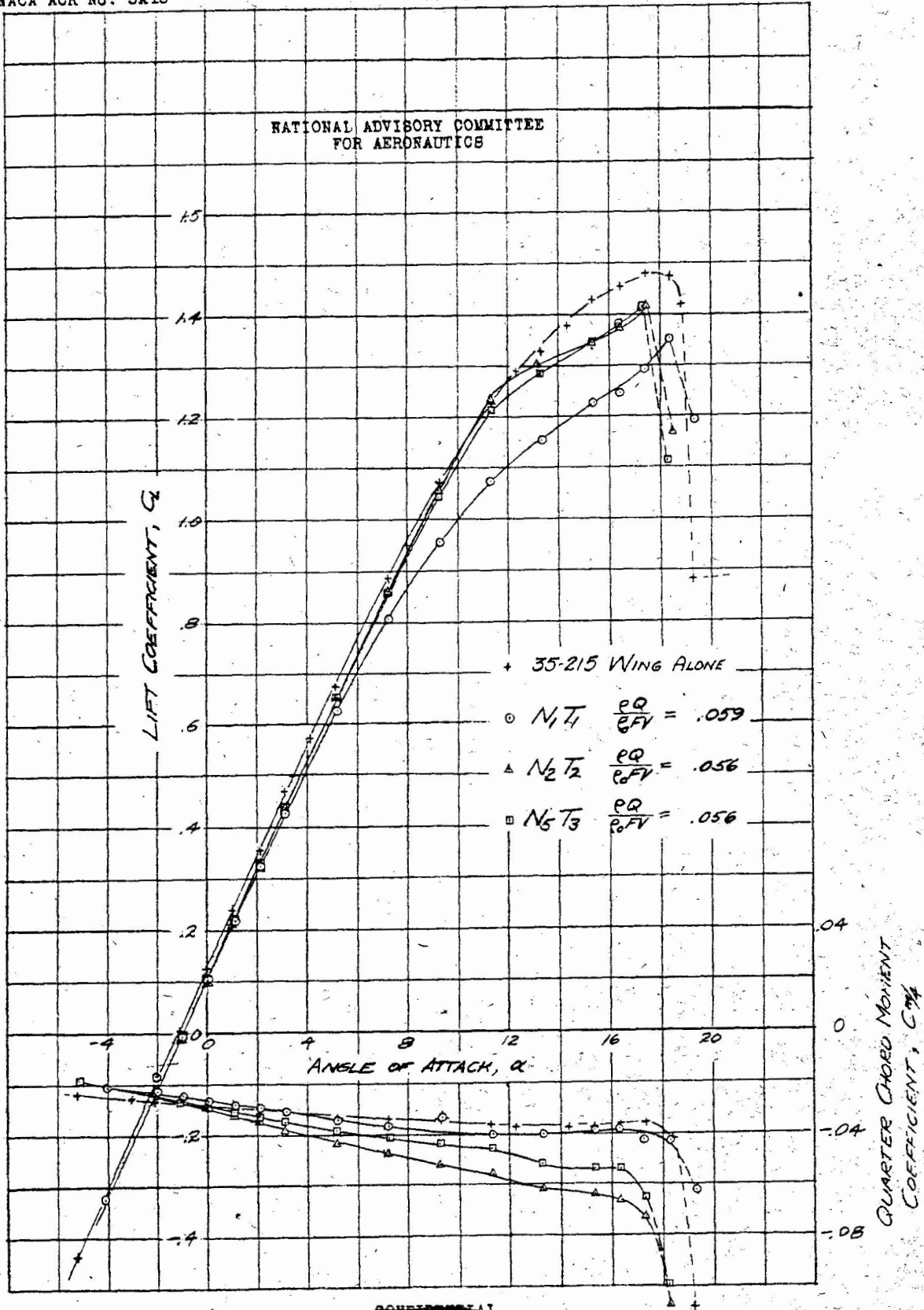


FIGURE 32.- CHARACTERISTICS OF WING-NACELLE COMBINATIONS AS DETERMINED FROM BALANCE FORCE MEASUREMENTS. REYNOLDS NUMBER =  $3.59 \times 10^6$ , MACH NUMBER = .13

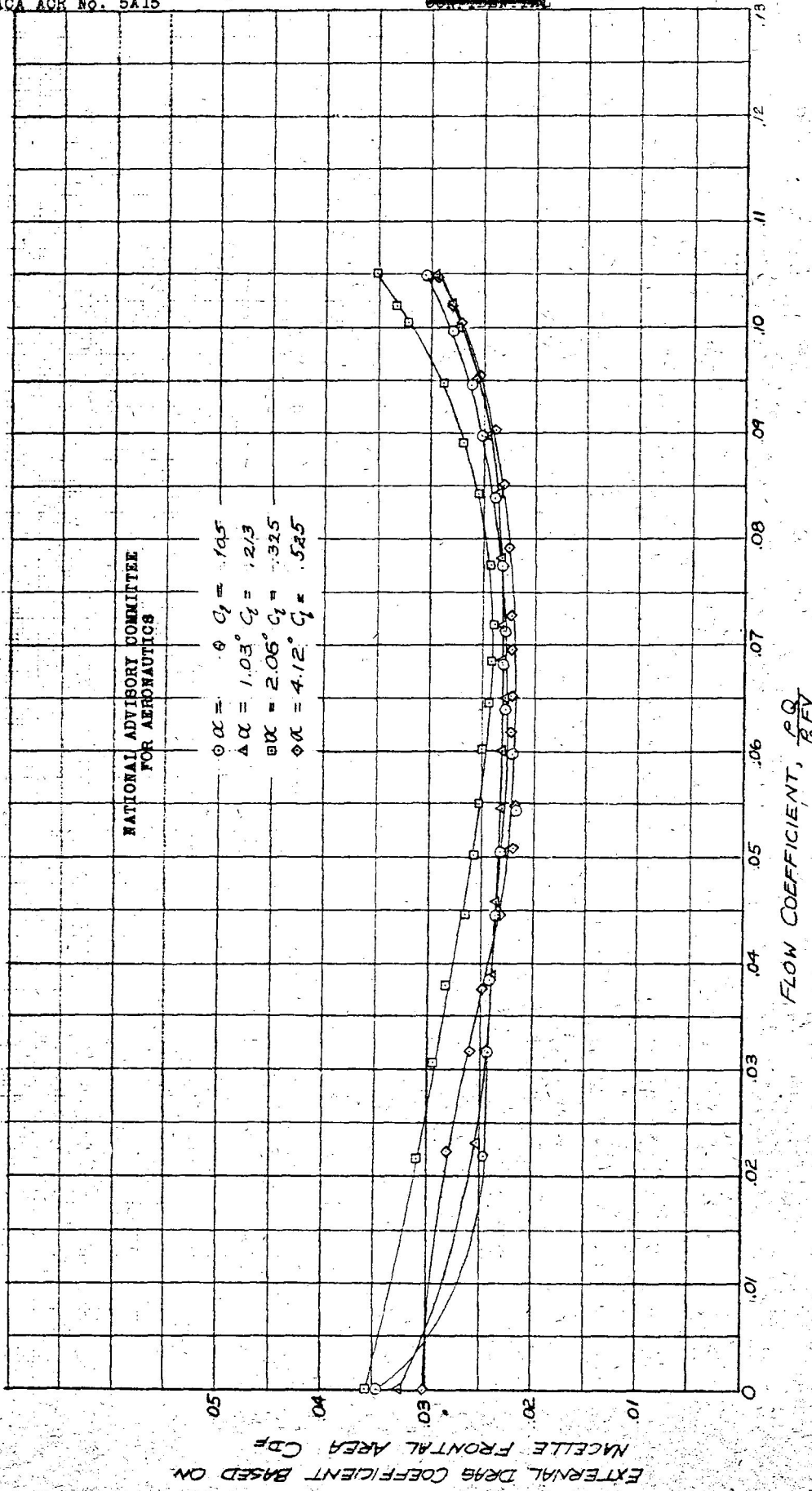
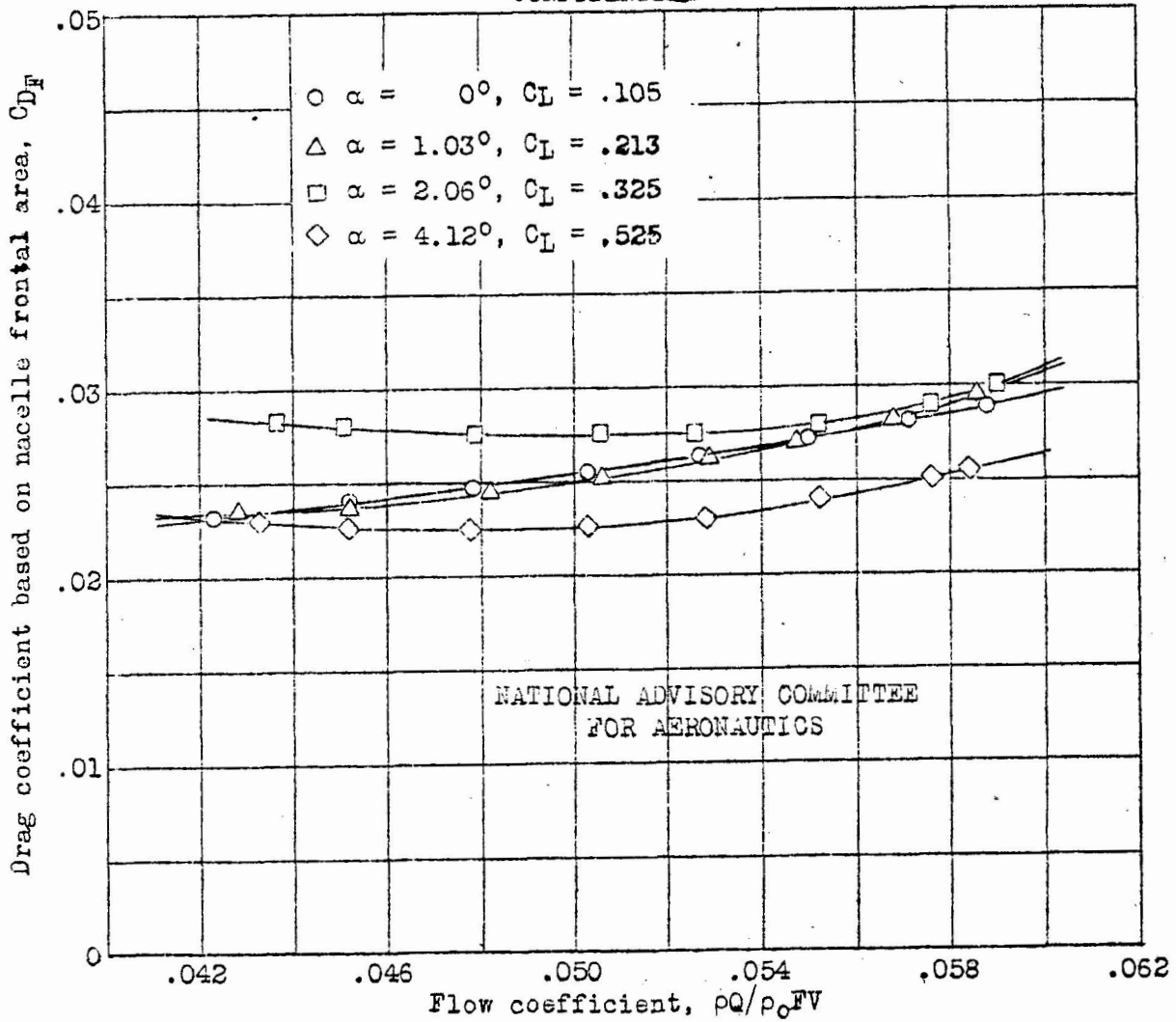


FIGURE 33. - VARIATION OF NACELLE  $N_{1/2}$  EXTERNAL DRAG COEFFICIENT WITH MASS FLOW COEFFICIENT. REYNOLDS NUMBER =  $4.02 \times 10^6$ . MACH NUMBER = .14

UNCLASSIFIED

~~CONFIDENTIAL~~



NATIONAL ADVISORY COMMITTEE  
FOR AERONAUTICS

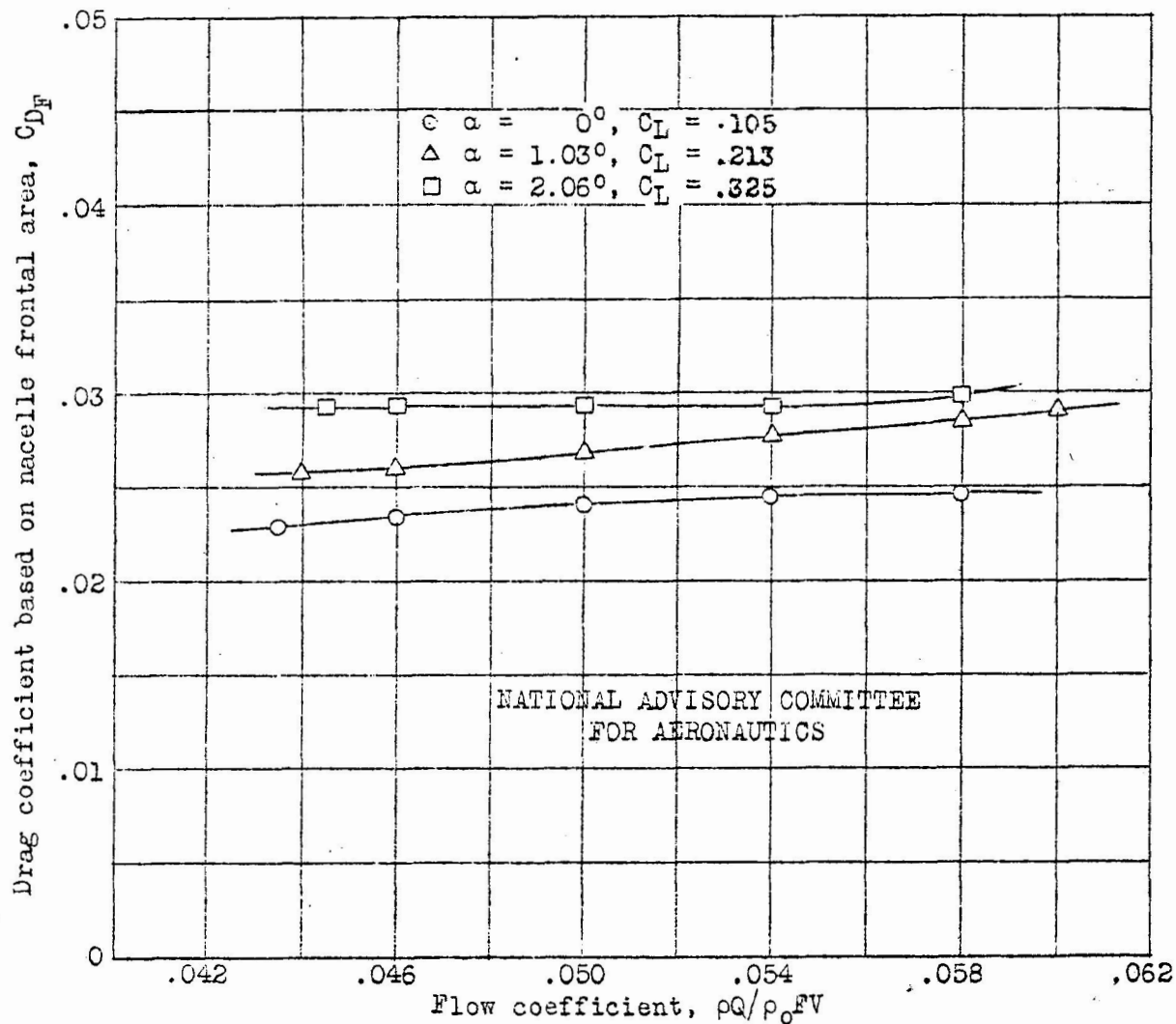
~~CONFIDENTIAL~~

UNCLASSIFIED

Figure 34.- Variation of nacelle N<sub>5</sub>T<sub>3</sub> drag coefficient with mass flow coefficient. Reynolds number =  $7.6 \times 10^6$ . Mach number = .27.

UNCLASSIFIED

~~CONFIDENTIAL~~

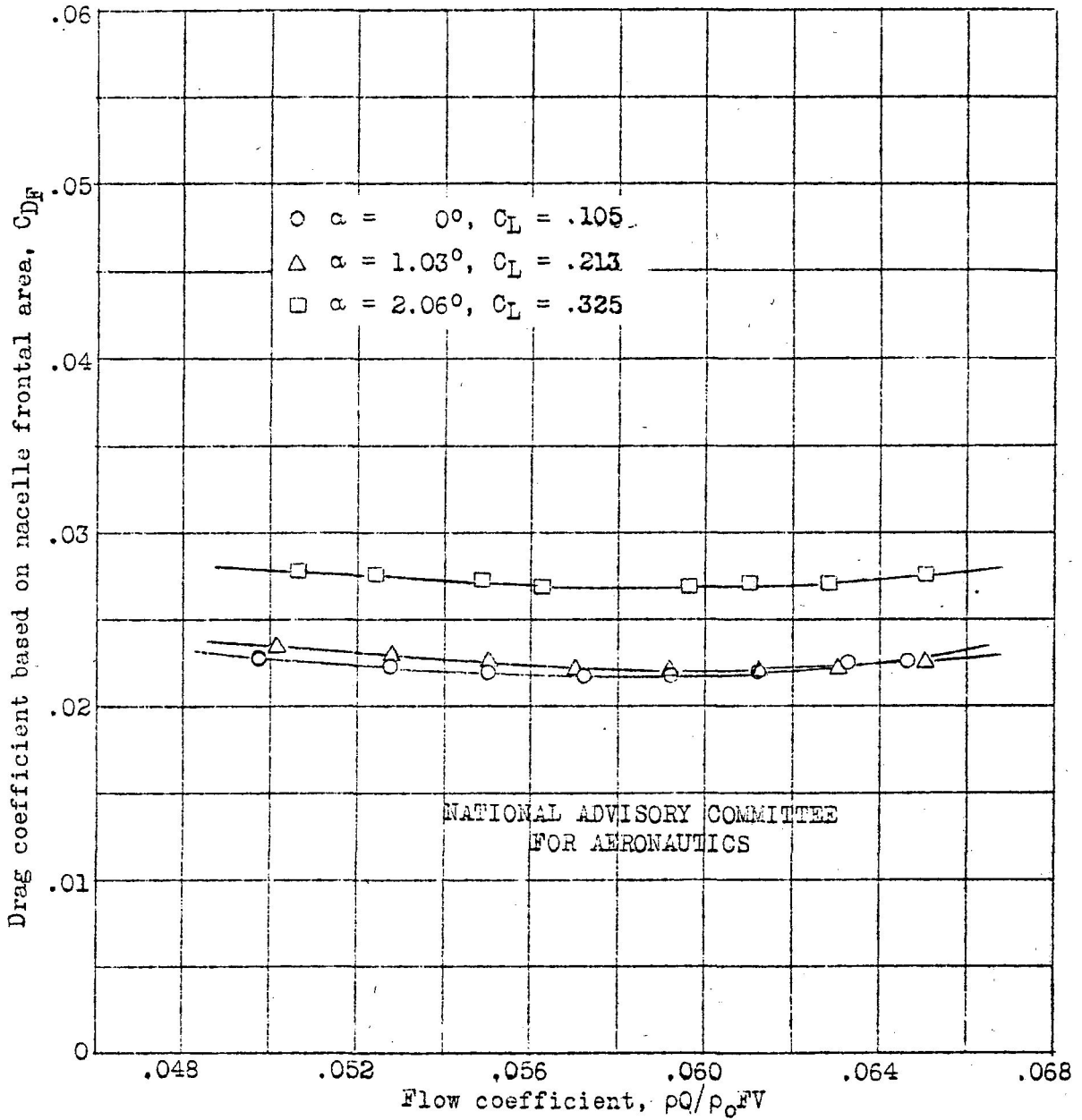


~~CONFIDENTIAL~~

UNCLASSIFIED

Figure 35a.- Variation of nacelle  $N_{5T_4}$  drag coefficient with mass flow coefficient. Reynolds number =  $7.6 \times 10^6$ , Mach number = .27.

UNCLASSIFIED  
~~CONFIDENTIAL~~

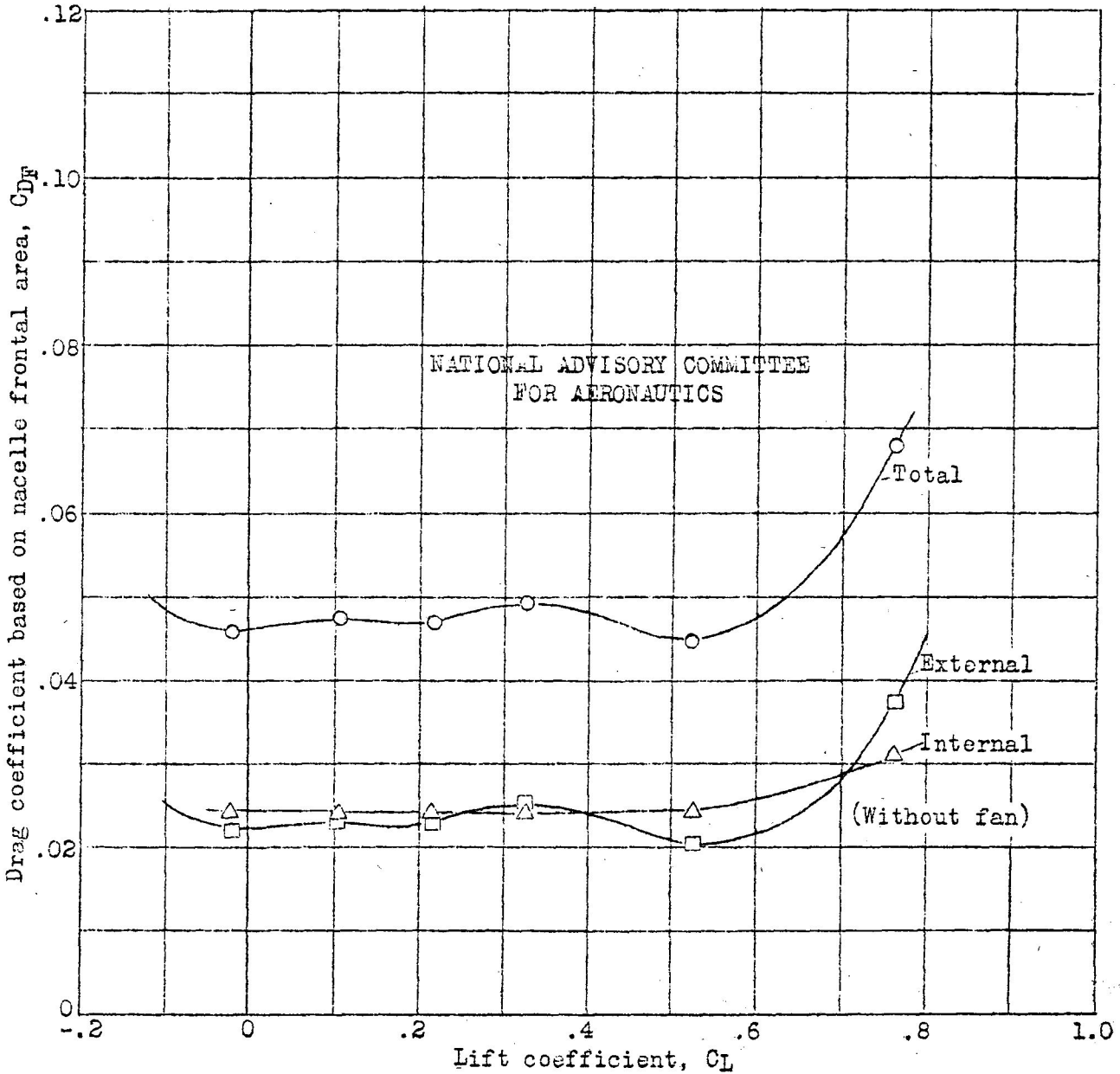


~~CONFIDENTIAL~~  
 UNCLASSIFIED

Figure 35b.- Variation of nacelle N5T5 drag coefficient with mass flow coefficient. Reynolds number =  $7.6 \times 10^6$ . Mach number = .27.



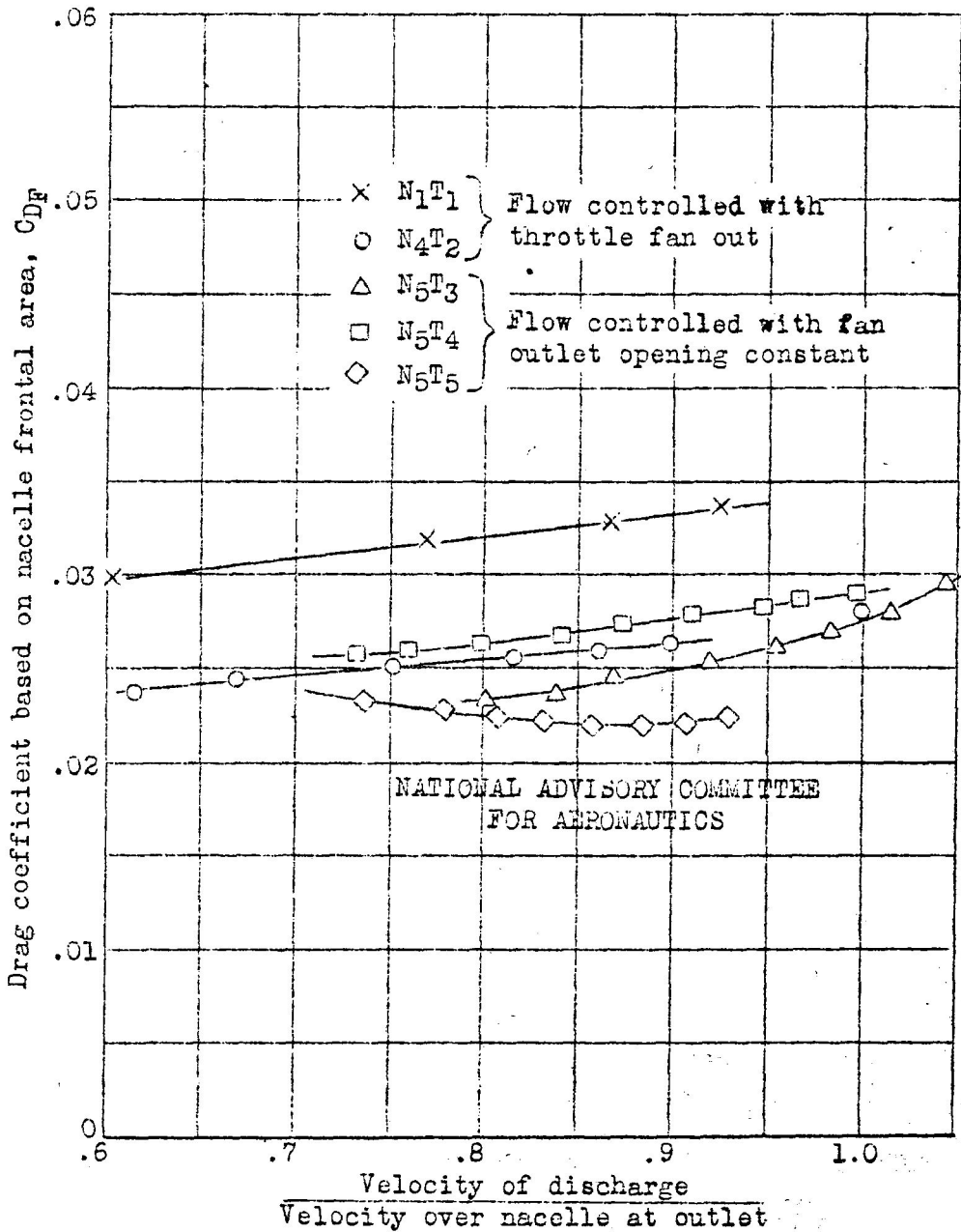
~~CONFIDENTIAL~~



~~CONFIDENTIAL~~

Figure 36.- Variation of nacelle drag coefficient with lift coefficient for nacelle  $N_4T_2$ ,  $\rho/\rho_0 Q/FV = .056$ , Reynolds number =  $3.7 \times 10^6$ , Mach number = .13.

~~CONFIDENTIAL~~



~~CONFIDENTIAL~~ UNCLASSIFIED

Figure 37.- Variation of nacelle external drag coefficient with the ratio of velocity of discharge from the outlet to the velocity over the nacelle at the outlet.  $\alpha = 1.03^\circ$ ,  $C_L = .213$ . Reynolds-number =  $7.6 \times 10^6$ , Mach number = .27.

~~CONFIDENTIAL~~  
UNCLASSIFIED

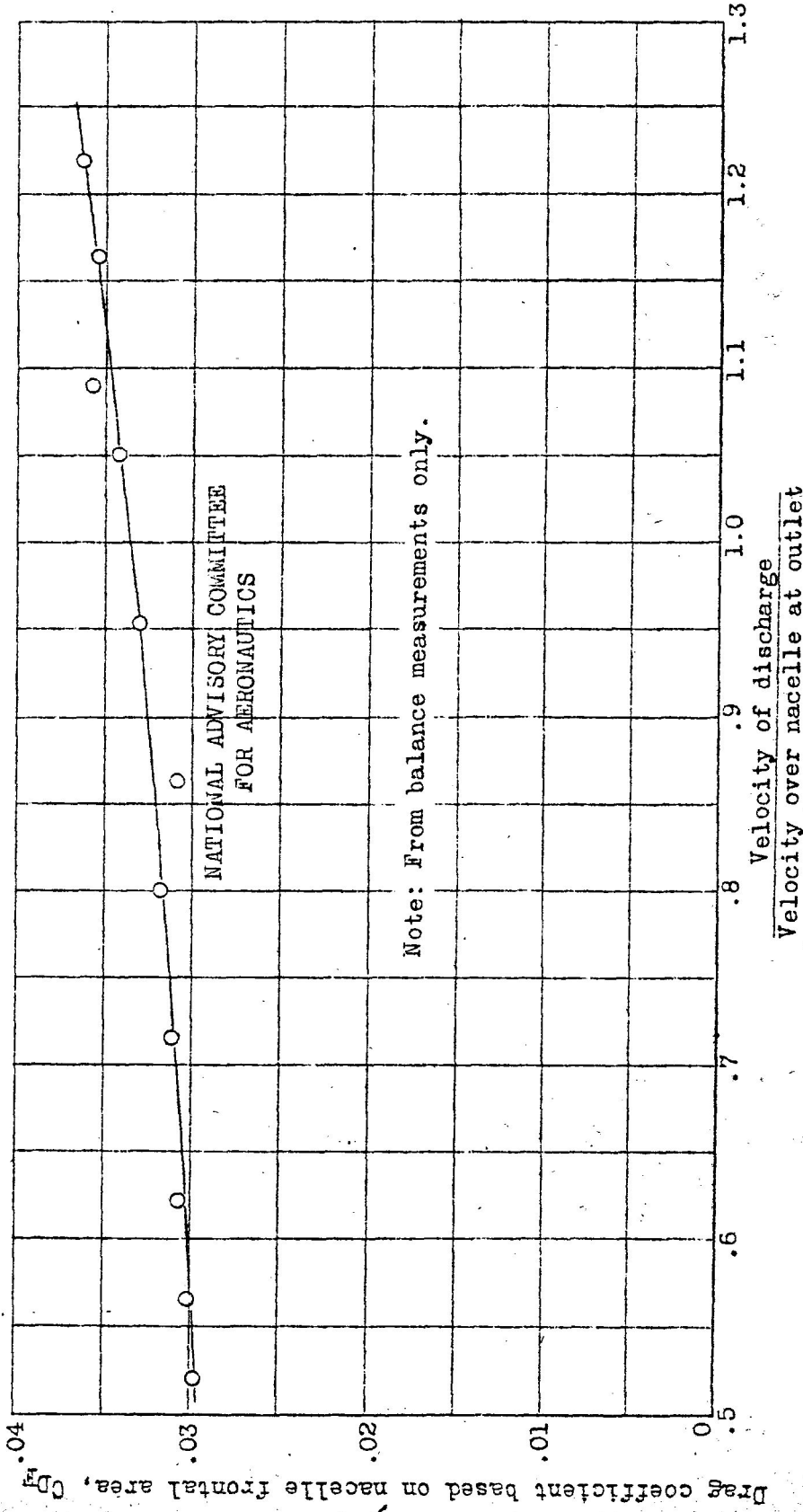


Figure 38.- Variation of nacelle  $N_{1T1}$  external drag coefficient with the ratio of velocity of discharge from the outlet to the velocity over the nacelle at the outlet at constant mass flow coefficient, fan operating  $p_0/\rho_0 V_0 = .055$ ,  $\alpha = 0^\circ$ ,  $C_L = .105$ , Reynolds number =  $5.03 \times 10^6$ , Mach number = .19.

~~CONFIDENTIAL~~  
UNCLASSIFIED

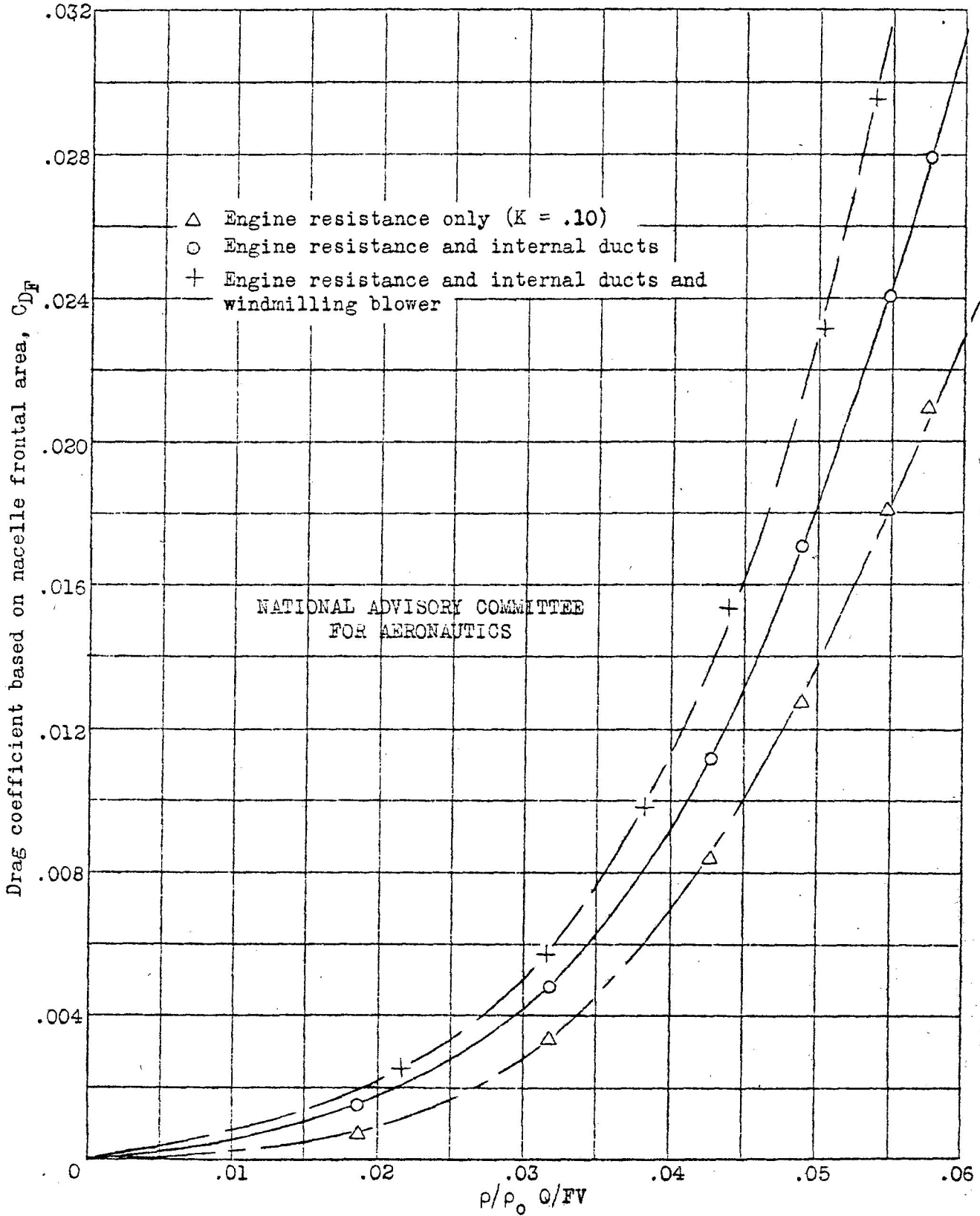
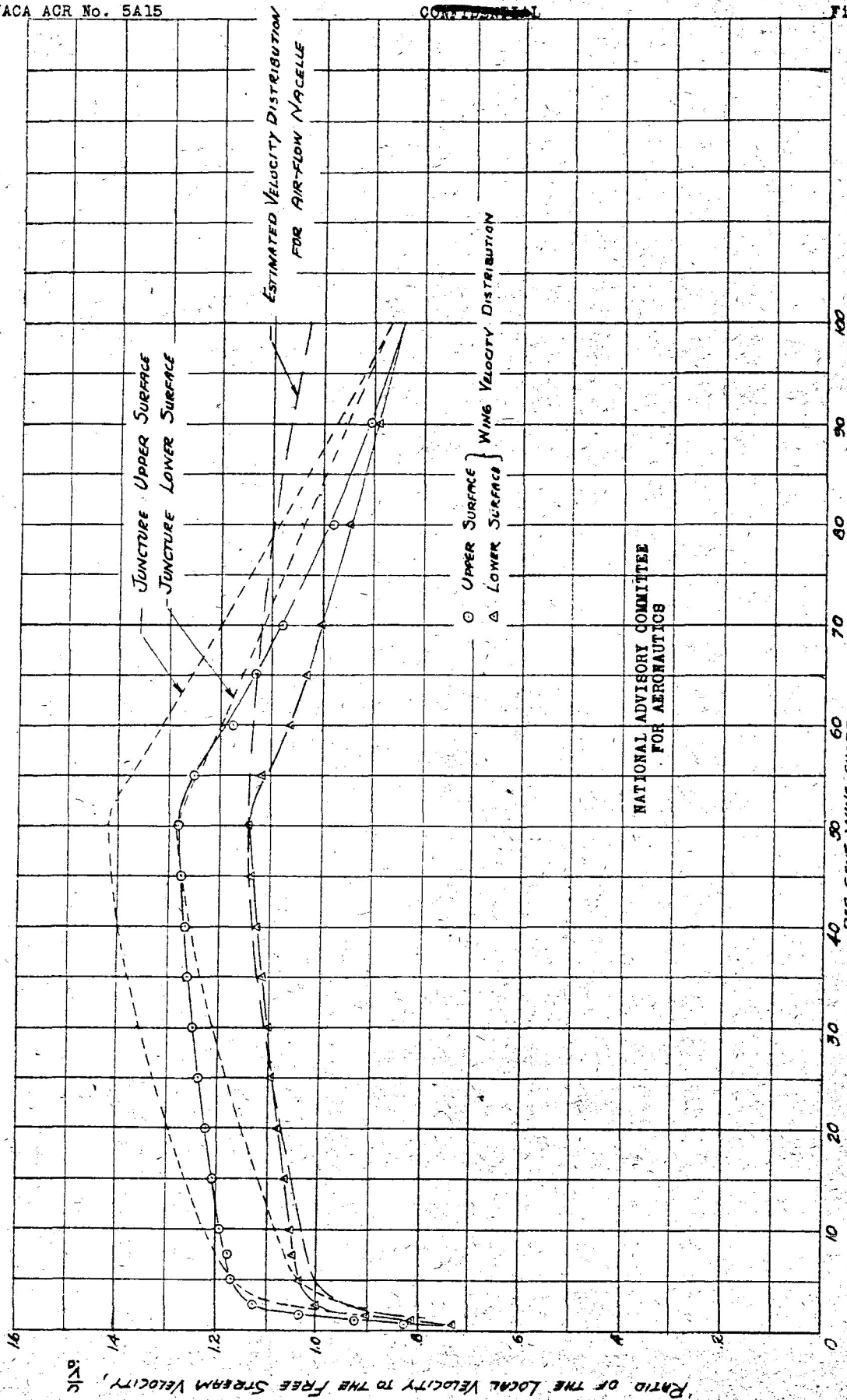


Figure 39.- Variation of internal drag coefficient with mass flow coefficient for nacelle  $N_4P_2$  for all angles between  $-1^\circ$  and  $4^\circ$  inclusive.



NATIONAL ADVISORY COMMITTEE FOR AERONAUTICS

FIGURE 40.— SUPERPOSITION OF VELOCITIES IN THE JUNCTURE OF THE NACA 35-215 WING AND THE MODIFIED NACA 133-30 NACELLE.

UNCLASSIFIED

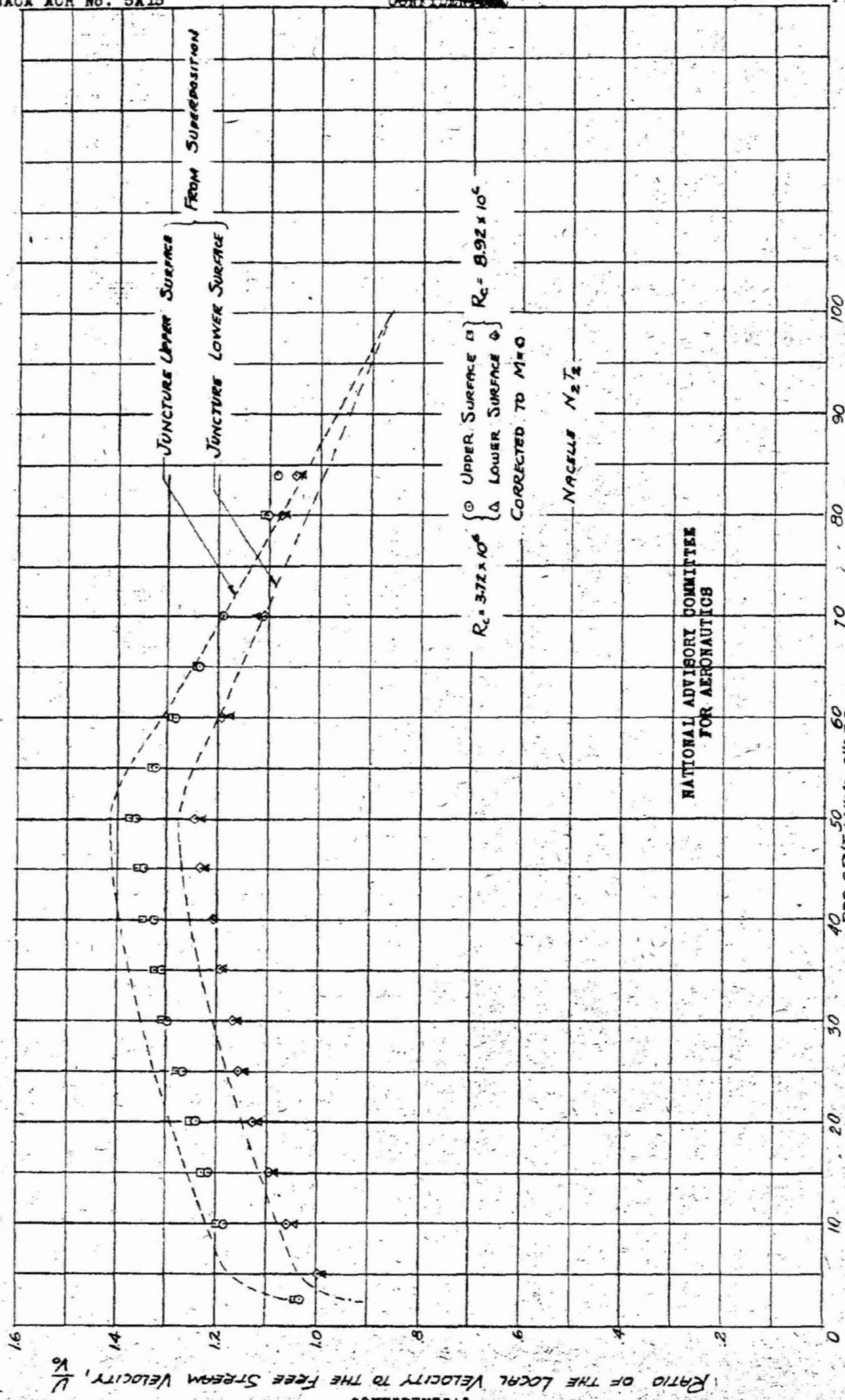


FIGURE 41.- COMPARISON OF THE MEASURED VELOCITY DISTRIBUTION WITH THAT CALCULATED BY SUPERPOSITION FOR THE JUNCTION.

NATIONAL ADVISORY COMMITTEE FOR AERONAUTICS

UNCLASSIFIED

UNCLASSIFIED

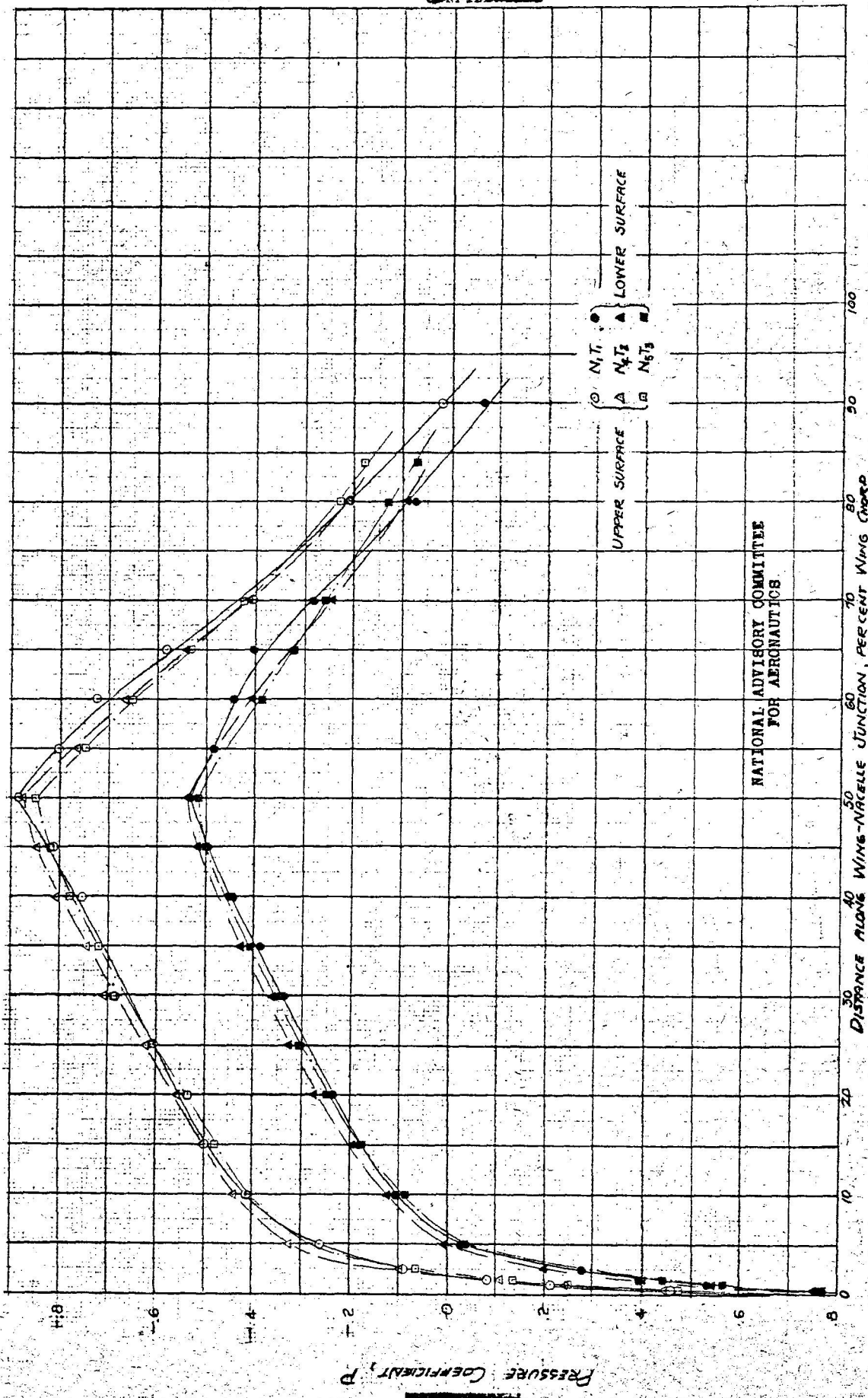


FIGURE 42.- COMPARISON OF PRESSURE DISTRIBUTION OVER THE WING-NACELLE JUNCTION FOR NACAELLS WITH VARIOUS TAILS.  $\frac{P}{P_\infty}$  vs.  $\frac{x}{c}$

NATIONAL ADVISORY COMMITTEE FOR AERONAUTICS

UNCLASSIFIED

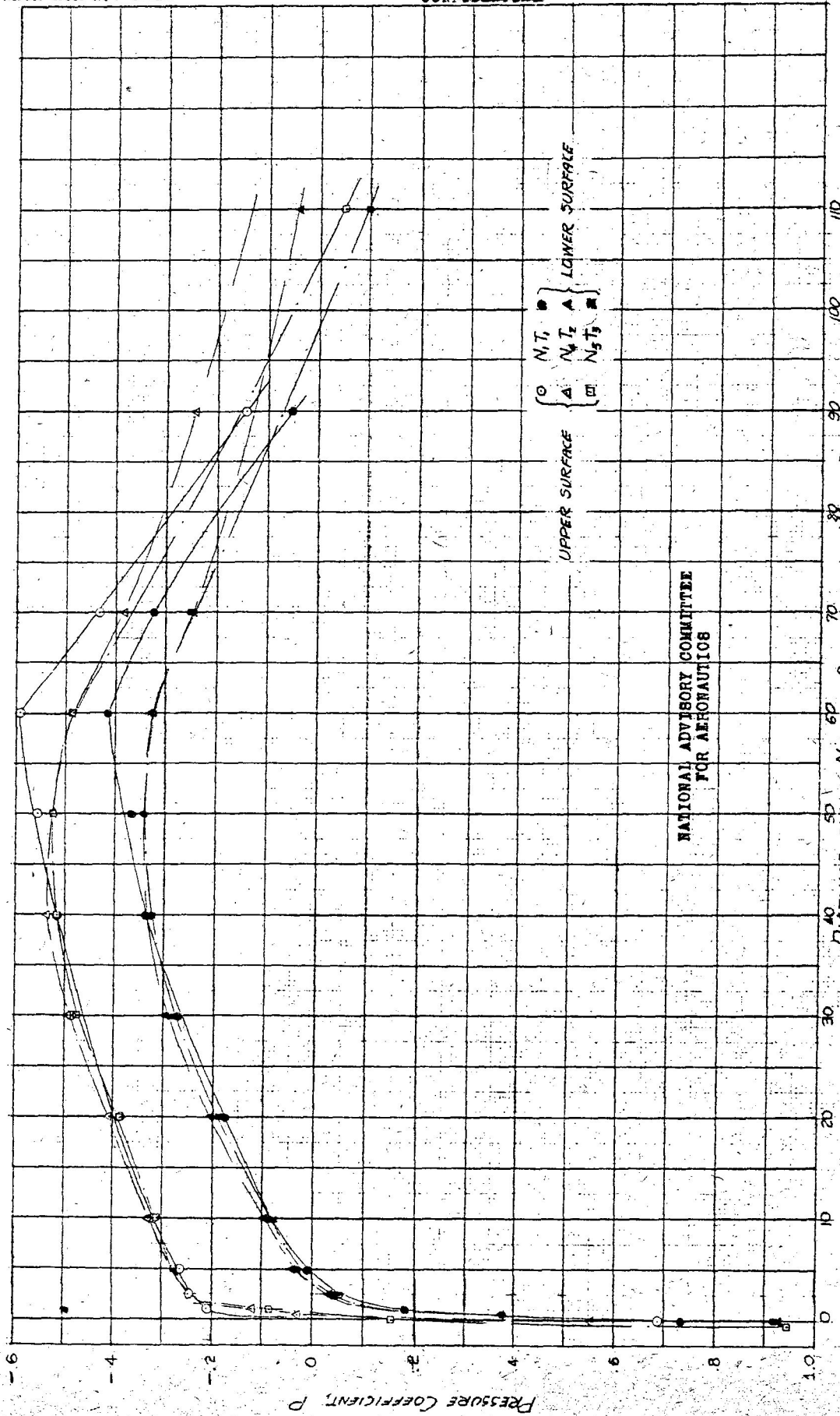


FIGURE 43.- COMPARISON OF PRESSURE DISTRIBUTION OVER BOTH SURFACES OF NACELLES WITH VARIOUS TAILS.  $\frac{P}{P_0} = 0.058$   $M = 0.65$



UNCLASSIFIED  
~~CONFIDENTIAL~~

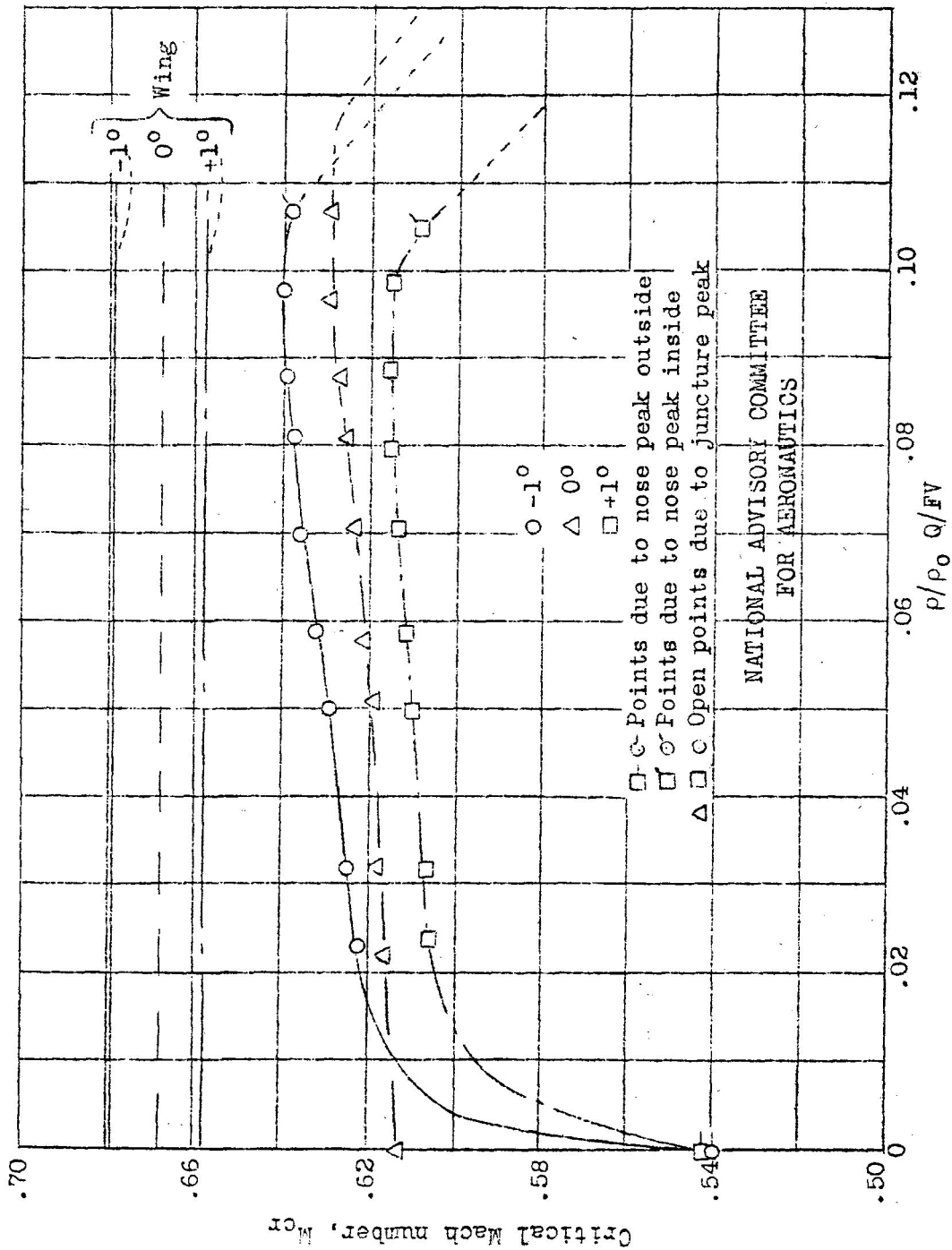
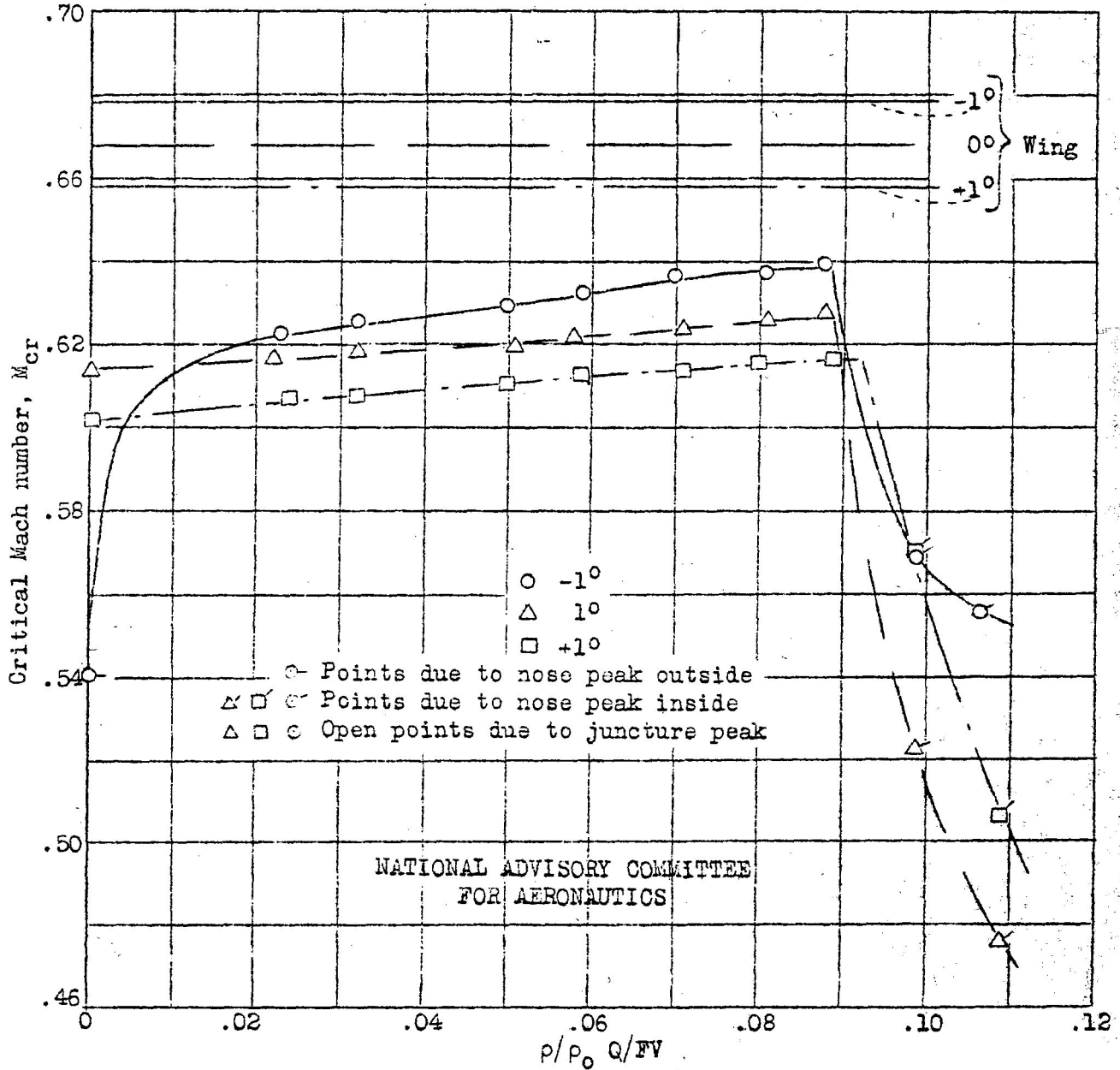


Figure 44.- Variation of predicted critical mach number with mass flow coefficient for nacelle N2T2. [ $v/V = 11.1 \rho/p_0 Q/FV$ ]

~~CONFIDENTIAL~~  
UNCLASSIFIED

UNCLASSIFIED  
CONFIDENTIAL

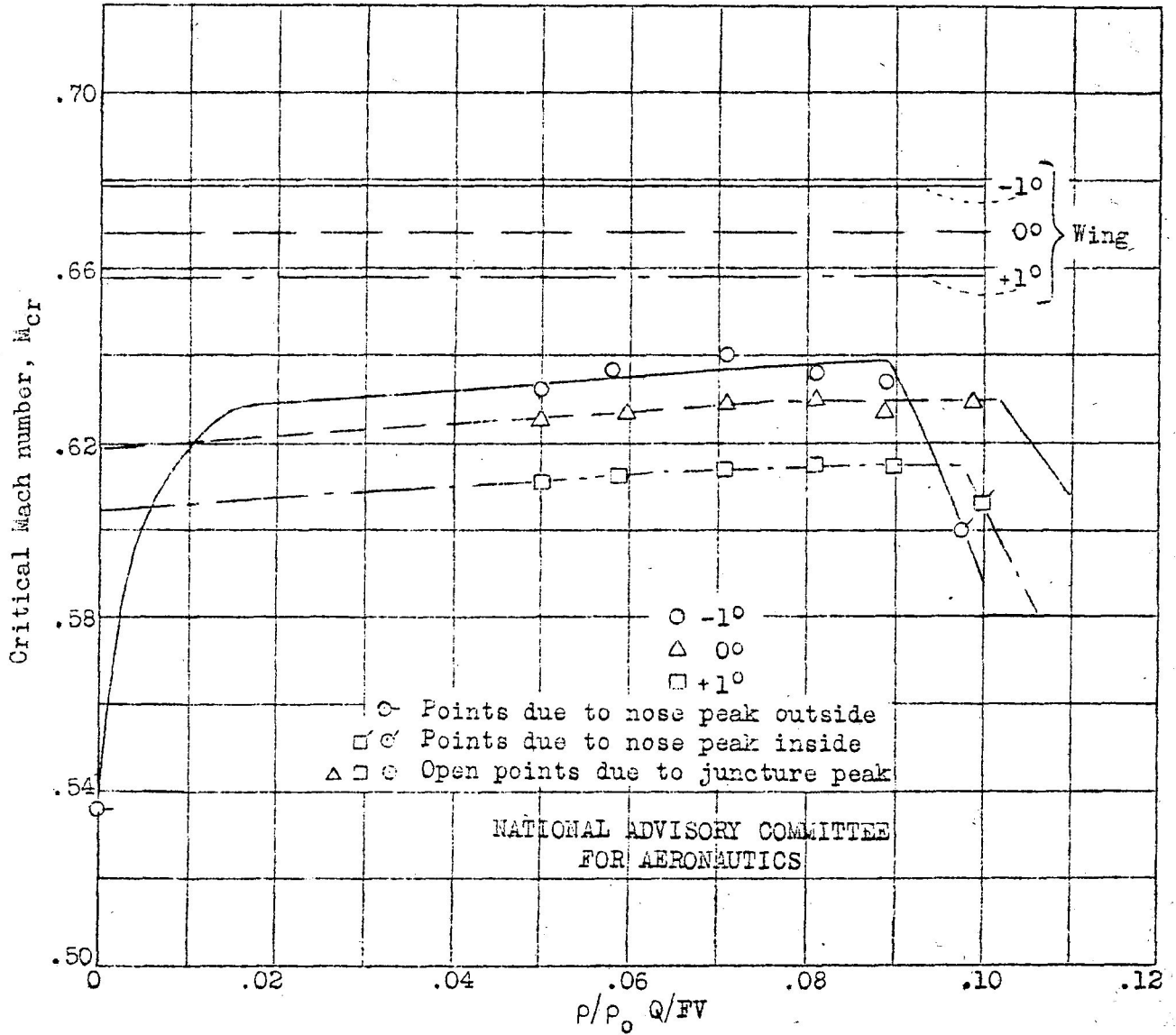


UNCLASSIFIED

Figure 45.- Variation of predicted critical Mach number with mass flow coefficient for nacelle  $N_4T_2$ . [ $v/V = 11.1 p/p_0 Q/FV$ ]

UNCLASSIFIED

~~CONFIDENTIAL~~



NATIONAL ADVISORY COMMITTEE  
FOR AERONAUTICS

~~CONFIDENTIAL~~

UNCLASSIFIED

Figure 46.- Variation of predicted critical Mach number with mass flow coefficient for nacelle N<sub>5T3</sub>. [ $v/V = 11.1 \rho/\rho_0 Q/FV$ ].